学位論文

Investigation on environmental dynamics of radioactive Cs released from Fukushima nuclear power plant accident

福島原発事故に伴い放出された放射性 Cs の環境動態についての研究

2019 年 (令和元年) 11 月

NGUYEN TAT THANH

Abstract

A prominent nuclear accident after Three Miles Island (1979) and Chernobyl (1986) - Fukushima Daiichi Nuclear Power Plant accident had occurred due to the massive earthquake and huge tsunami. By the Fukushima Nuclear Power Plant accident, tremendous radioactive materials, especially radiocesium with a quite long half-life had been released into the air and then deposited on the surface soil. Radiocesium causes harmfulness to human such as disordering the function and metabolic activity of kidneys, myocardium and so on if they get in the body. Recent research after the Fukushima Nuclear accident also pointed out that the significant impacts on the environment such as the morphological effects on pines, high abnormality rate in the pale grass blue butterfly, reduction of the body weight and head size of monkey babies. It is necessary to investigate their distribution and change following the time to protect humans and the environment from radiocesium. Some researchers have evaluated the distribution of radiocesium in the soil in the post-accident period; however, an investigation on the change of the radiocesium for later years and transfer of the radiocesium from soil to young tree growing on the contaminated soil is not conducted. Therefore, the environmental dynamic and transfer of radiocesium from depth profile soil to young pines is the purpose of this investigation.

－ This doctoral thesis is composed of 6 chapters in which content is summarized as below －

Chapter I: The background and circumstance of the Fukushima Nuclear Power Plant accident and its effects on the environment are introduced briefly. The reason for choosing the Iitate village as a research location and the purpose of the investigation are explained.

Chapter II: A method for soil sampling and young tree sampling is described in this investigation. These collected soil and young tree samples are prepared and measured by Imaging plate measurement and Ge detector. The acquired results are used for further analysis in the next Chapters.

Chapter III: A technique for determining the shape of the depth profile of radiocesium in soil by using an imaging plate combined with the unfolding algorithm and PHITS code simulation is introduced. By the proposed technique, the depth profile of radiocesium can be plotted with millimeter depth-bin width, which is quite difficult to be obtained by conventional techniques such as sliding soil core to thin soil layers.

Chapter IV: Migration velocity and diffusion coefficient are radiocesium movement indexes in soil, and they are solutions of an equation derived from Bossew and Kirchner-model for transportation of radionuclides in soil. The migration velocity, which is assumed as an exponential function of time, inserted to the equation above, and applied for fitting the depth profiles of those obtained by the method in Chapter III.

Chapter V: In this chapter, a soil-to-plant transfer coefficient formulation expressed using a soil-to-root transfer factor and root-to-plant translocation factor is proposed. The soil-to-root transfer coefficient is constructed to use for the homogeneous distribution and depth profile of radiocesium in the soil. The proposed formulation is applied for calculating the soil-to-plant transfer coefficient of young trees collected at the Iitate village.

Chapter VI: The research results are summarized, and future research prospect is suggested

CONTENTS

Chapter I. Introduction 6

1. Research background 6

1.1. The circumstance of Fukushima Daiichi nuclear power plant before and after the accident 6

1.2. Selection of location for research 9

2. Environmental dynamics of radiocesium in the environment and purpose of this study 11

Chapter II. Soil sampling and measurement method 16

1. Soil core sampling method 16

2. Young tree sampling method 22

3. Measurement of IP profiles 24

4. Gamma measurement of collected soil cores by a COAX type detector 28

5. Gamma measurement of ^{40}K in young trees by the COAX and Well-type detectors 28

Chapter III. Determination of ^{137}Cs depth profile soil 32

1. Introduction 32

2. Material and method 34

2.1. Calculation of response function by PHITS 34

2.2. Unfolding technique 40

3. Results 43

3.1. IP profile and gamma measurement results 43

3.2. Depth profile results of radionuclides 46

4. Discussion 48

5. Conclusion 53

Chapter IV. Migration velocity and diffusion coefficient 57

1. Introduction 57

2. Material and method 58

2.1. Migration velocity and diffusion coefficient from previous research 58

2.2. The equation for migration velocity and diffusion coefficient in Fukushima soil 58

2.3. Fitting method for obtained depth profiles 59

2.4. Depth profiles of radionuclides at other locations 61

3. Results 72

4. Discussion 81

5. Conclusion 84

Chapter V. Soil-to-plant transfer coefficient formulation proposal 86

1. Introduction 86

2. Soil-to-tree transfer coefficient formulation 88

3. Results 90

3.1. Depth profile of radiocesium in soil 90

3.2. Radioactivity concentration in the root 92

3.3. Soil-to-root transfer factor and soil-to-plant transfer coefficient 94

4. Discussion 98

5. Conclusion 103

Chapter VI. Summary 106

Acknowledgment 107

Chapter I. Introduction

1. Research background

1.1. The circumstance of Fukushima Daiichi nuclear power plant before and after the accident

Fukushima Daiichi nuclear power plant (FDNPP) located on the Okuma and Futaba towns of Fukushima prefecture and operated by the Tokyo Electric Power Company (TEPCO). In the FDNPP, there were six units on operating, and two units on preparing for construction. The reactors set up in the units of the FDNPP were boiling water reactor type (BWR), and electrical generators of each reactor were estimated to be 460 MWe (Unit 1), 784 MWe (Unit 2-5) and 1100 (Unit 6) in a total of 4.7 GWe [1]. This total amount of electrical generation made the FDNPP be one of the 15 largest nuclear power stations in the World.

On March 11th, 2011, at 14:46 a massive earthquake of 9.0 magnitude (the Tohoku earthquake) occurred at offshore of the pacific ocean and then ensuing tsunami had stuck off the northern coast of Honshu island [2] (named 東日本大震災- the Great East Japan Earthquake and Tsunami). Because of natural disasters, infrastructure systems, industrial facilities, residential houses along the coast of Fukushima, Miyagi prefectures were almost damaged and destroyed, and it affected to vast region of the north-east coast from Tochigi prefecture to Aomori prefecture. Collected data showed that human casualties included 14,508 dead and 11,452 missing people, and total damage costs were estimated to be between 16 and 25 trillion yen by the disaster [3].

The disasters also resulted in a losing a backup power system which was necessary for the cooling system of the FDNPP. The cooling system losing led to the fuel melting down, and then the hydrogen explosion happened to create a nuclear disaster considered as one of the largest scales of nuclear disaster on the world after the Three Mile Island (1979) and Chernobyl (1986) accidents. The accident had pushed nuclear power, and nuclear research facilities closing the

whole of Japan for several years to do re-estimation and set up new criteria for safety regulation. According to the data in early 2011, nuclear power contributed to around 30% in total of electricity in Japan [4], Closing nuclear power plant affected the electricity sector change in which the produced electricity from the fossil or oil fuel replaced the nuclear power. This replacement mediately thrust the Japanese economy to a crisis.

Together with the economic effects, the FDNPP accident brought about a severe consequence with the habitats and environment. There was a large amount of radioactive material released into the atmosphere and then deposited on the ground. The released radioactive materials caused a high radiation level surrounding the FDNPP and affected regions. Therefore, there were numbers of nearby towns such as Namie, Futaba, Okuma, Tomioka, Naraha towns had been evacuated to avoid the health effects of radiation. Moreover, The TEPCO had let out more than ten thousand tons of water with the high radiation level into the open ocean within three periods from April 1st to May 11th, 2011. The highest radioactivity in outflow water to the ocean was estimated to be 4.7 PBq (total radioactivity of ^{131}I, ^{134}Cs, and ^{137}Cs) of letting out on April 1st to 6th, 2011 [5].

The released radioactive materials included the short half-life radionuclides such as ^{132}I (2.33 hours), ^{132}Te (3.2 days), ^{129}Te, ^{129m}Te, ^{131}I (8.04 days), ^{136}Cs, and the long half-life radionuclides of ^{134}Cs and ^{137}Cs with 2.06 and 30.07 years, respectively. The short half-life radionuclides were decayed out after several months of the accident [6]; however, long half-life radionuclides exist in the environment for a long time after the accident. By the FDNPP, according to Nuclear and Industrial Safety Agency (NISA), the released radioactivities of ^{131}I, ^{132}Te, ^{134}Cs, and ^{137}Cs were estimated to be 160, 88, 18 and 15 PBq [7]. The radioactive materials mainly dispersed and deposited to large regions of Ibaraki Prefecture to Miyagi Prefecture and highly concentrated in the east region of Fukushima Prefecture [8] as shown in Fig. I-1.

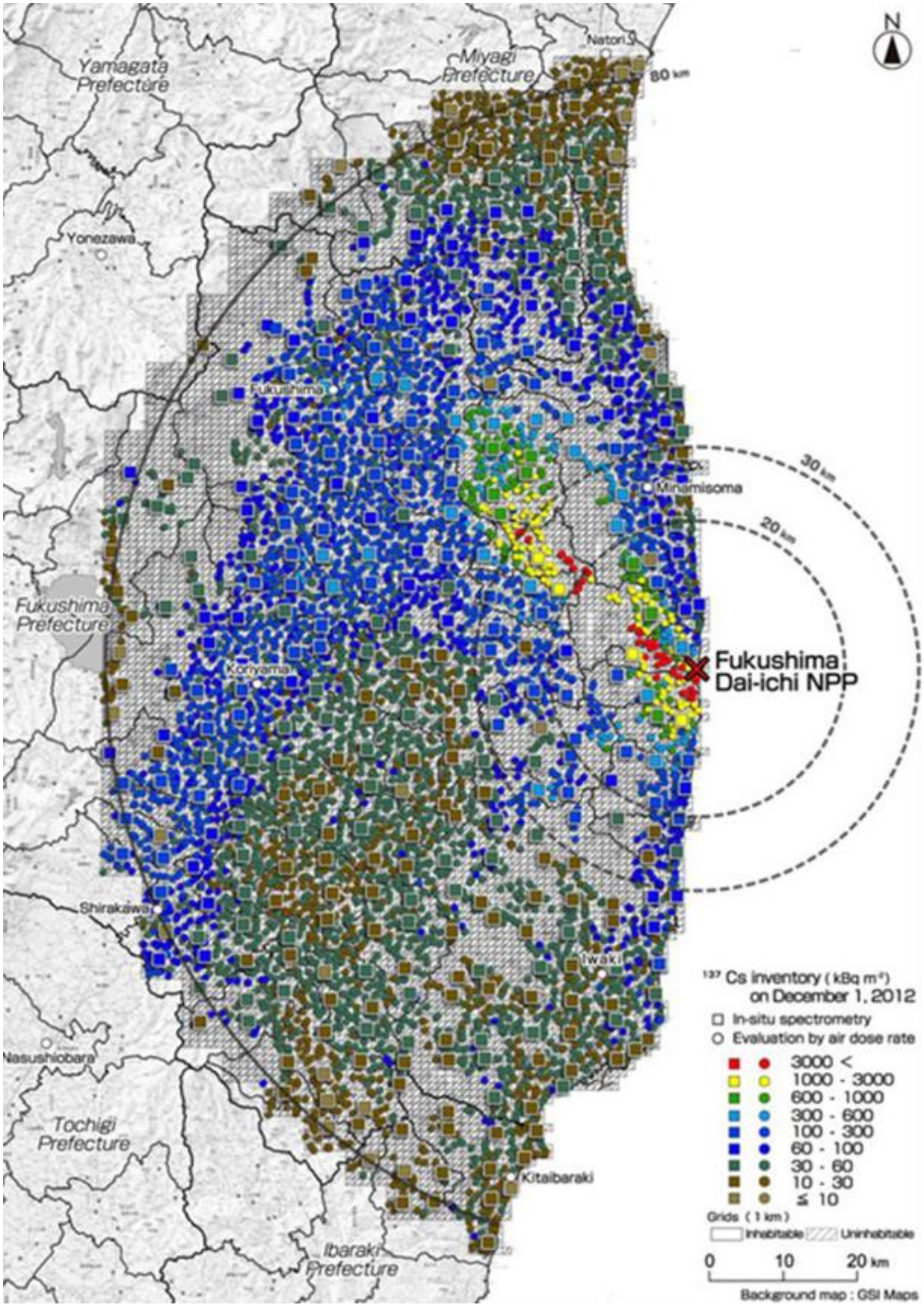

Fig. I-1: Distribution in/on the ground of radiocesium released from the FNPP accident [8]

1.2. Selection of location for research

Iitate village is a small village which is directly under Soma district and 25-45 km far from the FDNPP of northwest direction. Before the FDNPP accident occurring, the population of Iitate village was around 6,100 people [9] in 2010. The main works of people here were related to agriculture and raising cows within around 2,300 hectares of land [10]. After the nuclear accident in March 2011, because of the high radiation level, residents living in Iitate village were announced to evacuate to surrounding areas. Then, Iitate village was fixed boundaries of "Areas in which the residents are not permitted to live" and "Areas where it is expected that the residents have difficulties in returning for a long time" on July 17th, 2012 [11].

Early survey data of around 130 locations whole Iiate village shown that the radiation exposure rate at 1m height in the air was observed to be over 20 μSv/h in the southern part of the Iitate village in March 28-29th, 2011 [12]. The level of exposure rate at 1m height in the air changed the following time from 2011 to 2014 is shown in Fig. I-2. Fig. I-2 shown that in the early stage of the accident, because there was a contribution of both short half-life and long half-life radionuclides, therefore they made the radiation exposure rate to be quite high such as over 20 μSv/h. However, several months later, the short half-life had been decayed out, the radiation exposure rate reached a stable value.

Iitate village has a diversified flora with many vegetable plant types (fern plants, evergreen, edible wild plants so on) and wood plant types (pines, fir trees, cedars so on). After residents evacuated to other regions, the agricultural land was without any cultivation activity; therefore, these young trees invade a vast area of agricultural land use. Furthermore, at the Iitate village, some places in the northern region where had an exposure rate of less than 1 μSv/h which was quite low compared to the exposure rate in the air in the southern region (20 μSv/h). This condition allowed observing the impacts of radiation on baby plants more conveniently.

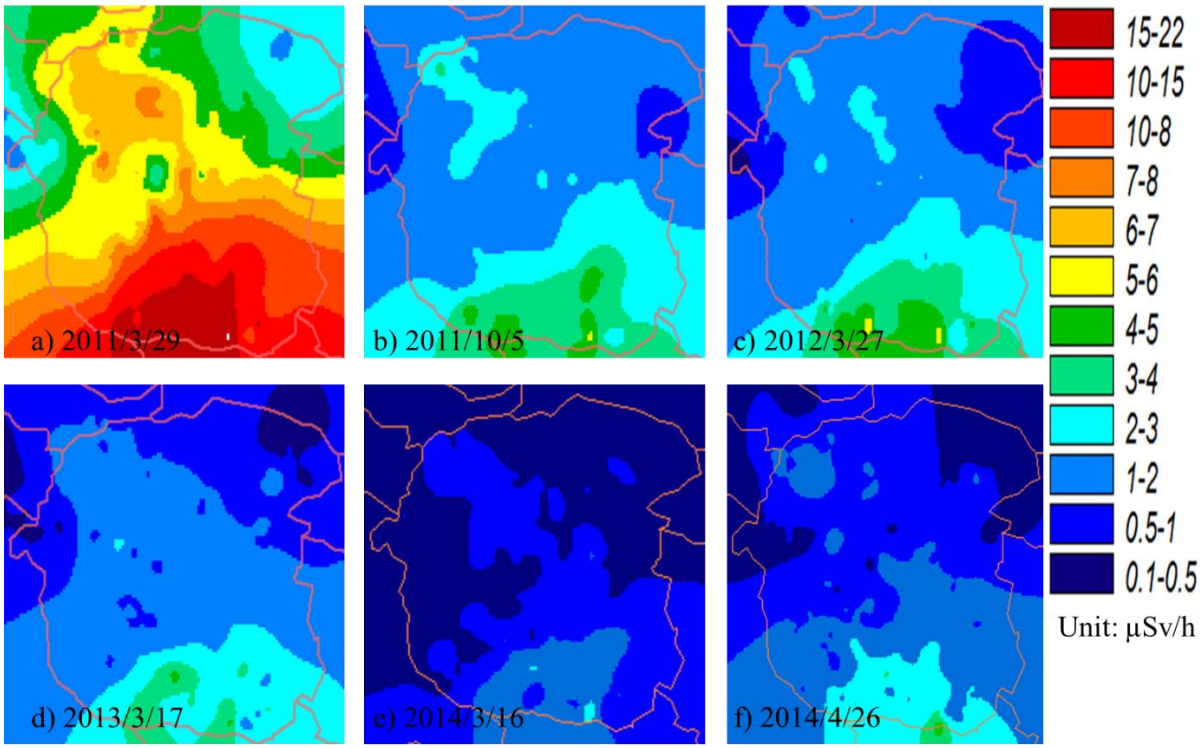

Fig. I-2: Change of exposure rate on time from 2011 – 2014 at Iitate village.

2. Environmental dynamics of radiocesium in the environment and purpose of this study

Because the short half-life radionuclides were decayed out after several months of the accident, the majority of the dose to environmental dose level derived by radiocesium in later years. The harmful effects of radiocesium on the human body have been investigated and reported by many researchers. Research results and surveys on the people living in highly contaminated regions after the Chernobyl accident indicated that radiocesium is highly concentrated in kidneys, myocardium, skeletal muscles, spleen, and lungs, testicle, and liver after they get in the human body. The internal exposure including exposure from β ray and γ ray of the radiocesium results in the function and metabolic activity disorders of these organizations [13]. Some death cases of people were noted with the radioactivity concentration of ^{137}Cs amounted to 192.8 Bq/kg with adults and 645.3 Bq/kg with children in kidneys [13]. The impact of ^{137}Cs on the human body shows that the protection of exposure to radiation, especially internal exposure, is crucial work.

On the other face of radiation impacts on the ecosystem, recently, researches on the effects of radiation on pines living in highly contaminated regions surrounding the Fukushima nuclear power plant showed that morphological effects of the pines are proportional to the exposure dose level of the ambient [14]. Besides, the impacts of radiation on the insects, birds, and animals have been pointed by the forewing size reduction, growth retardation, high mortality rates and high abnormality rate in the pale grass blue butterfly [15], the abundance reduction of birds [16], butterflies and cicadas [17], body weight and head size reduction of monkey babies [18].

To protect humans to radiation, and evaluate the impacts on the ecosystem, it is necessary to investigate the distribution and change in the environment of radiocesium following time. Some researchers have estimated the distribution of radiocesium in the soil in the post-accident period [19, 20]; however, an investigation on the change of the radiocesium for later years and

movement of them from soil to young trees growing on the contaminated soil is not made clear. Therefore, the environmental dynamic and transfer of radiocesium from a depth profile soil to young pines are chosen as a theme of the doctoral thesis to make clear for the migration process of radiocesium in the soil.

Ordinarily, for the radiocesium released from the Fukushima nuclear power plant, the movement directions are considered in two ways such as migration in the soil and dispersion in the aqua mediums. The thesis concentrates on the migration of radiocesium in the soil in which radiocesium was released from the FNPP and then deposited on the surface ground by wet/dry deposition process [21]. Radiocesium exists on the surface soil layer move to deeper layers under weather conditions that as rain, snow so on. Young trees grow up on the contaminated soil absorb radiocesium during the development period.

References

1. http://www2.jnes.go.jp/atom-db/en/general/atomic/ke02a13/info_f.html (accessed on 2018/09/24)

2. Ministry of Economy, Trade, and Industry, press release, October 20, 2011, http://www.meti.go.jp/press/2011/10/20111020001/20111020001/pdf

3. Nuclear Safety Commission of Japan. Press release, April 12, 2011. http://www.nsr.go.jp/archive/nsc/info/20110412.pdf (accessed on 2018/07/13)

4. http://www.world-nuclear.org/information-library/country-profiles/countries-g-n/japan-nuclear-power.aspx (accessed on 2018/09/24)

5. NERHQ. Report of Japanese government to the IAEA Ministerial Conference on nuclear safety – the accident at TEPCO's Fukushima nuclear power stations. 2011 http://www.kantei.go.jp/foreign/kan/topics/201106/iaea_houkokusho_e.html , released on 7 June 2011.

6. Finston H L and Berstein W. Decay scheme of ^{132}I. Phys. Rev. 1954. 96 (71)

7. NISA. Regarding the evaluation of the conditions on reactor cores of unit 1, 2 and 3 related to the accident at Fukushima Dai-ichi nuclear power station, Tokyo Electric Power Co. Inc. 2011 http://www.nisa.meti.go.jp/english/press/2011/06/en20110615-5.pdf , released on 6 June 2011.

8. S, Mikami, T. Maeyama, Y. Hoshide et al., 2015. Spatial distributions of radionuclides deposited onto ground soil around the Fukushima Dai-ichi Nuclear Power Plant and their temporal change until December 2012. Journal of Environmental Radioactivity. 139: 320-343.

9. Iitate village 2017 Information of Iitate village (http://vill.iitate.fukushima.jp/index.html)

10. NHK World-Japan news. Fukushima farmers struggle, https://www3.nhk.or.jp/nhkworld/en/news/editors/3/fukushimafarmersstruggle/index.html (accessed 2018.10.09)

11. Ministry of Economy, Trade and Industry 2012 Restricted areas and areas to which evacuation orders have been issued as of 30 November 2012 (www.meti.go.jp/english/earthquake/ nuclear/roadmap/pdf/20121130_01.pdf)

12. T. Imanaka, S. Endo, M. Sugai et al., 2012. Early radiation survey of Iitate village, which was heavily contaminated by the Fukushima Daiichi accident, conducted on 28 and 29 March 2011. Health Phys. 102(6): 680-686.

13. Bandazhevsky, Y. I., Medical and Biological Effects of Radiocesium incorporated into the Human. Organism （Institute of Radiation Safety "BELRAD", Minsk, 2000. ISBN 985-434-080-5.

14. Yoschenko Y, Nanba K, Yoshida S, Watanabe Y et al., 2016 Morphological abnormalities in Japanese red pine (Pinus densiflora) at the territories contaminated as a result of the accident at Fukushima Dai-Ichi Nuclear Power Plant. J. Environ. Radiact., 165:60-67

15. Taira W, Nohara C, Himaya A et al., 2014. Fukushima's Biological Impacts: The Case of the Pale Grass Blue Butterfly. Journal of Heredity, 105(5):710-722

16. Moller A P, Mousseau T A, Nishiumi I et al., 2015. Ecological differences in response of bird species to radioactivity from Chernobyl and Fukushima. J Ornithol, 156(1): S287-296

17. Moller A P, Nishiumi I, Suzuki H et al., 2013. Differences in effects of radiation on abundance of animals in Fukushima and Chernobyl. Ecological Indicators, 24:75-81

18. Hayama S, Tsuchiya M, Ochiai K et al., 2017. Small head size and delayed body weight growth in wild Japanese monkey fetuses after the Fukushima Daiichi nuclear disaster. Scientific Reports volume 7, Article number: 3528

19. Shiozawa, S., 2013. Agricultural implications of the Fukushima nuclear accident. In: Nakashima, T.M., Tanoi, K. (Eds.), Agricultural implications of the Fukushima Nuclear accident. Springer, Japan, Tokyo, pp. 49-60.

20. Takahashi, J., Tamura. K., Suda, T., *et al*., 2015. Vertical distribution and temporal changes of ^{137}Cs in soil profiles under various land uses after the Fukushima Dai-ichi Nuclear Power Plant accident. J. Environ. Radiact. 139, 351-361.

21. K. Tanaka, Y. Takahashi, A. Sakaguchi et al., 2012. Vertical profiles of Iodine-131 and Cesium-137 in soils in Fukushima Prefecture related to the Fukushima Daiichi Nuclear Power Station Accident. Geochemical Journal. 46: 73-76.

Chapter II. Soil sampling and measurement method

1. Soil core sampling method

Iitate village was severely affected by a tremendous amount of the radioactive materials released from the FDNPP accident, and the soil in this region was heavily contaminated [1]. Since 2011, our team has monitored the air dose rate and collected about 10 soil cores annually. For investigating the thesis, soil core samples at different locations such as paddy field, near the forest, farmland so on, have been collected at Iitate village from 2012-2017, as shown in Fig. II-1. The information of the samples is listed in Table II-1.

The sampler tool used in this research has a 5 cm diameter (DIK-110C, Daiki Rika Kogyo Co., Ltd). The sample consists of two tubes; the outer tube is made of stainless steel, and the inner tube is made of a 275 μm thickness of a polyvinyl chloride tube (PVC). The length of the sampler is enough to collect 30 cm of soil core and is illustrated as in Fig. II-2. The 5 cm diameter and 30 cm length of soil cores were fitted with the lid and tape to avoid soil falling outside. Then, the soil cores were put into cardboard inserted with cushion, and transfer to Lab for further treatment and measurement.

To propose a method for determining the depth profile of soil cores with the millimeter depth-bin width (Chapter III), soil cores of 4 locations are chosen with the different imaging plate (IP) intensity profiles. The IP intensity profiles of these locations are described as broad distribution (Nagadoro Jumonji 2013 – No.2-2013), narrow distribution (Nagadoro paddy – No.1-2013), two peaks distribution (Nagadoro Jumonji 2015 – No.2-2015), and center distribution (Komiya Magata-No.x-2013) of radiocesium from the soil surface. The soil types in these cores in the 4 sampling locations are referred from NIAES (2001) [2]. These depth profiles are shown in detail in Subsection 3.1 (Chapter III) - information of samples and the air dose rate is listed in Table II-2.

To estimate the migration velocity and diffusion coefficient, it is necessary to collect data of at least 1 depth profile with a less than centimeter scale of depth-bin width and a depth profile by gamma measurement of different years at the same location. Because decontamination works at Iitate village were deployed quickly; therefore, the samples at locations of Notegami paddy field, Notegami dam, Maeda Hasegawa, Usushi, Komiya Naka Nohara, Fukuya Ichiwa, Murakami house, and Murakami Komeri were not collected second times. The samples at Iitate farm were collected at different locations and decontaminated before sampling. Although there were some samples collected at different locations of Nagadoro Jumonji (2017) and Yamatsumi Shrine (2016, 2017) collected, they were enough for using the fitting function.

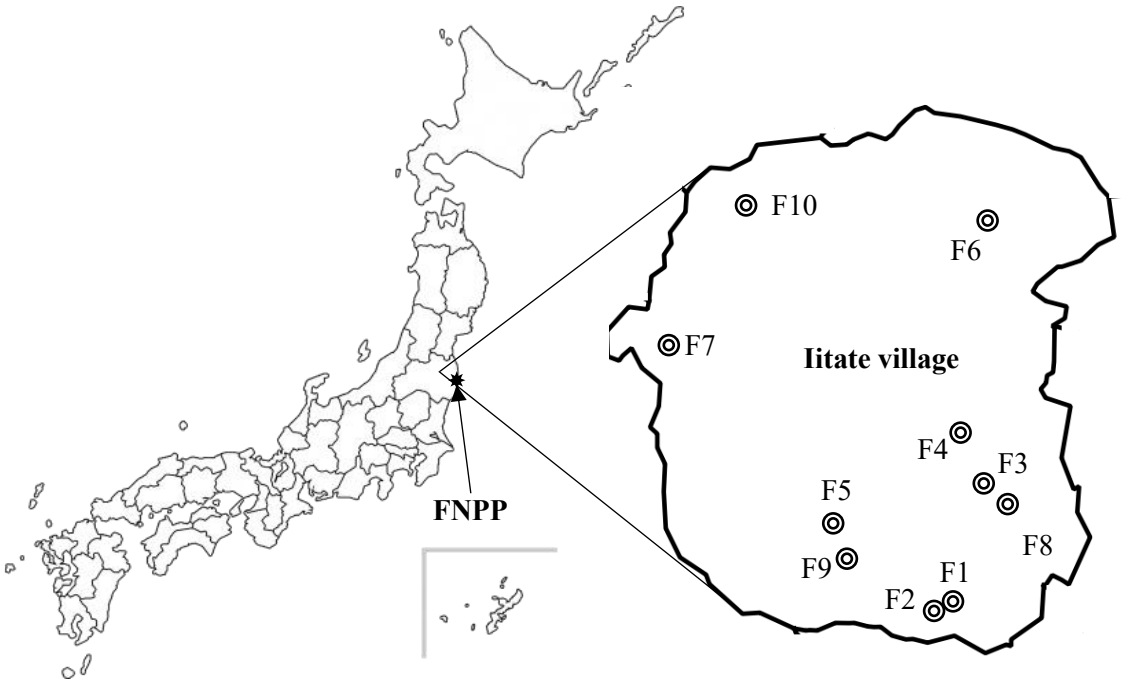

Fig. II-1: Sampling location

Table II- 1: Number of samples collected by years

No	Sampling location	Period	Total core	Without Unfold	Unfold
1	Nagadoro rice field	2012-2017	6	0	6
2	Nagadoro Jumonji[a] (2017)	2012-2015	4	1	3
3	Yamatsumi Shrine[a] (2016,2017)	2012-2017	6	2	4
4	Ochiai Komiya	2012-2015	4	1	3
5	Iitate village office	2012-2017	6	3	3
6	Warabi daida	2016, 2017	2	0	2
7	Nagadoro gate	2014, 2016, 2017	2	1	2
8	Nagadoro Magata (Flower)	2012-2014	3	2	1
9	Iitate farm[a]	2012-2016	4	1	3
10	Near Iitate farm	2016	1	0	1

[a]: samples collected at different locations or decontaminated locations

Fig. II-2: Soil core sampling method – (a): Sampler - (DIK-110C, Daiki Rika Kogyo Co., Ltd).; (b): 30 cm soil core

Table II-2: Information of samples and air dose rate at the height of 1 m from the ground used in Chapter III

Location	GPS		Dose rate
	Latitude	Longitude	(μSv/h)
No.2-2013	37.61281	140.7494	5.6
No.1-2013	37.6620	140.7746	0.8
No.x-2013	37.60396	140.7779	9.5
No. 2-2015	37.61281	140.7494	4.1

2. Young tree sampling method

I collected young trees (pine and fir trees) samples, which were grown on the contaminated ground at Iiitate village after FNPP accident occurred (age around 1-2 years) as shown in Fig. II-1. Young trees were collected at 10 locations in the Iitate village in March 2015, 2016 and 2017. The whole-body of the young tree was collected not to damage the root. The sampled trees were washed, wrapped by a wiper paper, and packed into a clear vinyl bag. At each location, a 30cm soil core (30 cm deep, 5 cm in diameter) was collected together with young tree samples by a soil sampler. The air dose rate at the time of sampling was measured by a survey meter (PDR-101, Hitachi Aloka Medical LTD). Information on soil and air dose rate at the sampling locations are listed in Table II-3. The age of young trees was estimated based on the number of branches as no-branch for 1 year; 2 branches for 2 years. Young tree samples are used for the calculation of the transfer coefficient in Chapter V.

Table. II-3: Air dose rate, Inventory of collected soil core, and information of collected young trees (samples collected at a little far away, not at same position year by year)

Location	Air dose rate (μSv/h)			Collected trees			Note
	2015	2016	2017	2015	2016	2017	
Warabidaida (F1)	-	1.25	2.0	-	2 trees; Age 1 y	1 tree; Age 1 y	Forest hill, soil with poor humus
Nagadoro rice field (F2)	6.1	4.24	4.2	2 trees; Age 2 y	2 trees; Age 2 y	1 tree; Age 1 y	Paddy field, soil with rich humus on surface
Iitate farm (F3)	2.1	-	0.8	1 tree; Age 1 y	-	1 tree; Age 1 y	Paddy field edge, black soil
Near Iitate farm 1 (F4)	-	1.2	1.6	-	2 trees; Age 1 y	1 tree; Age 1 y	
Nagadoro gate (F5)	-	2.21	2.5	-	1 tree; Age 2 y	1 tree; Age 1 y	Forest hill, soil with poor humus
Manodam (F6)	-	0.43	-	-	2 trees[a]; Age 2 y	-	Roadside, soil with poor humus
Nimabashi (F7)	-	0.43	-	-	1 tree; Age 1 y	-	Forest hill, soil with poor humus
Near Iitate farm 2 (F8)	-	1.17	-	-	1 tree; Age 2 y	-	Paddy field, soil with rich humus on surface
Nagadoro Jumonji (F9)	-	-	2.76	-	-	1 tree[a]; Age 2 y	Forest hill, soil with rich humus to deep soil
Yamatsumi (F10)	2.1	-	1	2 trees; Age 2 y	-	1 tree[a]; Age 1 y	Forest hill, soil with rich humus on surface

[a]: Collected sample included young pine and young fir tree;

y: is represented for the year of plant. Year of young pine was determined based on the number of branches on tree (no-branch:0-1 year; 2 branches: 1-2 years)

3. Measurement of IP profiles

In principle, the measurement method of imaging plate based on Photo-stimulated Luminescence (PSL) phenomenon, in which after absorbing radiation energy photo-stimulated phosphor crystals inside the sensitive layer of IP film emits the luminescence excited by heat or laser beams [3]. The procedure of photo-stimulated Luminescence is described by image as in Fig. II-3. Based on this physical phenomenon, IP film has been produced since 1980 and used for medical diagnose. Nowadays, The IP film with different sizes manufactured by Fuji film Co., Ltd.

The outside of polyvinyl chloride tubes enclosing the soil cores is cleaned and covered with a skinny layer of plastic wrap to avoid contamination to the film. Then, IP film (BAS-IP MS 2040, size: 20 × 40 cm) were used to wind around the soil cores. The wrapped soil cores are pushed into a lead chamber around 24 hours for radiation exposure. Two-Dimension (2D) images were obtained by the Typhoon FLA 7000 reader (GE Healthcare Life Science Co.) of Hiroshima University. The average IP profile corresponding to a depth of soil core is extracted with 0.5 mm steps (0 to 30 cm corresponding to 600 steps) from the 2D imaging by an Image Quant TL software (GE Healthcare Life Science Co.). The IP and reader equipment are shown in Fig. II-4, II-5. The IP profiles are applied for further investigations in Chapter III.

The young tree samples (including root part) are soaked in water with radio-isotope soap for 24 hours. After, the soil stuck on the tree is washed off with fresh water. The samples are put in a room for draining, and then, they are set on the IP film and fixed by a case. These samples are put in the lead chamber for around two weeks for exposure. The 2D images of these samples use to observe the distribution of radiocesium in samples.

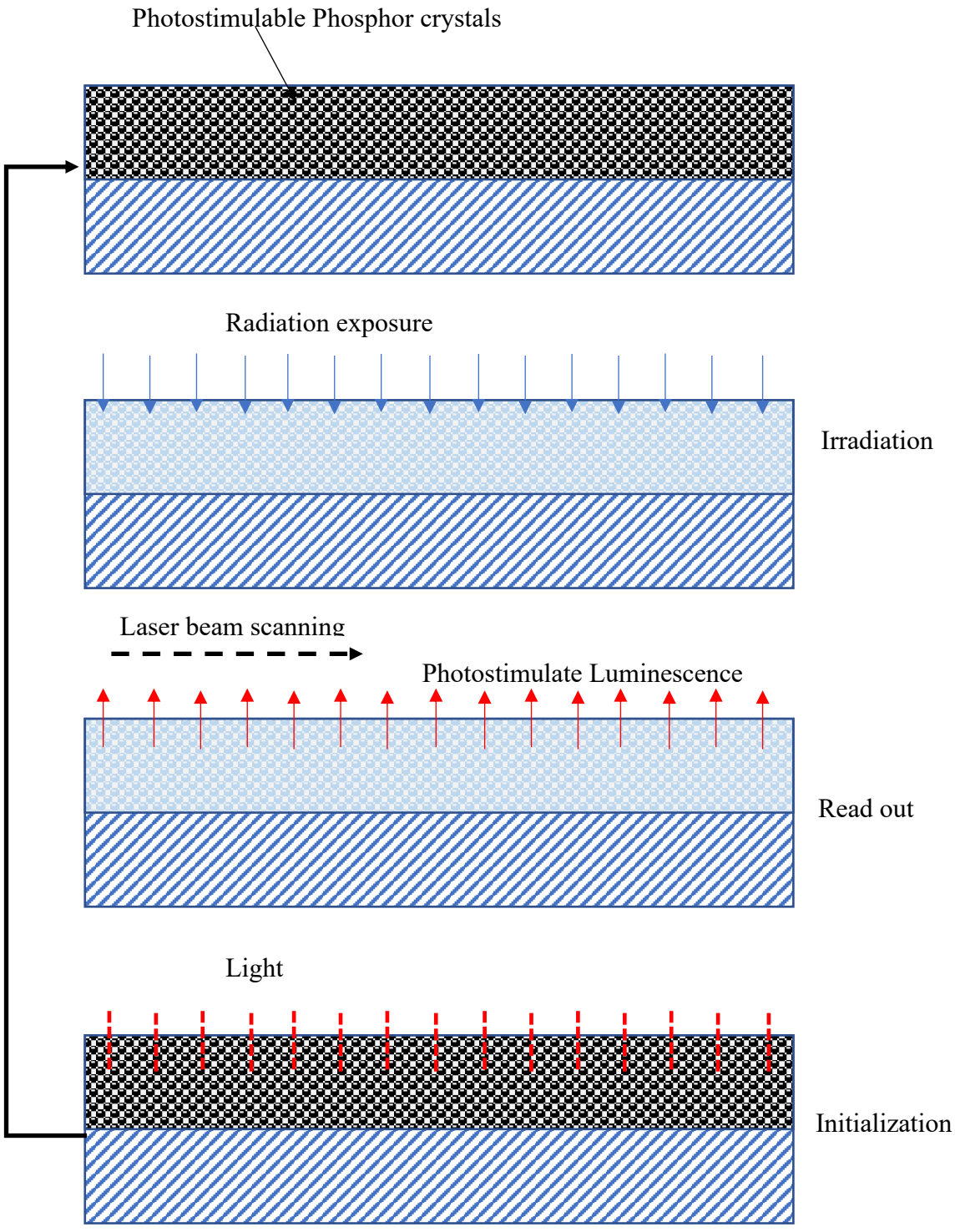

Fig. II-3: Photo-stimulated Luminescence procedure

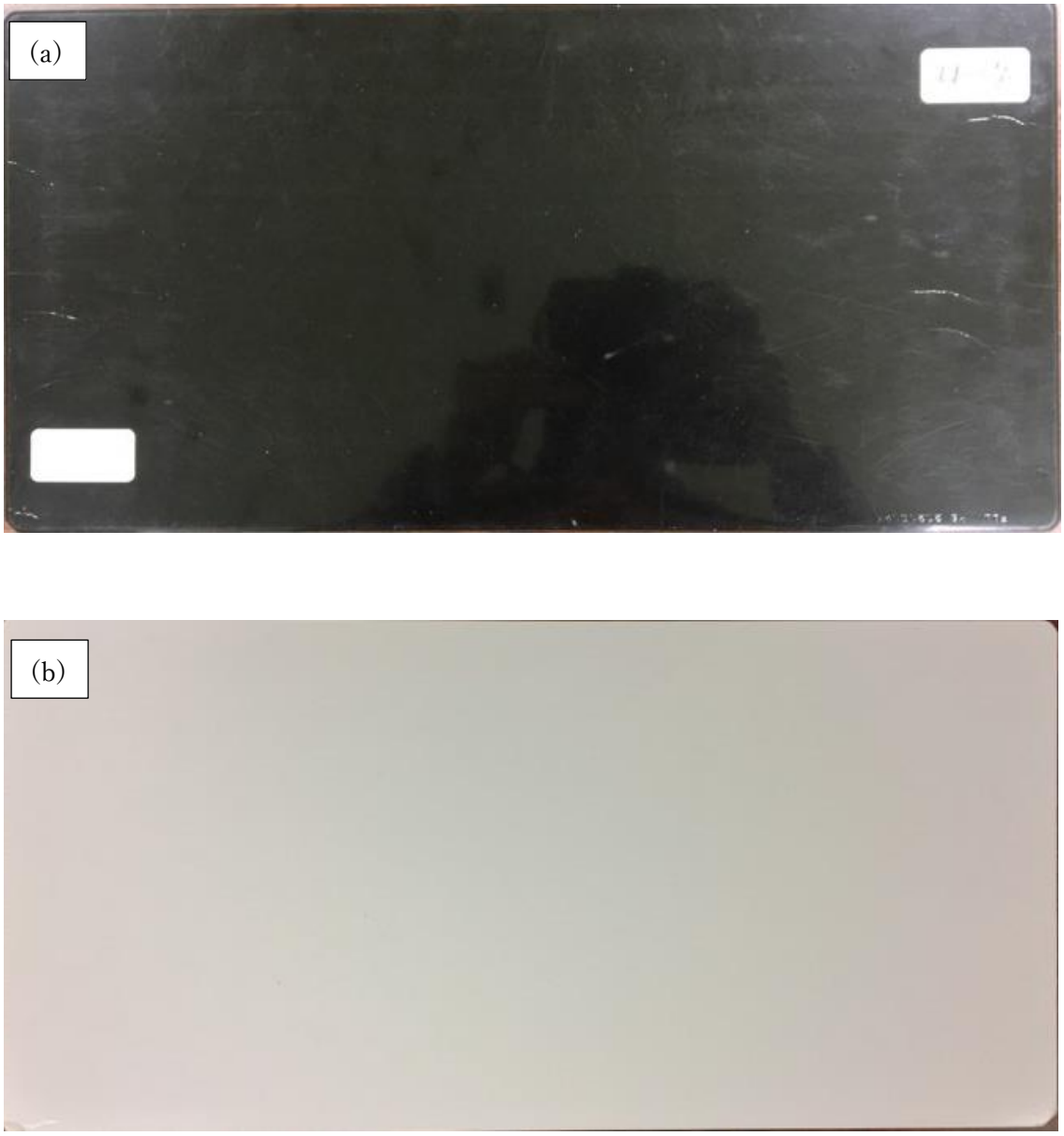

Fig. II-4: Imaging plate (a) backside (b) front side

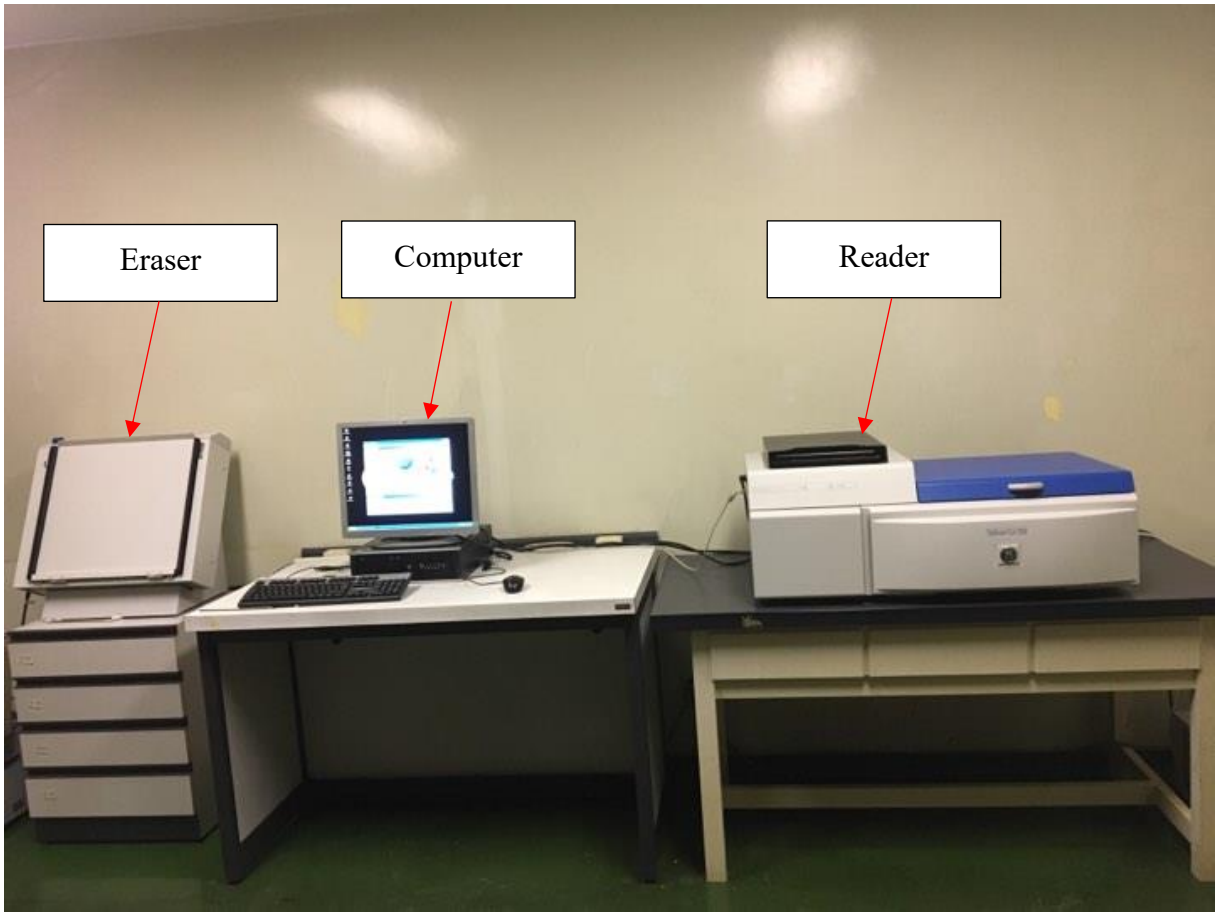

Fig. II-5: Typhoon FLA 7000 measurement system

4. Gamma measurement of collected soil cores by a COAX type detector

The soil cores were separated into thin layers from the surface to a depth of 30 cm: from the soil surface to 5 cm soil layer is divided to 2 layers (2.5 cm thickness of each layer) and remaining part of 5-30 cm is cut to 5 layers (5 cm thickness of each layer). These soil layers were desiccated at around 100 °C for one day in an oven, then grind to small soil particles to make them pass a mesh (2 mm size) and remove stone and roots. The samples obtained from treating soil layers were filled into a U-9 container and acquired the gamma spectra by a low-background Ge detector (GMX-30200-P, ORTEC) as in Fig. II-6. The samples were measured for 20000 seconds with 2 samples of surface layer soil and for 80000 seconds with samples in deep soil layers. The detection efficiencies of the Ge detector with the energy of γ-ray peaks in the emission energy range of ^{134}Cs, ^{137}Cs, and ^{40}K were calculated based on fitting the detection efficiency curve of γ rays energy emitted from ^{109}Cd, ^{57}Co, ^{139}Ce, ^{51}Cr, ^{85}Sr, ^{137}Cs, ^{54}Mn, ^{88}Y, and ^{60}Co in standard volume sources (MX-033, Japan Isotope Association). The detection efficiency of the Ge detector was calculated with a statistical error and a systematic uncertainty of less than 1%, 5%, respectively [4]. The cascade summing effect at 605 keV for ^{134}Cs was estimated to be 1.15 [5].

5. Gamma measurement of ^{40}K in young trees by the COAX and Well-type detectors

The young trees after the IP measurement were naturally dried up for two weeks in room temperature conditions. Dried samples were cut into the tree and root parts. The tree parts were minced small pieces and filled in a U-9 container for gamma-ray measurement by the COAX. The tree samples were measured for 80000-160000 seconds. Detection efficiency of the COAX detector for gamma-ray peaks of 605, 662, and 1461 keV emitted from ^{134}Cs, ^{137}Cs, and ^{40}K, respectively, are referred to in **Section 4** above.

The roots were put on a clean paper and their shape was made as grown in soil, and then they were cut into 4 segments as distributed in soil layers of 2.5, 2.5, 5 and 5 cm from the surface. Each root segment was also minced to small pieces and fill into a polyethylene tube for gamma-ray measurement by a Well-type Ge detector (GWL 120230-S, Seiko EG&G). Each root sample was measured for around 160000- 250000 seconds.

For determining the detection efficiency of the Well-type Ge detector with gamma-ray peaks of 605, 795, and 662 keV, the radioactively contaminated soil collected at Iitate village, Fukushima prefecture in August 2013 was used as a standard source with radioactivity of ^{137}Cs and ^{134}Cs determined by the COAX. Detection efficiency of 1461 keV emitted from ^{40}K of the Well-type Ge detector was determined using a ^{40}K source included in NaCl and KCl mixed salt (NaCl:KCl = 50:50 of weight percent). Detection efficiency as a function of the sample height in the polyethylene tube was obtained from fitting the detection efficiencies of different heights. The uncertainty was estimated to be less than 5%.

Fig. II-6: Gamma measurement system (COAX) in Hiroshima University

References

1. Imanaka, T., Endo, S., Sugai, M., *et al*., 2012. Early Radiation Survey of Iitate Village, Which Was Heavily Contaminated by the Fukushima Daiichi Accident, Conducted on 28 and 29 March 2011. Health physics 102 (6), 680-686.

2. National Institute for Agro-Environmental Sciences (NIAES), 2001. Soil map, http://agrimesh.dc.affrc.go.jp/soil_db/ (accessed 07.03.17)

3. http://home.fujifilm.com/products/science/ip/principle.html (accessed in 2019.01.07)

4. Endo, S., Kajimoto, T., Shizuma, K., 2013. Paddy-field contamination with ^{134}Cs and ^{137}Cs due to Fukushima Dai-ichi Nuclear Power Plant accident and soil-to-rice transfer coefficients. J. Environ. Radiact.116, 59-64.

5. Kajimoto. T., Endo. S., Nguyen. T. T., Shizuma. K. Calculation of coincidence summing in gamma-ray spectrometry with the EGS5 code. Applied Radiation and Isotopes 95, 53-58

Chapter III. Determination of ^{137}Cs depth profile soil

1. Introduction

Because of the FDNPP disaster, a tremendous number of radioactive materials were released to the environment [1]. Radiocesium deposits and exists on the soil, they possibly result in harmfulness to people via inhaling (internal exposure) and animals living in that contaminated region. To estimate the air dose, solving amount to underground water and root uptake by the plant, the depth profile of radiocesium in the soil is necessary. Based on this information, it needs to make clear the movement characteristics and the change of radiocesium in the soil. The movement of radiocesium in the soil is described by the migration velocity and diffusion coefficient indexes. These indexes are derived by fitting the radiocesium depth profile [2-5]. Generally, the depth profile is often obtained by measurement of radioactivity in the separated soil layers form a soil core. The depth profile obtained by this method is available for estimating the vertical movement of radiocesium in medium with centimeter per year of migration velocity.

For uncultivated upland field soil contaminated by the FDNPP accident, the migration velocities of radiocesium were 4–7 mm per month during the first 3–4 months after the accident, and 0.4–1.4 mm/y 1 year after the accident, and they would decrease with time [6]. Besides, other estimation results of the relaxation depth of radiocesium (mean migration depth) for different types of land in contaminated areas of Fukushima Prefecture show that migration velocity was small 4 to 21 months after the accident. The reported migration velocities of 1.6 mm/y in meadowland, 3.7 mm/y in farmland, 1.2 mm/y in tobacco fields, and 10.1 mm/y in paddy fields [7]. By the previously reported results, it suggested that it is difficult to obtain the migration velocity and diffusion coefficient by fitting depth profiles with the depth-bin width of the centimeter scale. It is challenging to cut thinner layers from soil cores to get millimeter depth-bin width by the common technique.

In this chapter, I develop a method to solve the problem meet on the depth profile by the common technique. The method uses an IP film and the unfolding technique and is conducted by unfolding the IP profile obtained from 2D images of IP film with a response matrix of the deposited energy emitted from point sources (^{134}Cs, ^{137}Cs, and ^{40}K) in a soil core. The method is verified with the samples described in chapter II. The unfolding results are compared with those measured by the gamma measurement method. The confidence of this method is also confirmed by the reproduced depth profiles (^{134}Cs, ^{137}Cs, and ^{40}K) by unfolding analysis comparing with those by the assumption.

2. Material and method

2.1. Calculation of response function by PHITS

The response function depends on the energy deposition in the IP sensitive layer and the depth from thin radionuclide sources at a specific depth, and it was calculated with PHITS code [8]. The PHITS calculation for the deposition energy on the sensitive layer from a radionuclide is separately conducted with the energy deposition of γ rays and β rays emitted from that radionuclide. Particularly, in this chapter, the radionuclides of ^{134}Cs, ^{137}Cs, and ^{40}K, which are mainly contented in the soil, are chosen. The geometry for the calculation is shown in Fig. III-1. A soil core having a dimension of Φ5.0 cm diameter and a 30.0 cm length is contained by a 275 μm thickness of polyvinyl chloride tube (PVC), as shown in Fig. II-2 (b) of Chapter II. This soil core is wrapped by an IP film which is assembled from 5 layers of a 190 μm thickness of PET layer, a 115 μm thickness of the sensitive layer ($BaFBr_{0.85}I_{0.15}$:Eu), a 12 μm thickness of a back layer, and a 160 μm thickness of iron oxide layer [9]. The chemical compositions of soil were referred from the literature [10]. Because the soil density of soil cores collected at Iitate village has a range from 0.6 to 0.9 g/cm^3; therefore, it was chosen with a value of 0.7 g/cm^3 for the calculation. The PHITS calculation for deposition energy on the sensitive layer of the IP was done at every 1 mm depth step.

The data of γ ray, including energies and their emission rates for ^{134}Cs, ^{137}Cs, and ^{40}K, were referred from the National Nuclear Data Center [11]. The β ray energy spectra of ^{134}Cs, ^{137}Cs, and ^{40}K were calculated and plotted as in Fig. III-2. The calculated β ray energy, emission rate, and the internal conversion electrons [11] are shown in Fig. III-2. The referred parameters for ^{134}Cs, ^{137}Cs, and ^{40}K are shown in Table III-1. One case of the energy deposition profile results for these radionuclides with the sources setting at a depth of 15 cm is shown in Fig. III-3. Because the β ray has a weak penetration compared with the β ray, in the obtained profiles of

the radionuclides (^{134}Cs, ^{137}Cs, and ^{40}K), the sharp peak regions are mainly contributed from β rays; on the contrary, the tail regions are mainly contributed from γ rays.

In an IP profile, which consists of the ratio of β and γ rays energy deposition emitting from the radionuclides on the sensitive layer (response function). The response function of a radionuclide is the sum of the calculated results of β and γ rays combining with their emission rate emitted from that own radionuclide. Because the ratio of ^{137}Cs and ^{134}Cs released from the Fukushima nuclear power plant accident was almost 1, therefore the response function of radiocesium was calculated based on their ratio on the IP measurement date. By this method, it is the sum of the response function of ^{137}Cs, and ^{134}Cs multiplied by the ratio of the radioactivity concentration of ^{134}Cs to ^{137}Cs on the IP measurement date, f_d. The f_d is the activity ratio of ^{134}Cs to ^{137}Cs by the gamma measurement method. The response matrix, R^k_{ij} (k = radiocesium or ^{40}K), for further unfolding analysis is a set of the energy deposition profile at different depth in the IP sensitive layer from thin radionuclide sources of ^{134}Cs, ^{137}Cs, and ^{40}K at a depth of soil core as follow:

$$\begin{aligned} R_{ij}^{radio-Cs} &= f_d[2.23E_\gamma^{Cs-134}(d_i;z_j)+E_\beta^{Cs-134}(d_i;z_j)]+[0.85E_\gamma^{Cs-137}(d_i;z_j)+E_\beta^{Cs-137}(d_i;z_j)] \\ R_{ij}^{K-40} &= 0.11E_\gamma^{K-40}(d_i;z_j)+0.89E_\beta^{K-40}(d_i;z_j) \end{aligned} \quad (1)$$

where, $E(d_i;z_j)$ is energy deposition profile; d_i is i-th depth from thin radionuclides sources of ^{134}Cs, ^{137}Cs, and ^{40}K; z_j is j-th depth of soil core.

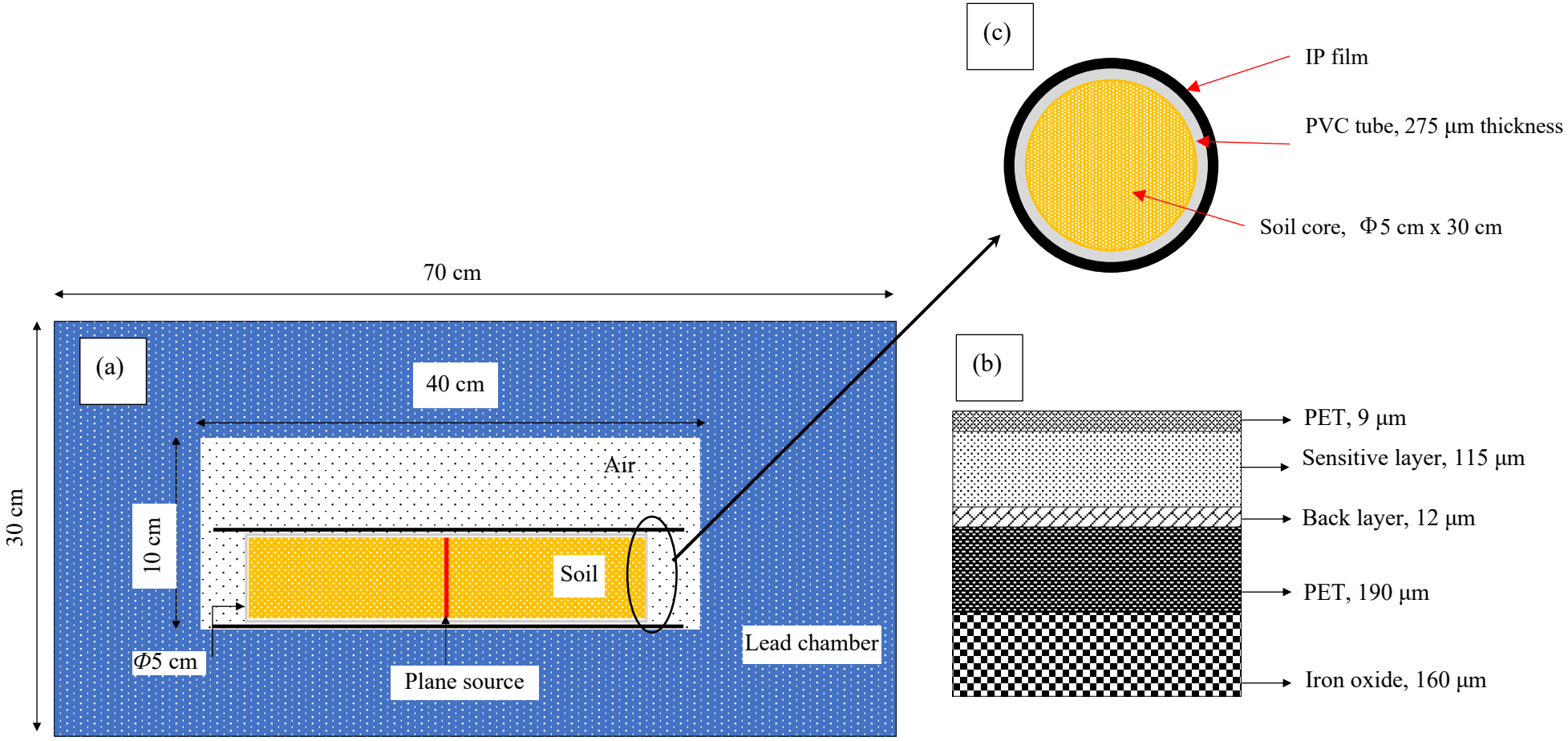

Fig. III-1: PHITS calculation geometry; (a): Set up of soil core in the lead chamber; (b): design of an imaging plate (IP) film; (c): Cross-section of the soil core wrapped by an IP film

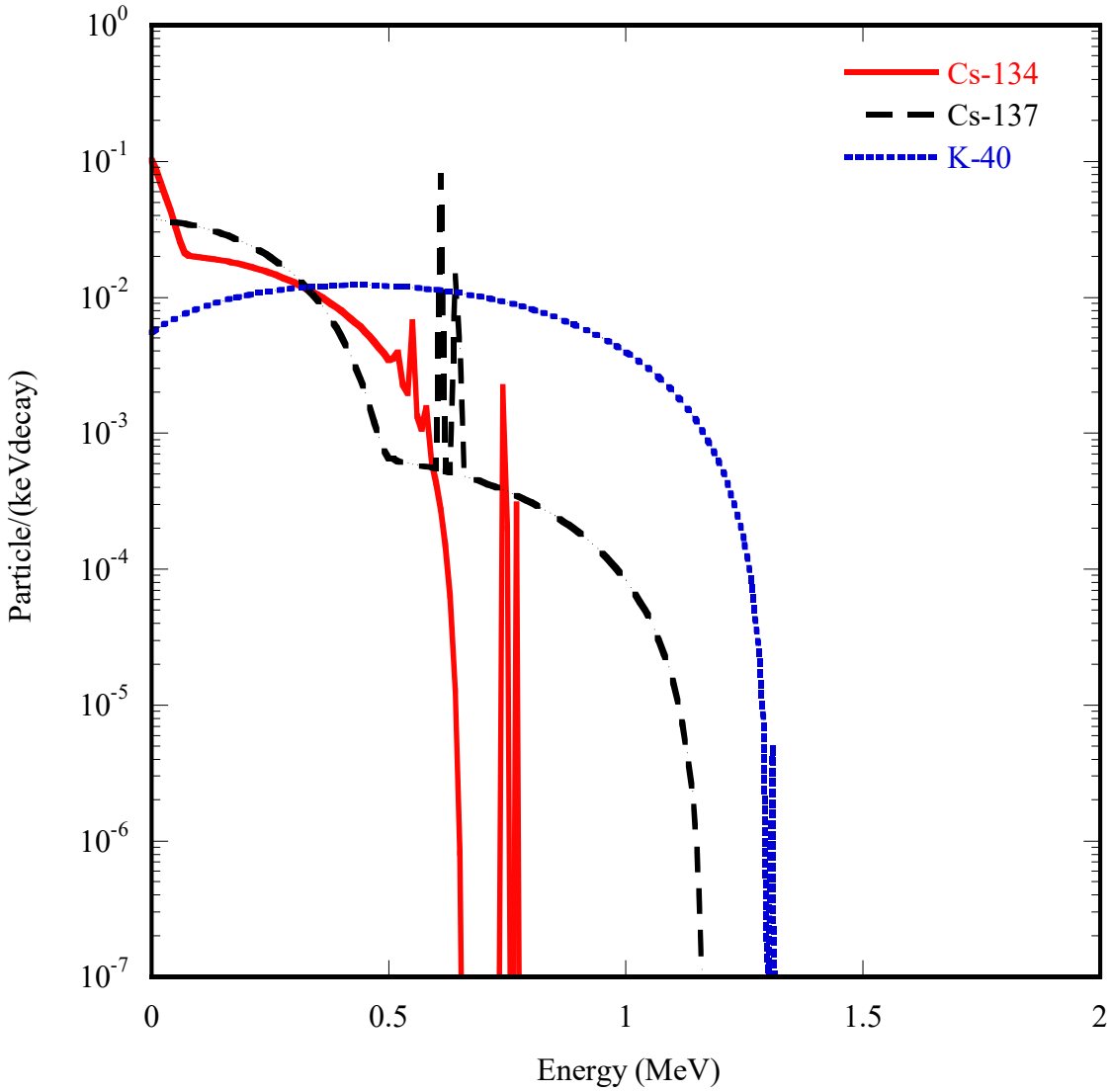

Fig. III-2: β ray source term for ^{134}Cs (solid red curve), ^{137}Cs (dashed black curve), and ^{40}K (dashed blue curve)

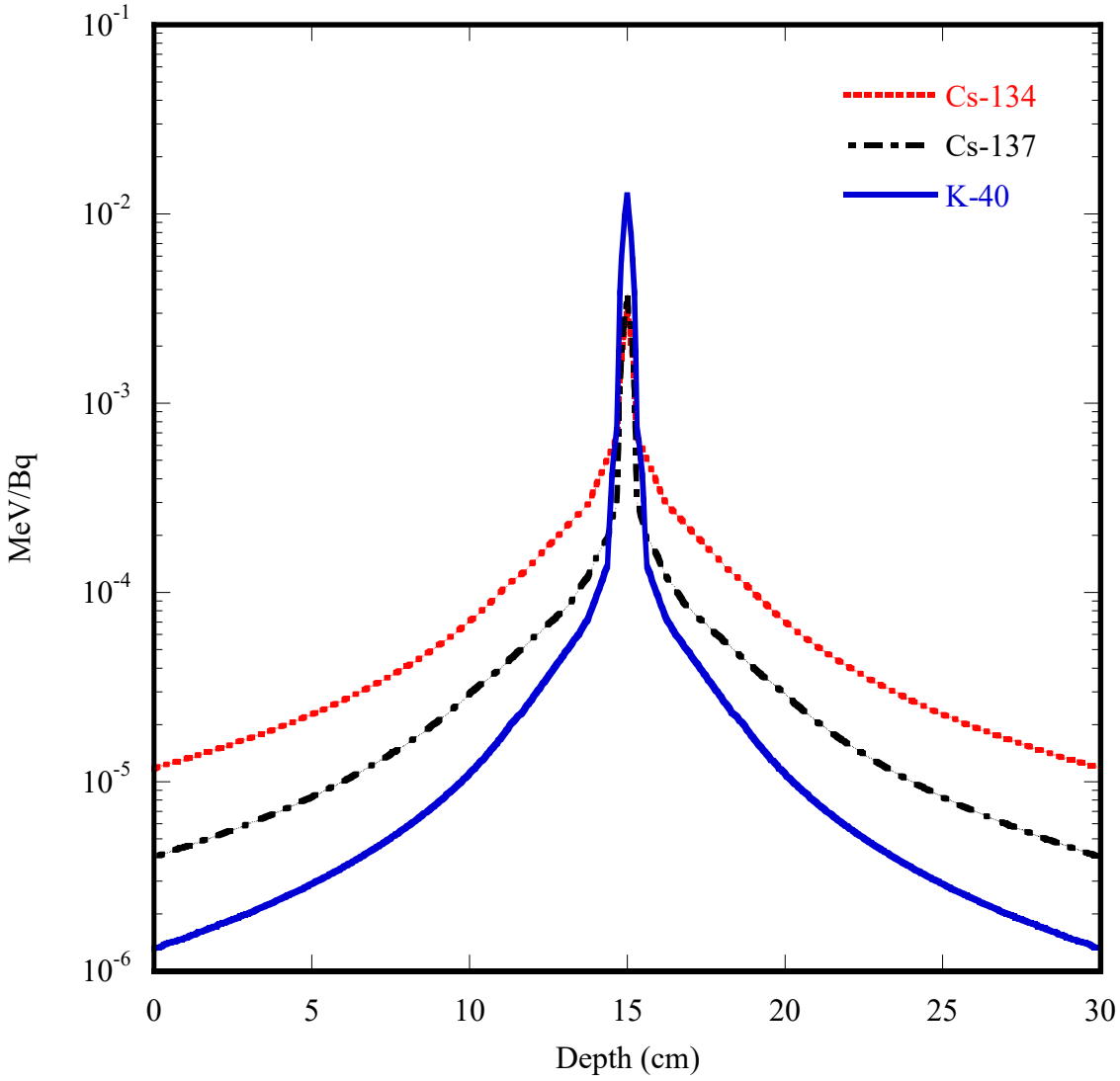

Fig. III-3: One case of the response functions of ^{134}Cs (dashed red curve), ^{137}Cs (dashed black curve), and ^{40}K (solid blue curve) with sources at 15 cm.

Table III-1: β ray endpoint energies, γ ray energies, internal conversion electron (IC) energies, and emission rates for ^{134}Cs, ^{137}Cs, and ^{40}K (NNDC, 2006) [11]

Radionuclide	β ray		γ ray		IC	
	Endpoint energy (keV)	Emission rate (%)	Energy (keV)	Emission rate (%)	Energy (keV)	Emission rate (%)
^{134}Cs	88.8	27.3	475.4	1.5	525.8	0.05
	415.4	2.5	563.3	8.3	531.9	0.13
	658	70.2	569.3	15.4	563.3	0.02
	-	-	604.7	97.6	567.28	0.49
	-	-	795.9	85.5	598.7	0.07
	-	-	802	8.7	758.4	0.22
	-	-	1038.6	1.0	764.5	0.02
	-	-	1168	1.8	789.9	0.03
	-	-	1365.2	3.0	-	-
^{137}Cs	514	94.7	661.7	85.1	661.6	0.01
	892.1	5.8×10^{-4}	-	-	661.4	0.06
	1175.6	5.3	-	-	660.4	0.3
	-	-	-	-	655.7	1.4
	-	-	-	-	624.2	7.79
^{40}K	1311.1	89.1	1460.8	10.7	-	-

2.2. Unfolding technique

A measured IP intensity at a particular point on the IP profile obtained from a 2D image is not only contributed from the radioactive sources existed in the same position of soil core, but is also smeared by those distributed along with the length of soil core. Therefore, the unfolding technique is carried out to separate the real IP intensity at a particular point from the smeared IP intensity.

The IP intensity, I_i [pxl] at a depth of d_i (i = 0 to 600, 0 to 30 cm, 0.5 mm steps) is represented by response matrix R^k_{ij} [MeV/Bq] and radioactivity A_j [Bq] at source position z_j, exposure time, t, and pixel intensity η [pxl/MeV] as

$$I_i^k = t\eta \sum_j R_{ij}^k A_j^k, \qquad (k = \text{radiocesium or } {}^{40}\text{K}) \tag{2}$$

The parameter $t\eta A_j^k$, is proportional to A_j^k when t and η are considered as constant, therefore, the radioactivity A_j^k can be rewritten with A_j^k as

$$I_i^k = \sum_j R_{ij}^k A_j^k. \tag{2'}$$

The unfolding technique in this investigation is performed as finding the inverse matrix of the response function. The value of radioactivity output of radiocesium and ^{40}K in soil cores is multiplication of the IP intensity by the inverse response function. Hence, the Bayesian unfolding technique with the iterative algorithm is applied for further calculation [12].

By the Bayesian unfolding technique, the reduced chi-square ($\chi_v{}^2$) is used for determining the number of iterations. The reduced chi-square is expressed as in Eq. (3). For my calculation, the reduced chi-square values in a range from 1.48 to 1.95 are suitable for the reproduction of the depth profile. With this condition, seven iterations were chosen to use in this method. The iterations change following the reduced chi-square for the four types of profiles are shown in Fig. III-4.

$$\chi_v^2 = \frac{1}{300}\sum_k \sum_j \left(\frac{I_j^k - \sum_i R_{ij}^k A_i^k}{\sigma_j} \right)^2 , \quad (3)$$

where σ_j calculated by the standard deviation of the IP intensity at depth d_j.

Radiocesium and natural ^{40}K are the main components that contribute to the IP profiles of the soil core. By the gamma measurement results, the distribution of ^{40}K is quite homogeneous from the soil surface to deep layers. Hence, for unfolding analysis, the IP profile of ^{40}K was considered as a constant from 0 – 30 cm of soil core. In the plateau of the IP intensity, the ^{40}K dominantly contributes to the IP profile of the soil core. Therefore, it was assumed to be an average of the IP profile in the dominant region of ^{40}K multiplied by the radioactivity ratio of ^{40}K to radiocesium + ^{40}K by gamma measurement in that region. The IP intensity profile of radiocesium was obtained based on subtracting the IP profile of the soil core and the IP profile of ^{40}K. The calculated IP profile of radiocesium and ^{40}K are used for the separate unfoldings to find the depth profiles of them combining to response matrices.

Because the depth profile obtained by the unfolding technique has the relative values, the unfolded depth profile of $A_i^{Radio-Cs}$ (or A_i^{K-40}) is converted to the Bq/kg unit of radioactivity by a conversion factor. The conversion factor is the ratio of the average value by unfolding analysis to that by the gamma measurement within 10 cm from the surface of the soil for radiocesium and 20-30 cm in the plateau for ^{40}K.

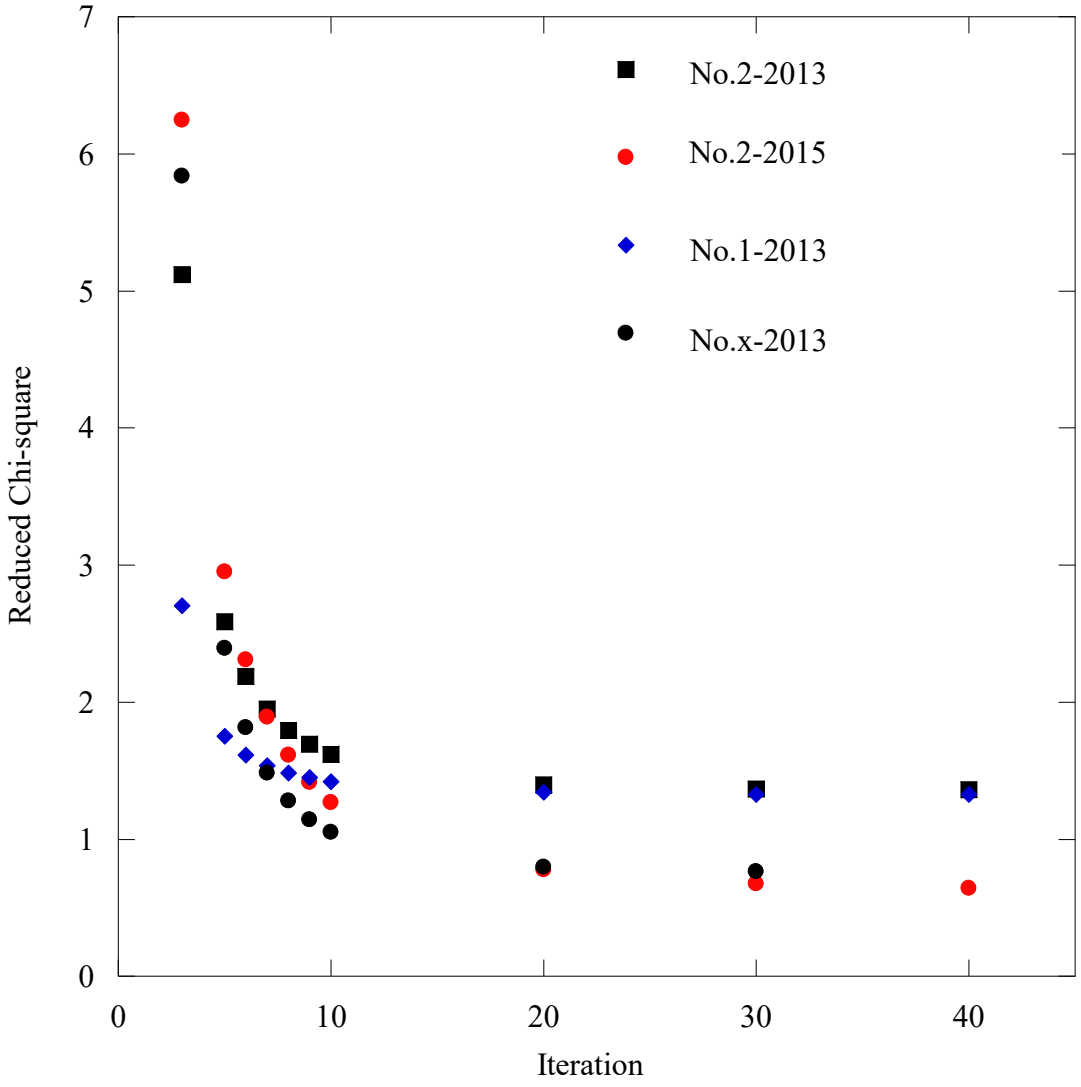

Fig. III-4: Reduced chi-square change following iterations

3. Results

3.1. IP profile and gamma measurement results

The 2D images obtained by the image analyzer are shown in Fig. III-5. These images were used for getting the IP profile as in Fig. III-6. The IP profile and gamma measurements of the samples are plotted in Figs. III-6(a–d). In this figure, the value in the high-intensity region of the IP profiles is adjusted to fit with the maximum value obtained by the gamma measurement to compare the shapes of the IP profiles and depth profiles. The shapes of IP profiles are different: large distribution shape (Fig. III-6(a)); narrow distribution shape (Fig. III-6(b)); two peaks distribution (Fig. III-6(c)); and central distribution (Fig. III-6(d)). Figs. III-6(a, b) suggested that the un-disturbing soil at the collected location. Fig. III-6(a, c) shows that the depth profiles at the same location No.2 (collected in 2013, 2015) were quite different which might result in a disturbed ground of soil core collected in 2015. The decontamination works have been conducted at the Komiya Magata before the soil core sample is collected. Hence, the profile in Fig. III-6(d) was typical in which the uncontaminated soil replaced the 5 cm of the surface soil.

The results by gamma measurement show that the radioactivity concentration of ^{40}K is the same from 0-30 cm the depth of soil cores, and its distribution is dominant (10 times higher) than radiocesium at a depth of 20-30 cm. Also, the depth profiles by gamma measurement indicate that the plateaus in the 20-30 cm region of the soil cores because of ^{40}K existing in nature. Conversely, in the dominant region of the IP profile, the shapes of the IP profiles were completely different from those measured with the gamma measurement. These differences were explained by effects from γ ray emitted from radiocesium.

T13007: 長泥曲田水田（未除染）

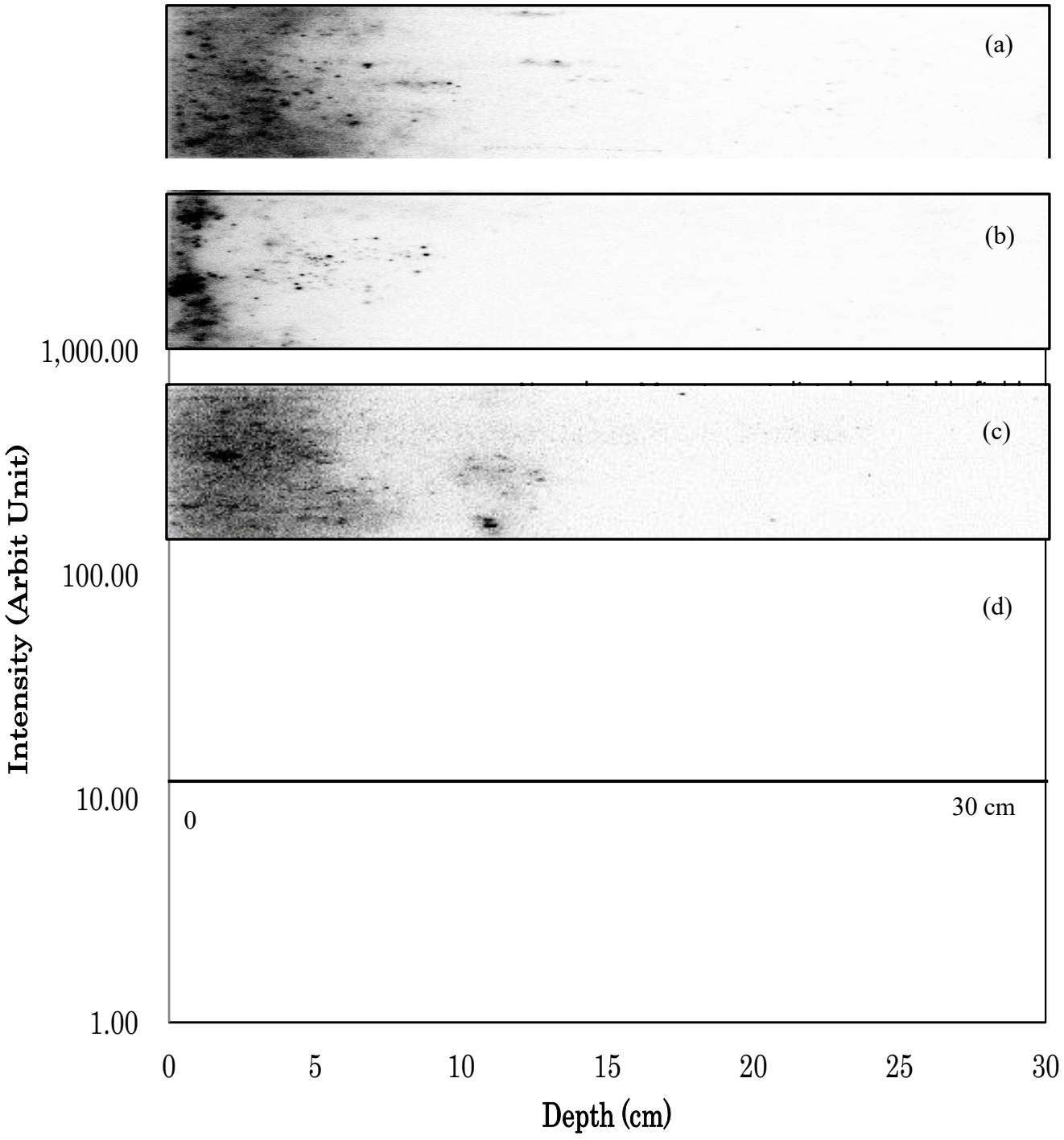

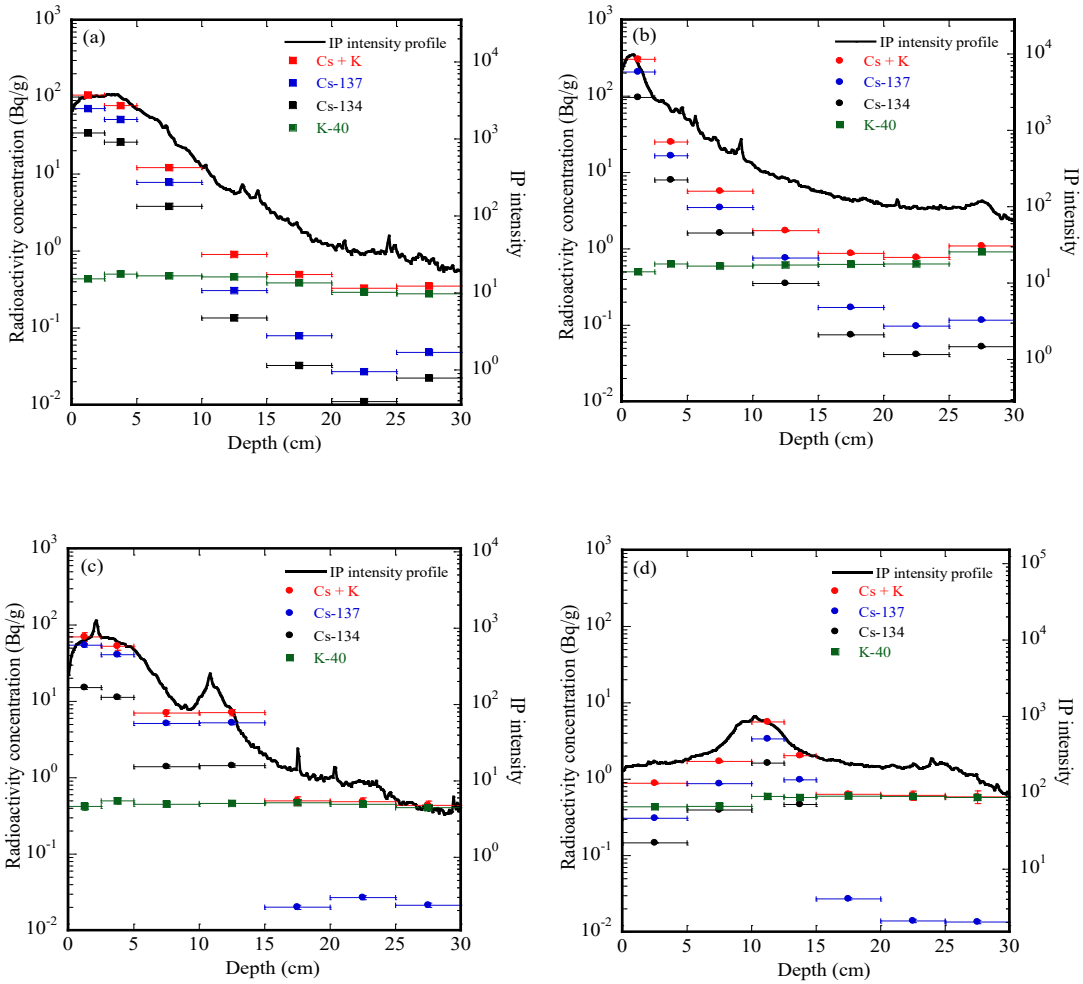

Fig. III-6: IP depth profiles (black solid lines), and gamma measurements of the samples collected at (a) No.2- 2013, (b) No.1- 2013, (c) No.2- 2015, and (d) No.x- 2013. The blue, black, green, and red solid circles denote ^{137}Cs, ^{134}Cs, ^{40}K, and the sum of radiocesium and ^{40}K, respectively.

3.2. Depth profile results of radionuclides

The results obtained by the unfolding technique and gamma measurement of the samples from No.2- 2013, No.1- 2013, No.2- 2015, and No.x 2013 are illustrated in Figs. III-7(a–d). The radiocesium depth profile by the proposed method agrees well with the gamma measurement results in the region 0-20 cm. In the region of 20-30 cm, the radiocesium concentrations of the samples at No.2 (-2013, and -2015) obtained by both methods have no difference (Figs. III-7(a, c)). In 20-30 cm region, the unfolding analysis results radioactivity of radiocesium obtained by unfolding has a gap with those by the gamma measurement of the samples at No.1- 2013 and No.x- 2013 (Figs. III-7(b, d)); however, they are in the range of the unfolding analysis uncertainty. The obtained results show there is good agreement between the sums radioactivity of the radiocesium and ^{40}K by both methods within the uncertainty.

By the proposed method, the depth-bin width of the depth profile can be changed to any scale to make the depth profile of radiocesium at a high concentration region clearer. In this doctoral thesis, the depth-bin width of depth profiles is chosen 1-millimeter scale and used for estimating the migration velocity and diffusion coefficient of radiocesium in chapter IV.

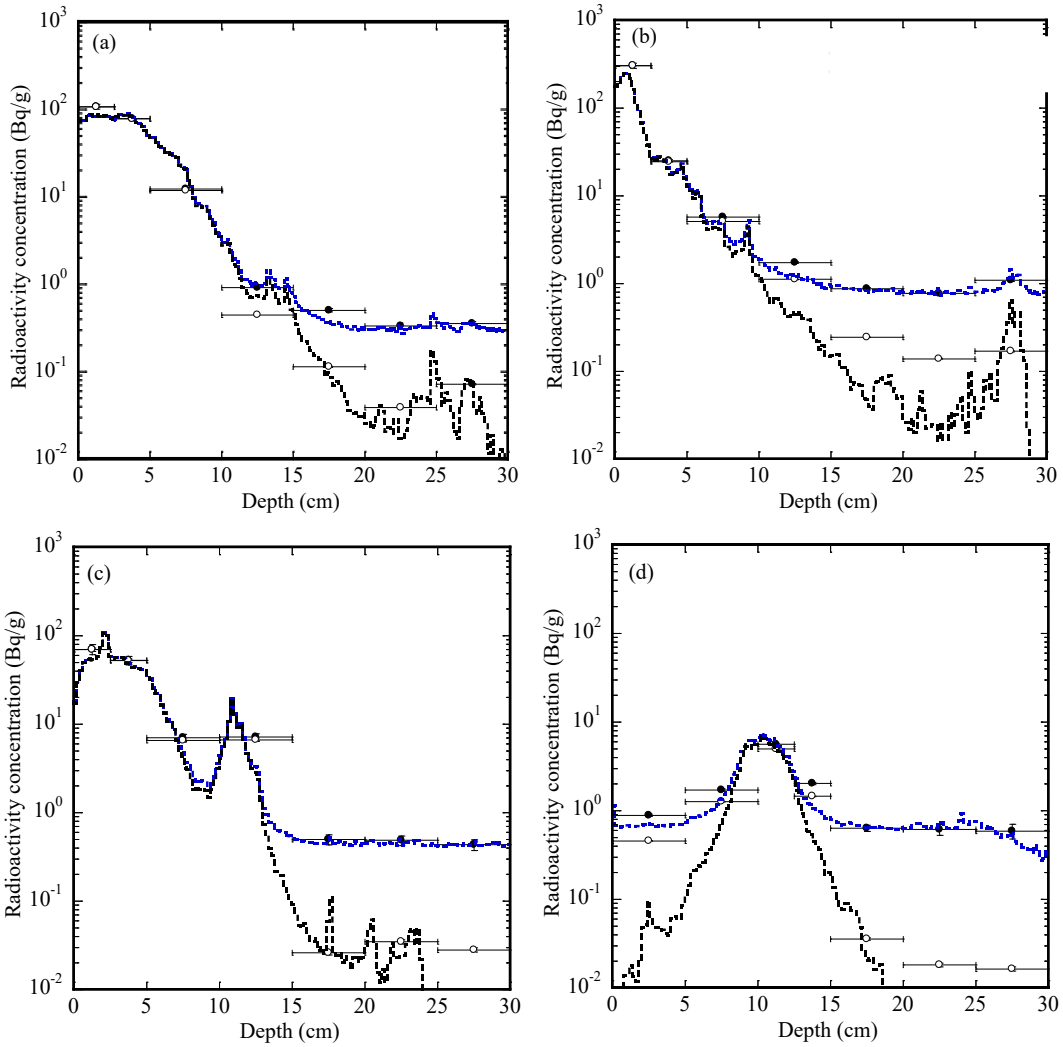

Fig. III-7: Unfolding analysis and gamma measurement results. (a) No.2- 2013, (b) No.1- 2013, (c) No.2- 2015, and (d) No.x- 2013. Blue and black dashed step lines describe the sum of the radiocesium and ^{40}K radioactivity concentration, and the radiocesium radioactivity concentration, respectively, obtained by the unfolding analysis. Black open circles describe the sum of the radiocesium and ^{40}K radioactivity concentration and solid black circles describe the radiocesium radioactivity concentration obtained by the gamma measurement.

4. Discussion

To verify the assumption of the IP profile of ^{40}K, the gamma measurement depth profiles of samples collected at No.1 location were used to calculate the verifying profiles of radiocesium and ^{40}K by interpolating. IP profiles were calculated based on response matrices and the verifying profiles as in Fig. III-8(a). Next, the calculated IP profiles of radiocesium and ^{40}K were applied for the proposed method to get back the depth profile. The confidence of the proposed method is validated by comparing the verifying profiles with the reproduced depth profiles. The Comparison of the unfolded depth profiles of radiocesium and ^{40}K was shown in Fig. III-8(b).

The unfolded depth profile of radiocesium and ^{40}K by the proposed method agreed well with those of test profiles in the region of 0-20 cm and 20-30 cm, respectively. The difference of radiocesium depth profile in the region 0-20 cm was approximately 10%. However, the depth profile of ^{40}K near the surface and the depth profile of radiocesium in deep layers were different from the test profiles. The average difference and unfolding error were estimated to be around 30% for ^{40}K, and 35.1% for radiocesium in the respective region.

To estimate the capacity of the proposed method using for low activity region of radiocesium, in which ^{40}K mainly contributes to the IP profile and conceals radiocesium contribution. The proposed method was verified by the changing of radiocesium activities of 1.3, 13, 54, and 134 Bq/g in the depth profiles. The unfolded results suggested that the depth region where the radioactivity distribution is reproduced expanded as the radioactivity of the radiocesium increased. Particularly, reproducible regions of 1.3, 13, 54 and 134 Bq/kg are 0-5 cm, 0-10 cm, 0-15 cm, and 0-20 cm, respectively. The average differences in these regions were estimated to be less than 20%.

Possible contamination of core samples caused by slipping soil in a vinyl tube was also tested. The contamination by this phenomenon would be expected to be no higher than

remaining radioactivity on the inner surface of vinyl-tube by the slipping high radioactivity soil. The vinyl-tube by an imaging plate (IP) after extracting soil has been measured. Fig. III-9 shows the IP intensity profile for the vinyl-tube with soil core, vinyl-tube after extracting soil and clean vinyl-tube (not used tube). The IP profile of the vinyl-tube extracting soil is slightly higher than that of clean vinyl-tube and 1 to 2 orders lower than the data for a vinyl tube containing soil. This shows that a small amount of soil attached to the inner surface of the vinyl-tube. However, the IP profile has a small position dependence, and the intensity is negligibly smaller than the IP intensity profile of the soil core as 0.19% for 0-10 cm depth and 1.73% for 10-20 cm, even if low radioactivity region of the 20-30 cm depth to be 2.03%. It shows that the contamination is not so high by the present soil sampling.

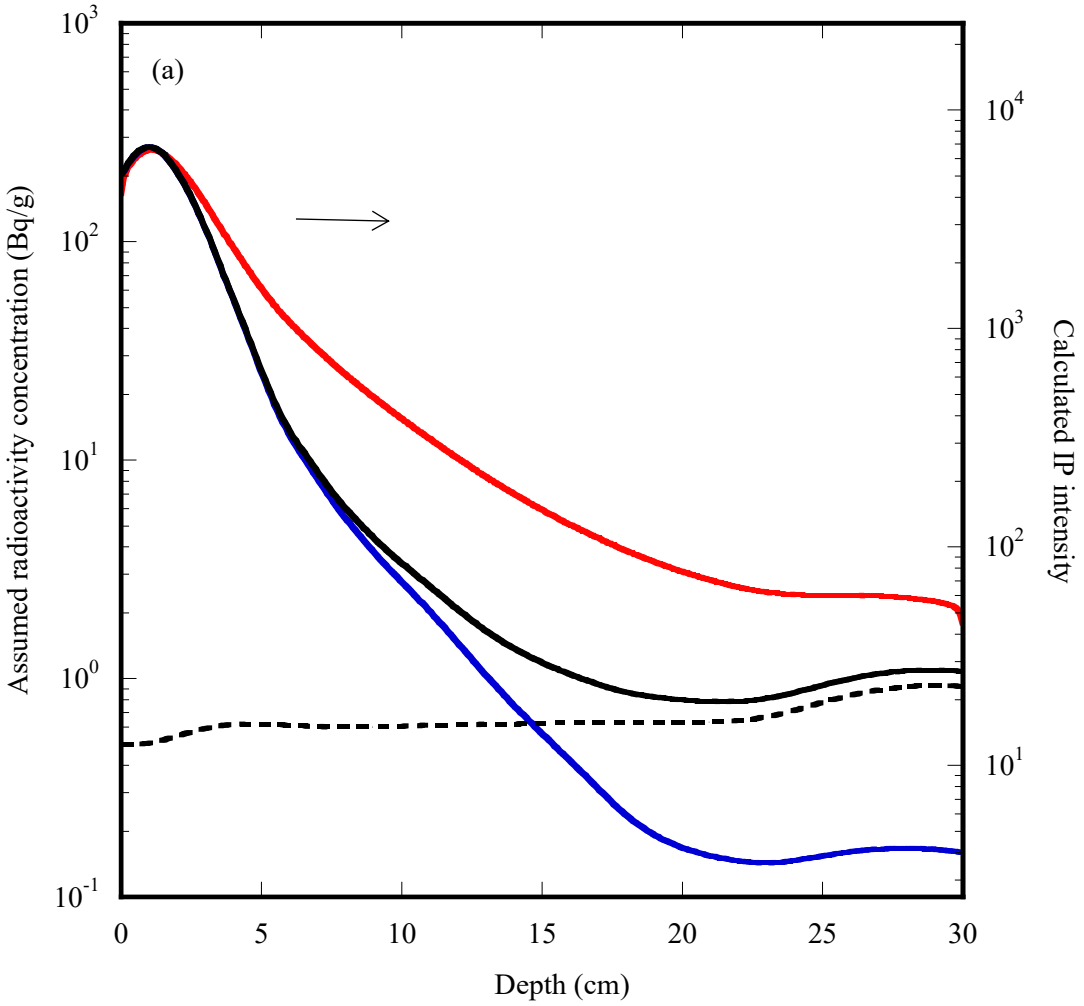

Fig. III-8: (a) IP profile of radiocesium (solid red curve) from the assumed values of radiocesium (solid blue curve), ^{40}K (black dashed curve), and the sum of radiocesium and ^{40}K (black solid curve).

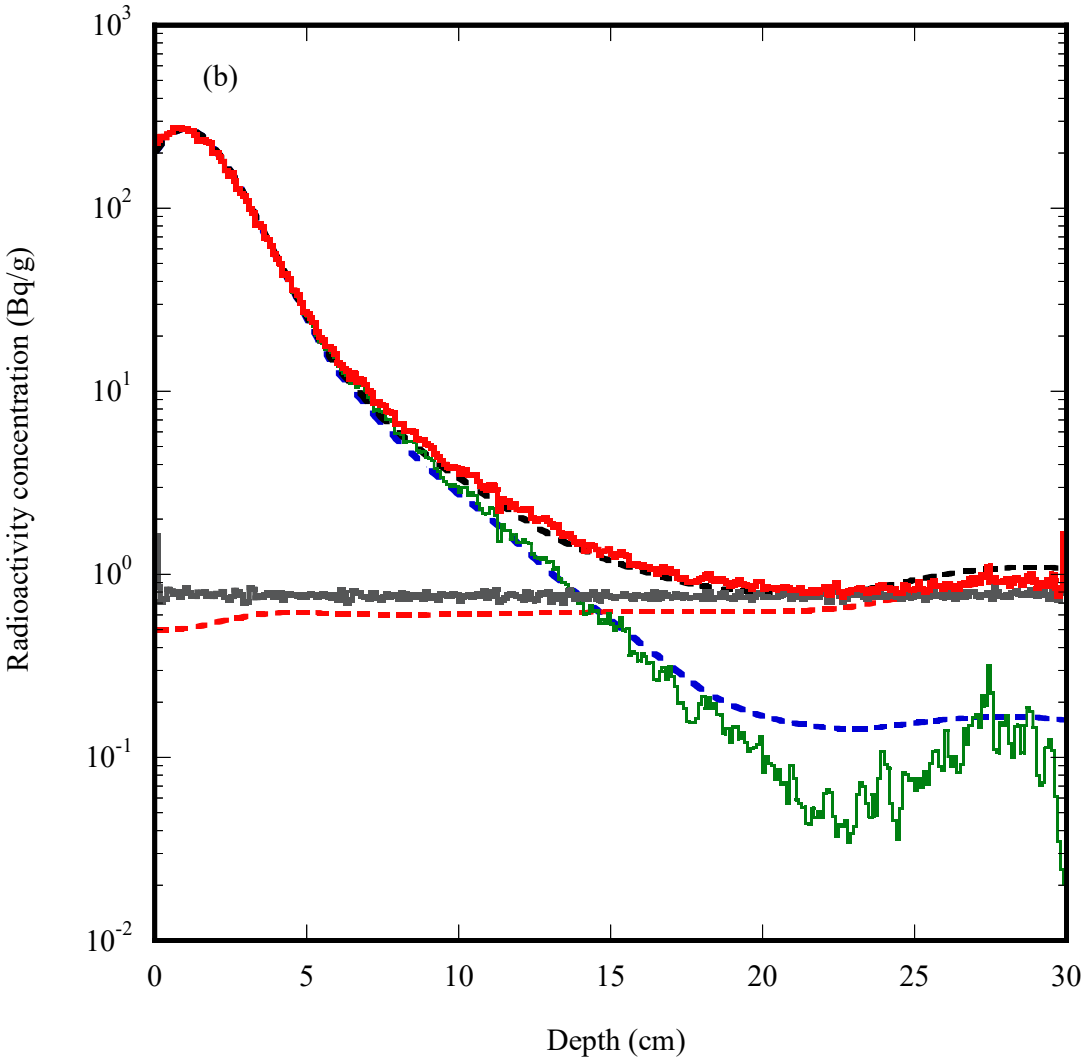

Fig. III-8: (b) Unfolding results of radiocesium (solid green line), ^{40}K (solid black line), and the sum of radiocesium and ^{40}K (solid red line) from the assumed values of radiocesium (black dotted line), ^{40}K (blue dotted line), and sum of radiocesium and ^{40}K (solid blue line).

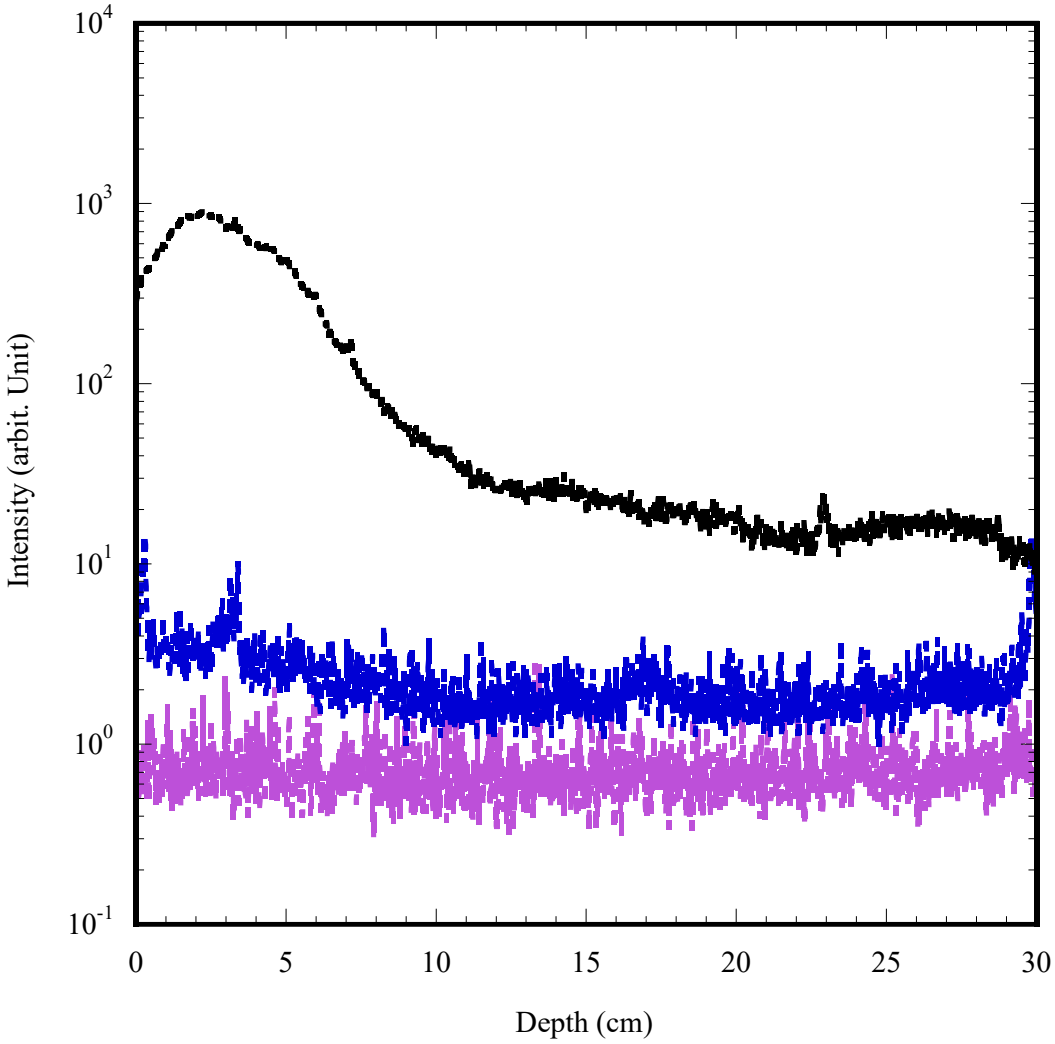

Fig. III-9: IP profile of clean vinyl-tube (pink dotted line), a vinyl tube from which soil extracted (blue dotted line) and a vinyl tube containing soil (black dotted line).

5. Conclusion

A method for determining the radiocesium depth profile with a depth-bin width of millimeter-scale to overcome the limitation of the normal technique was successfully constructed. To apply the proposed method, an IP depth profile obtained from the 2D images of the imaging plate, the response functions of radiocesium and ^{40}K of β and γ rays emitted from these radionuclides calculated by PHITS code are necessary. The response function of β ray seems to distribute surrounding the source. However, the response function of γ rays is quite different from that of β ray, the response function of γ rays have a large tail; therefore, the contribution of them is significant to the other positions. The response function matrices included response function of β and γ rays have been used for the proposed method. The depth profiles obtained by this method have a good agreement with those by gamma measurement.

Validation of the method was also conducted in this research. The verifying depth profiles of radiocesium and ^{40}K, which were interpolated from the depth profile of a sample collected at the No.1 location to evaluate the reproducibility was used. The IP profiles calculated based on the verifying depth profiles were used for reproducing depth profiles by the proposed method. The reproduction results indicated there was good agreement between the initial and reproduced depth profiles. The average differences are 10% and 35% at a depth of 0-20 cm and 20-30 cm, respectively.

On the other hand, for low radioactivity concentration of radiocesium, the unfolded results suggested that the radioactivity of radiocesium increases, the reproducible region is expanded. Particularly, reproducible regions of 1.3, 13, 54 and 134 Bq/kg are 0-5 cm, 0-10 cm, 0-15 cm, and 0-20 cm, respectively. The average differences in these regions were estimated to be less than 20%.

Possible contamination of core samples caused by slipping soil in the vinyl-tube was also estimated. The IP profile has a small position dependence, and the intensity is negligibly smaller

than the IP profile of the soil core as 0.19% for 0-10 cm depth and 1.73% for 10-20 cm, even if low radioactivity region of the 20-30 cm depth to be 2.03%. The present soil sampling method does not affect the investigation results.

References

1. Endo, S., Kajimoto, T., Shizuma, K., 2013. Paddy-field contamination with ^{134}Cs and ^{137}Cs due to Fukushima Dai-ichi Nuclear Power Plant accident and soil-to-rice transfer coefficients. J. Environ. Radiact.116, 59-64.

2. Arapis, G., Petrayev, E., Shagalova, E., *et al*., 1997. Effective migration velocity of ^{137}Cs and ^{90}Sr as a function of the type of soils in Belarus. J. Environ. Radiact.34(2), 171-185.

3. Szerbin, P., Koblinger-Bokori, E., Koblinger, L., *et al*., 1999. Caesium-137 migration in Hungarian soils. Sci Total Environ. 227, 215-227.

4. Krstic, D., Nikezic, D., Stevanovic, N., *et al*.,2004. Vertical profile of ^{137}Cs in soil. Appl. Radiat. Isot. 61, 1487-1492.

5. Almegren, S., Isaksson, M., 2006. Vertical migration studies of 137Cs from nuclear weapons fallout and the Chernobyl accident. J. Environ. Radiact. 91, 90-102.

6. Shiozawa, S., 2013. Agricultural implications of the Fukushima nuclear accident. In: Nakashima, T.M., Tanoi, K. (Eds.), Agricultural implications of the Fukushima Nuclear accident. Springer, Japan, Tokyo, pp. 49-60.

7. Takahashi, J., Tamura. K., Suda, T., *et al*., 2015. Vertical distribution and temporal changes of ^{137}Cs in soil profiles under various land uses after the Fukushima Dai-ichi Nuclear Power Plant accident. J. Environ. Radiact. 139, 351-361.

8. Sato, T., Niita, K., Matsuda, N., et al., 2013. Particle and heavy ion transport code system, PHITS, version 2.52. J. Nucl. Sci. Technol. 50(9), 913-923.

9. Tanaka, K., Endo, S., Toyoda, S., et al., 2007. Monte Carlo-based calculation of imaging plate response to 90Sr in teeth: experimental validation of the required correction on sample thickness. Radiat. Environ. Biophys. 46, 215-220.

10. Kerr, G. D., Pace, J. V., III, and Scott, W. H., Jr., 1983. Tissue kerma vs distance relationships for initial nuclear radiation from the atomic bombs: Hiroshima and Nagasaki. In U.S.-Japan joint workshop for reassessment of atomic bomb radiation dosimetry in Hiroshima and Nagasaki, pp. 57-103. Hiroshima: Radiation Effects Research Foundation.

11. National Nuclear Data Center-Brookhaven national laboratory (NNDC), 2006. Chart of nuclides, http://www.nndc.bnl.gov/chart/ (accessed 17.02.17).

12. Antcheva, I., Ballintijn, M., Bellenot, B., et al., 2009. ROOT — A C++ framework for petabyte data storage, statistical analysis and visualization. Computer Physics Communications 180(12), 2499-2512.

Chapter IV. Migration velocity and diffusion coefficient

1. Introduction

Theoretically, the migration velocity and diffusion coefficient are originated from the diffusion-convection model and expressed by the Folker-Plank equation. Some researchers had been solved the Folker-Plank equation by assumptions of the homogeneous Green function for infinite medium Szerbin et al. (1999) [1] or setting boundary conditions at the soil-air of interface for Green function [2] o find out these factors.

Bossew and Kirchner (2004) have pointed out that the assumptions above lead to underpredicts the solute concentration in soil and proposed a new model for describing the vertical profile of ^{137}Cs (radiocesium) [3]. The new concept of this model is based on three processes of diffusive-convective transport, continuity or conservation, and the interaction (sorption). The migration velocity and diffusion coefficient are assumed to be constants of time.

However, the investigation results for Fukushima soil contaminated by radioactive material from the Fukushima Daiichi Nuclear Power plant have shown that the migration velocity of radiocesium is quite fast for several months after deposition and then slows down. Particularly, the migration velocity of radiocesium was 4–7 mm per month during the first 3–4 months after the accident, and 0.4–1.4 mm/y 1 year after the accident [4]. Estimation of radiocesium movement in the soil for other soil types also suggested the migration velocity was small 4 to 21 months after the accident and migration velocities of 1.6 mm/y in meadowland, 3.7 mm/y in farmland, 1.2 mm/y in tobacco fields, and 10.1 mm/y in paddy fields.

Therefore, in this research, migration velocity is assumed to be an exponential function of time and replaced the equation solved by Bossew and Kirchner [2] for fitting the experimental data. The obtained results are discussed with previous results.

2. Material and method

2.1. Migration velocity and diffusion coefficient from previous research

Movement of radionuclides in the soil is considered based on the processes of the diffusive-convective transport, conservation, and interaction of radionuclides. Migration velocity and diffusion coefficient are indexes of radionuclides movement and derived from a set of differential equations from 3 processes above (Bossew and Kirchner, 2004). The vertical profile of radiocesium is expressed by Eq. (1) as:

$$C(x,t) = C_0 e^{-\lambda t}\left\{\frac{1}{\sqrt{\pi D t}} e^{-\frac{(x-vt)^2}{4Dt}} - \frac{v}{2D} e^{\frac{vx}{D}} erfc\left(\frac{v}{2}\sqrt{\frac{t}{D}} + \frac{x}{2\sqrt{Dt}}\right)\right\} \quad (1)$$

where, $C(x, t)$: Radioactivity concentration of radionuclide at depth-x and time-t;

C_0: Initial radioactivity concentration of radionuclide (radiocesium);

v: Migration velocity;

D: Diffusion coefficient;

λ: Decay factor.

Concerning Eq. (1), radionuclide movement in soil governs the migration in soil and their interaction with the soil particles. The positive part of Eq. (1) describes for the convection and diffusion (transport mechanism), the negative part is expressed for the interaction mechanism of radionuclide in liquid and solid phase. This equation has been consistently described for radiocesium released from the Chernobyl accident and Nuclear weapon test.

2.2. The equation for migration velocity and diffusion coefficient in Fukushima soil

There were some researches about the movement of radiocesium in Fukushima soil. The results indicated that radiocesium quickly moves to deeper layers after 3-4 months of the

accident, and then migration velocity is slowed down due to the absorption of soil particles with radiocesium (Shiozawa, 2013; Takahashi et al. 2015). On the other hand, real data collected in present research shows the migration velocities are not constant, which was assumed as in Eq. (1). In this investigation, the migration velocity of radiocesium in the soil is assumed to be an exponential relation as in Eq. (2).

$$v = v_0 e^{-at} \tag{2}$$

where, a: absorption factor.

By this assumption, the migration distance, d in Eq. (1) is considered as total of migration distance and should be rewritten by

$$d = \int_0^t v dt = \int_0^t v_0 e^{-at} dt = \frac{v_0}{a}(1 - e^{-at}). \tag{3}$$

The radioactivity concentration of radionuclide at depth-x and time-t is rewritten as,

$$C(x,t) = C_0 e^{-\lambda t}\left\{\frac{1}{\sqrt{\pi D t}} e^{-\frac{(x - v_0(1-e^{-at})/a)^2}{4Dt}} - \frac{v_0(1-e^{-at})/a}{2Dt} e^{\frac{v_0(1-e^{-at})/ax}{Dt}} erfc\left(\frac{v_0(1-e^{-at})/a + x}{2\sqrt{Dt}}\right)\right\}. \tag{4}$$

2.3. Fitting method for obtained depth profiles

Event soil cores are collected at the same location, the results always have a fluctuation. In this investigation, the fluctuations of the value of depth profiles in region 0-2 cm and 2-5 cm from surface soil obtained by the unfolding method are chosen to be 0.2 and 0.5. The obtained data from chapter III and the gamma measurements are applied for fitting.

Fitting works are conducted by finding the minimum value of reduced chi-square (theory of reduced chi-squared was mentioned in Chapter III) corresponding to change of relative activity, migration velocity, absorption factor, and diffusion coefficient, as shown in Fig. IV-1. The final reduced chi-square values are chosen in the range from 0.56 to 2. The calculated reduced chi-squares are summarized as in Table IV-1.

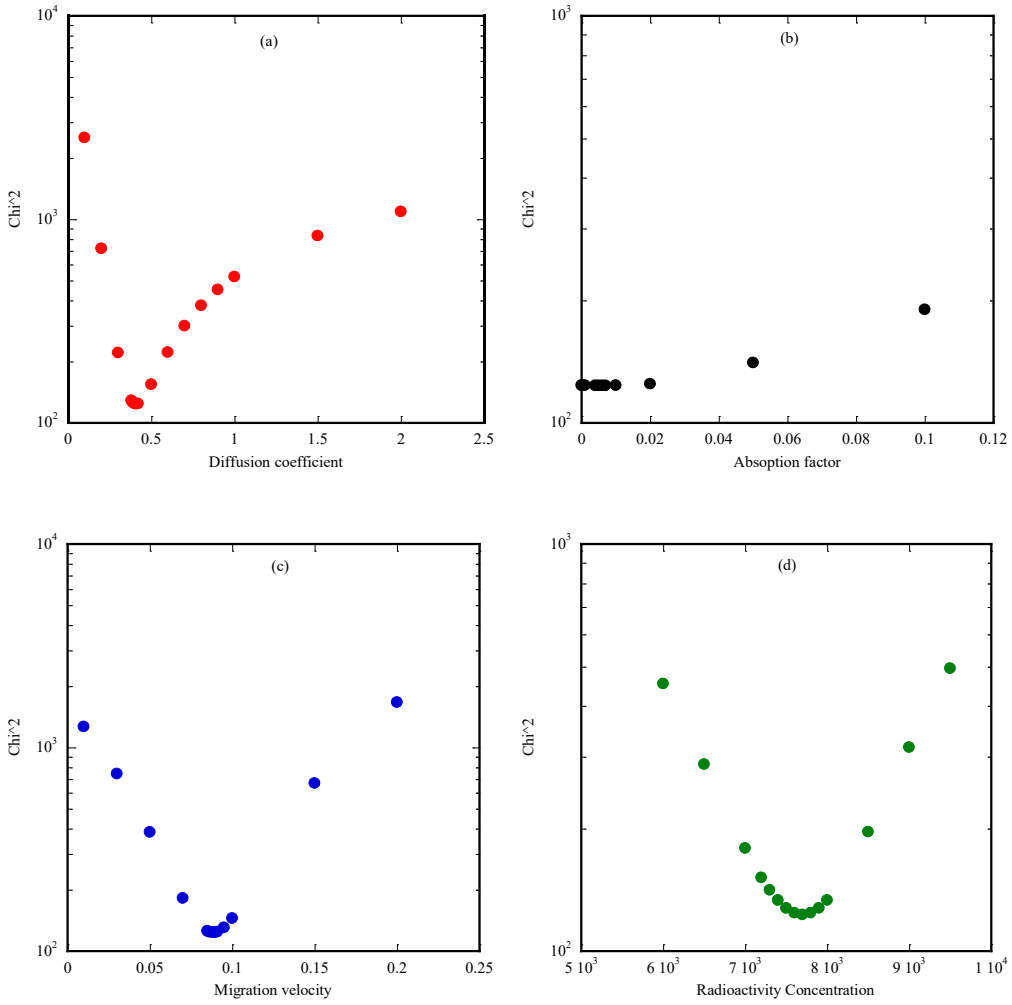

Fig. IV-1: Values of diffusion coefficient (a), absorption factor (b), migration velocity (c) and radioactivity concentration (d) chosen so that Chi-square is minimum

2.4. Depth profiles of radionuclides at other locations

The radiocesium is mainly concentrated in the region from 0-5 cm from the soil surface. In this research, the depth profile of the samples collected from 2012 to 2017at Iitate village is plotted in the region from 0-10 cm. These depth profiles were obtained by applying the technique in Chapter III. The results by the gamma measurement method and unfolding method were shown in Fig. IV-2 (a-j). Depth profiles by gamma measurement and depth profiles by unfolding method have a good agreement.

Depth profiles at the same location collected in different years almost have the same shape. However, there are some quite differences of depth profile in a specific year in some locations. These depth profiles are in the Nagadoro paddy field (2017), Ochiai (2013, 2015), Iitate Village office (2016), Iitate farm, and Near Iitate farm. These differences of the depth profile might cause sampling; for instance, samples were collected at locations that were disturbed by wild animals or other natural conditions. The depth profiles which have different shape will be excluded for fitting to obtain migration velocity and diffusion coefficient.

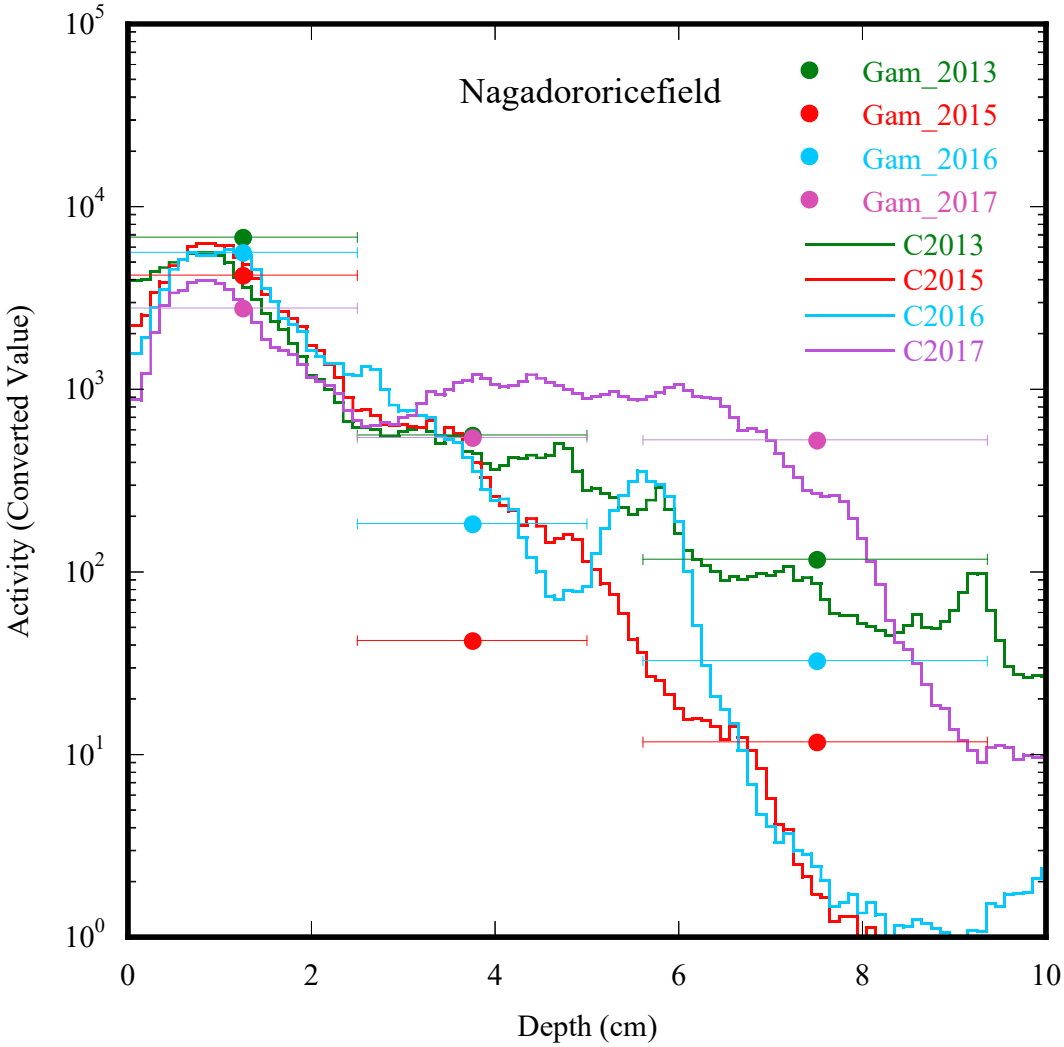

Fig. IV-2 (a): Depth profile of soil cores collected at Nagadoro paddy field. Green, red, light blue and pink solid dots describe for gamma measurement results plotted with uncertainty bar of cores collected from 2013, 2015, 2016, and 2017, respectively. Green, red, light blue and pink step lines describe for depth profiles of cores collected from 2013, 2015, 2016, and 2017, respectively, by Unfolding method

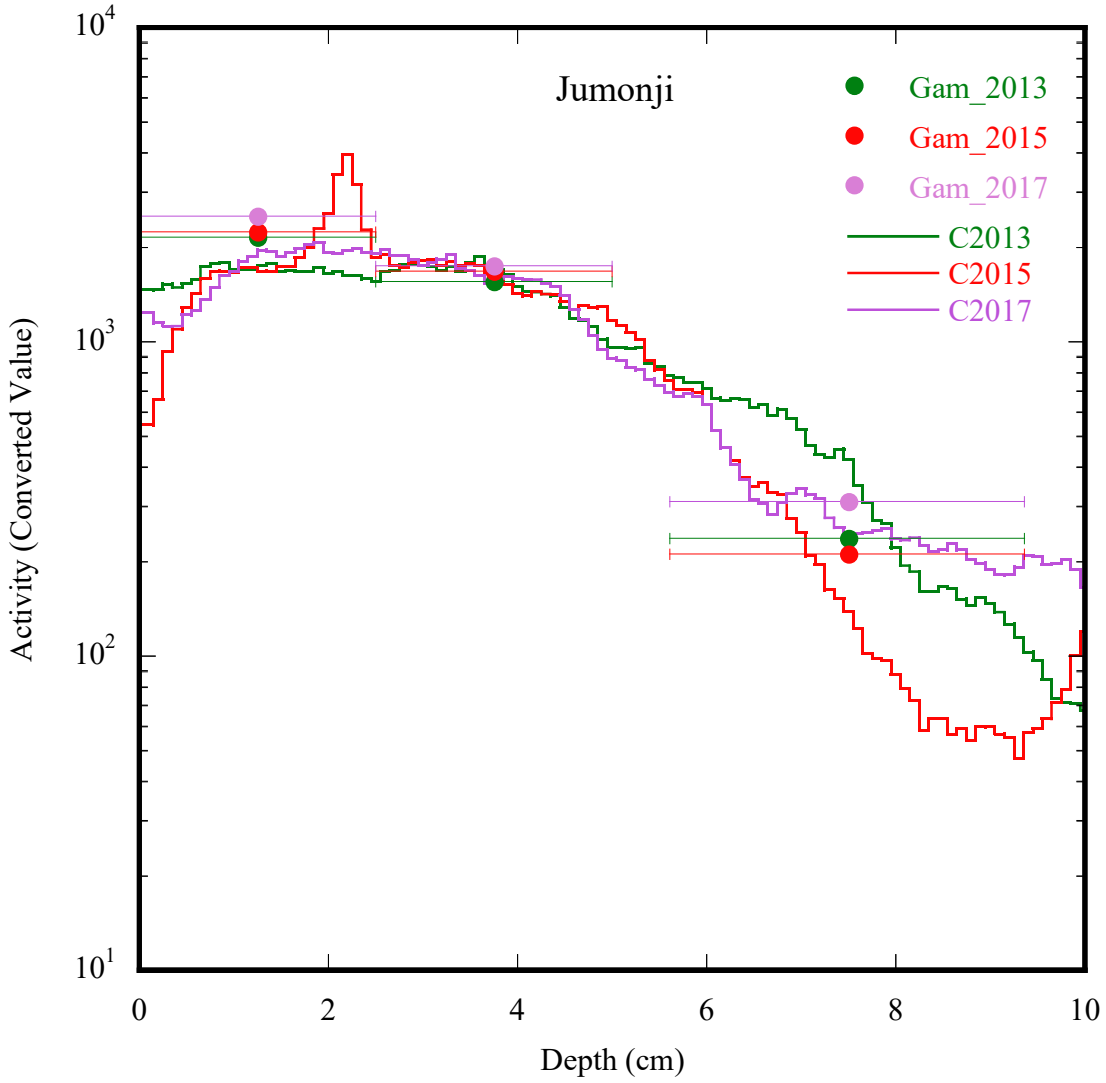

Fig. IV-2 (b): Depth profile of soil cores collected at Nagadoro Jumonji. Green, red, and pink solid dots describe for gamma measurement results plotted with the uncertainty bar of cores collected from 2013, 2015, and 2017, respectively. Green, red, and pink step lines describe for depth profiles of cores collected from 2013, 2015, and 2017, respectively, by unfolding method

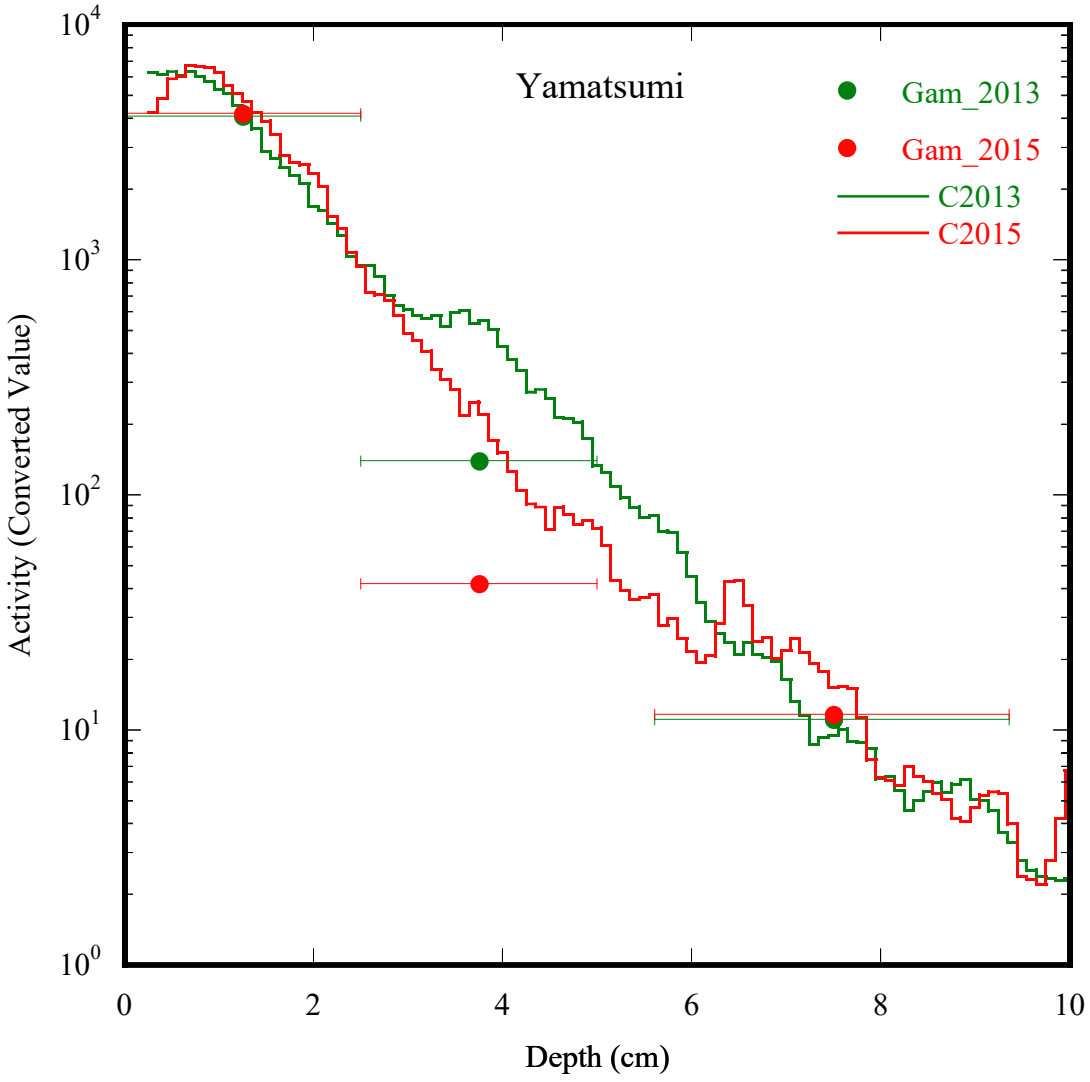

Fig. IV-2 (c): Depth profile of soil cores collected at Yamatsumi. Green and red solid dots describe for gamma measurement results plotted with uncertainty bar of cores collected from 2013, and 2015, respectively. Green and red step lines describe for depth profiles of cores collected from 2013, and 2015, respectively, by unfolding method

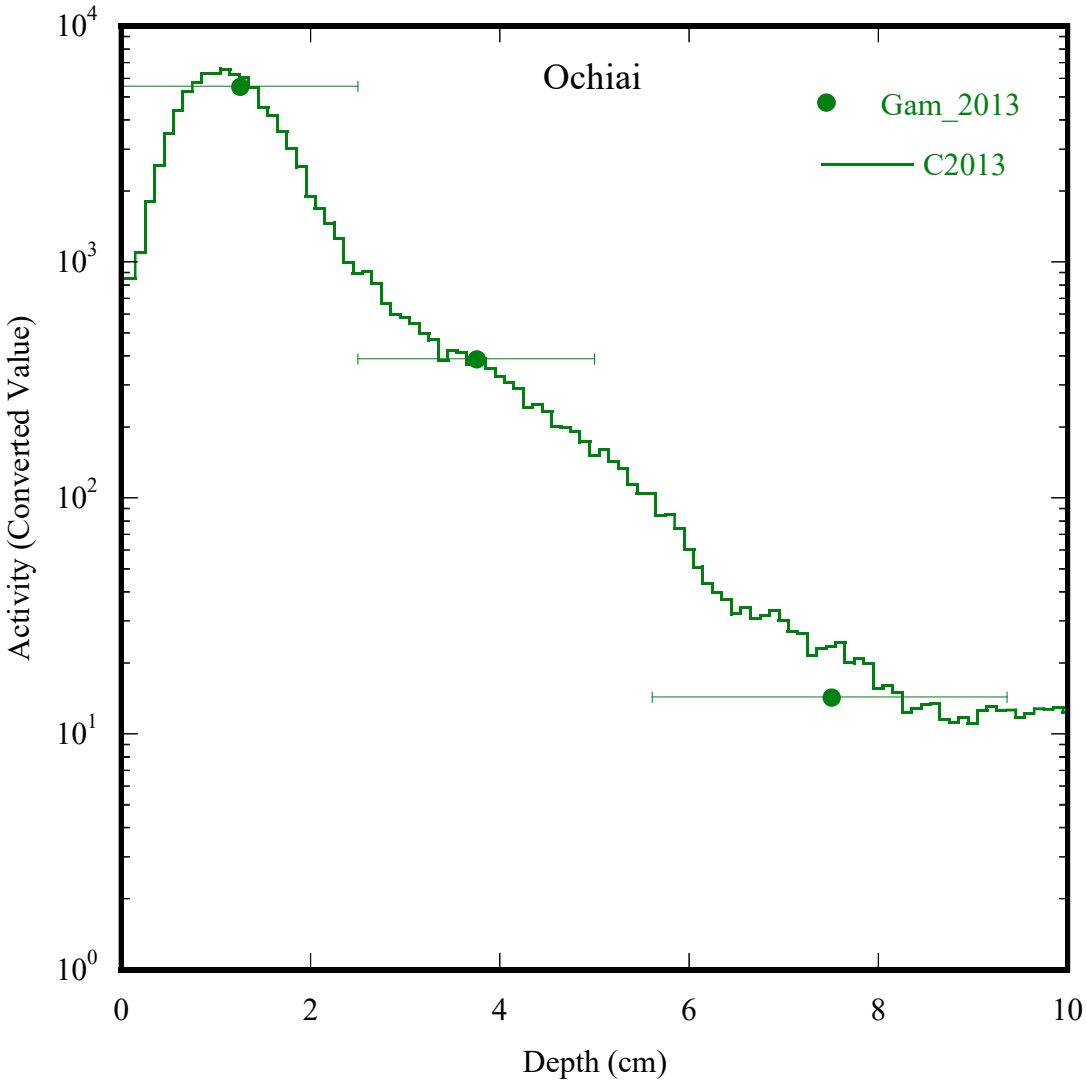

Fig. IV-2 (d): Depth profile of soil cores collected at Ochiai. Green solid dot describes for gamma measurement results plotted with the uncertainty bar of cores collected from 2013. Green step line describes for depth profiles of cores collected from 2013 by unfolding method

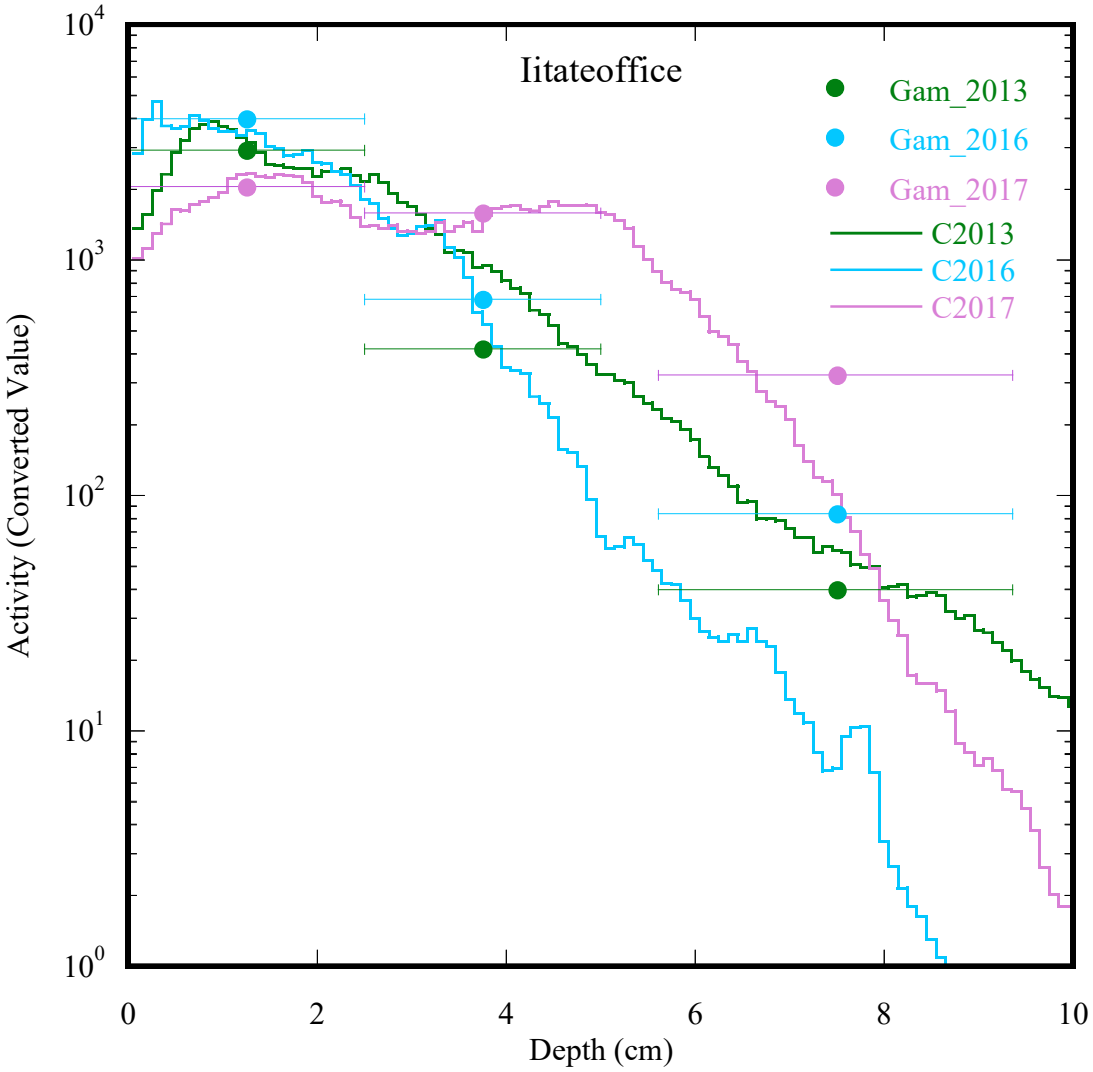

Fig. IV-2 (e): Depth profile of soil cores collected at Iitate Office. Green, light blue, and pink solid dots describe for gamma measurement results plotted with the uncertainty bar of cores collected from 2013, 2016, and 2017, respectively. Green, light blue, and pink step lines describe for depth profiles of cores collected from 2013, 2016, and 2017, respectively, by unfolding method

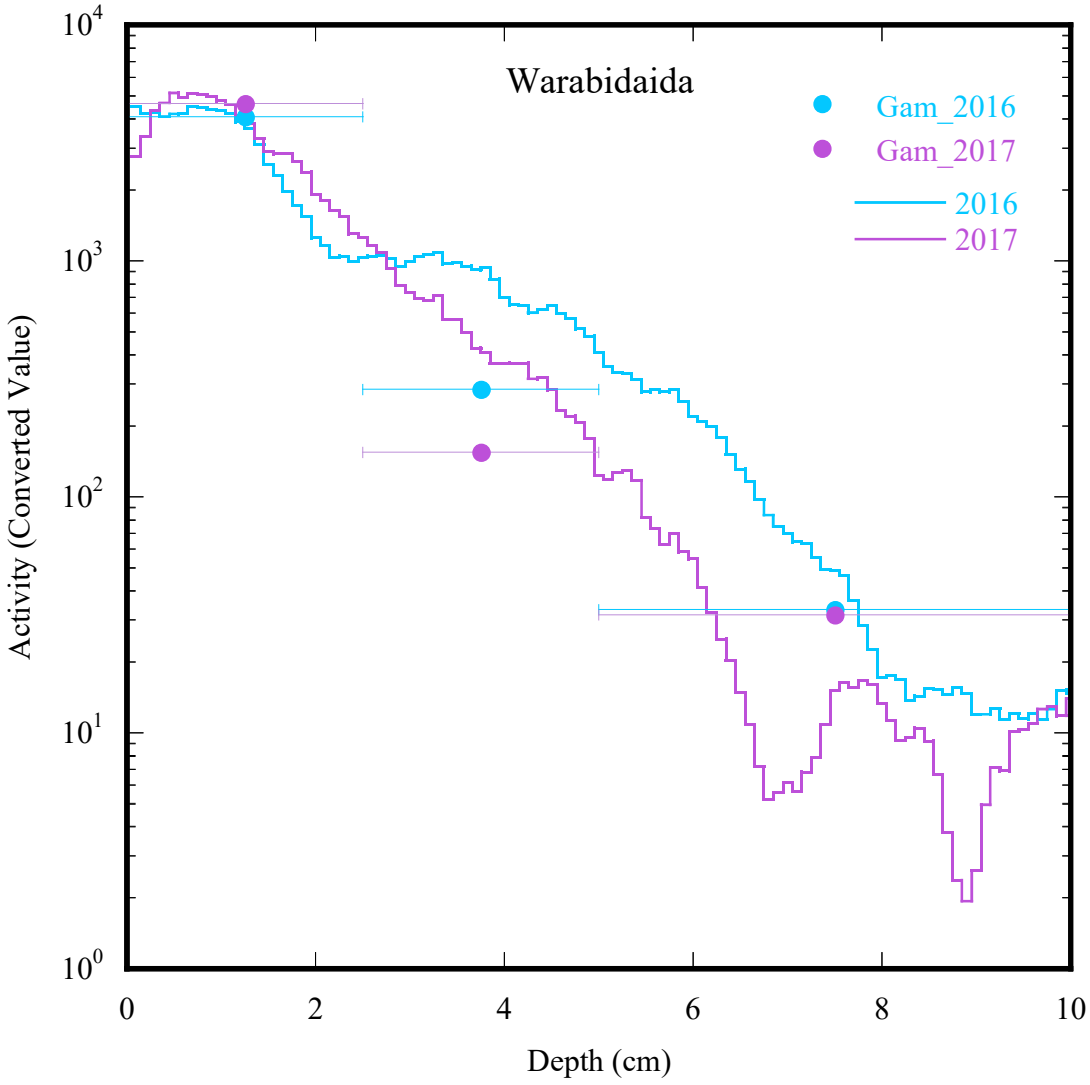

Fig. IV-2 (f): Depth profile of soil cores collected at Warabidaida. Light blue and pink solid dots describe for gamma measurement results plotted with the uncertainty bar of cores collected from 2016, and 2017, respectively. Light blue and pink step lines describe for depth profiles of cores collected from 2016, and 2017, respectively, by unfolding method

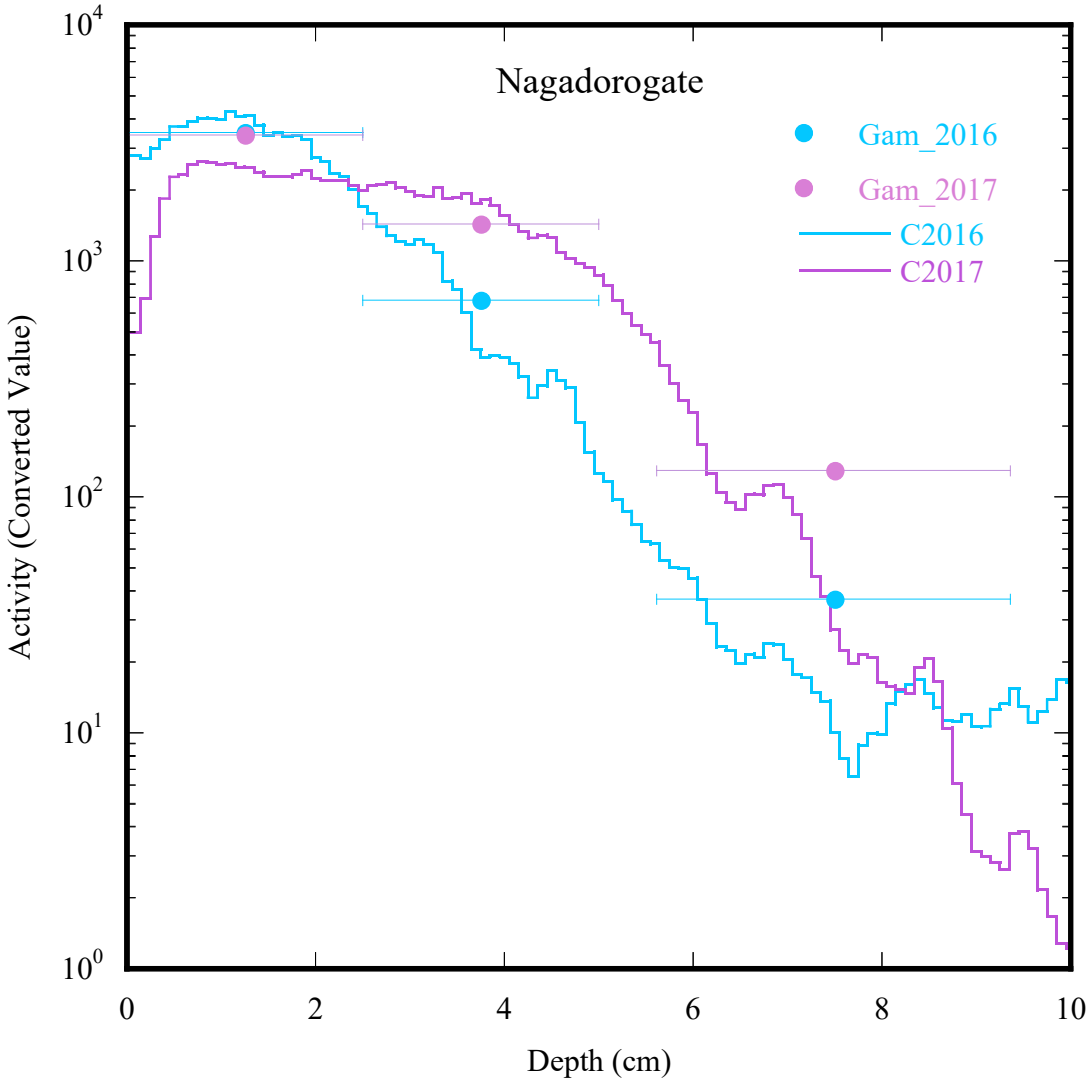

Fig. IV-2 (g): Depth profile of soil cores collected at Nagadoro gate. Light blue and pink solid dots describe for gamma measurement results plotted with the uncertainty bar of cores collected from 2016, and 2017, respectively. Light blue and pink step lines describe for depth profiles of cores collected from 2016, and 2017, respectively, by unfolding method

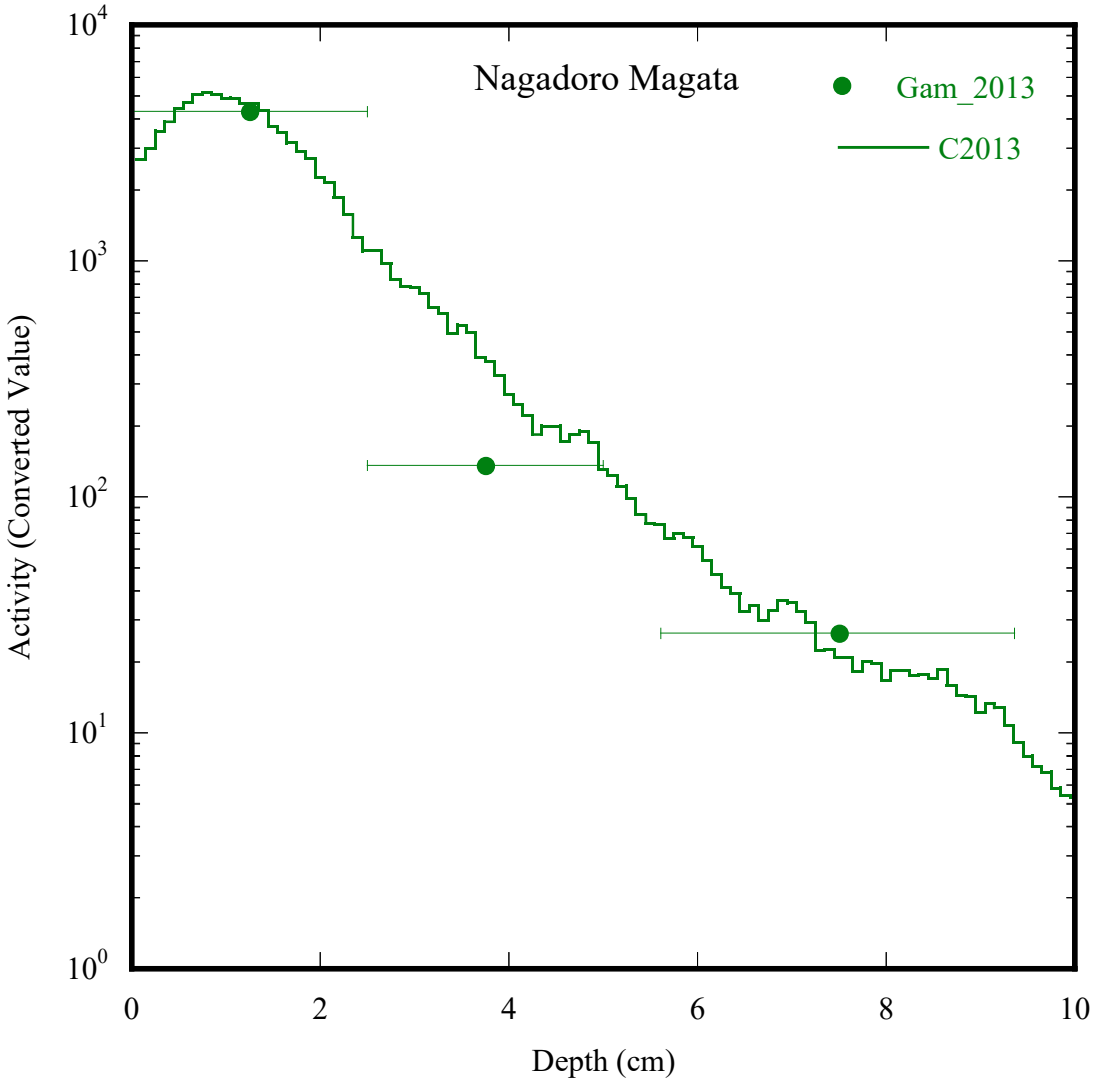

Fig. IV-2 (h): Depth profile of soil cores collected at Nagadoro Magata. Green solid dot describes for gamma measurement results plotted with the uncertainty bar of cores collected from 2013. Green step line describes for depth profiles of cores collected from 2013 by unfolding method

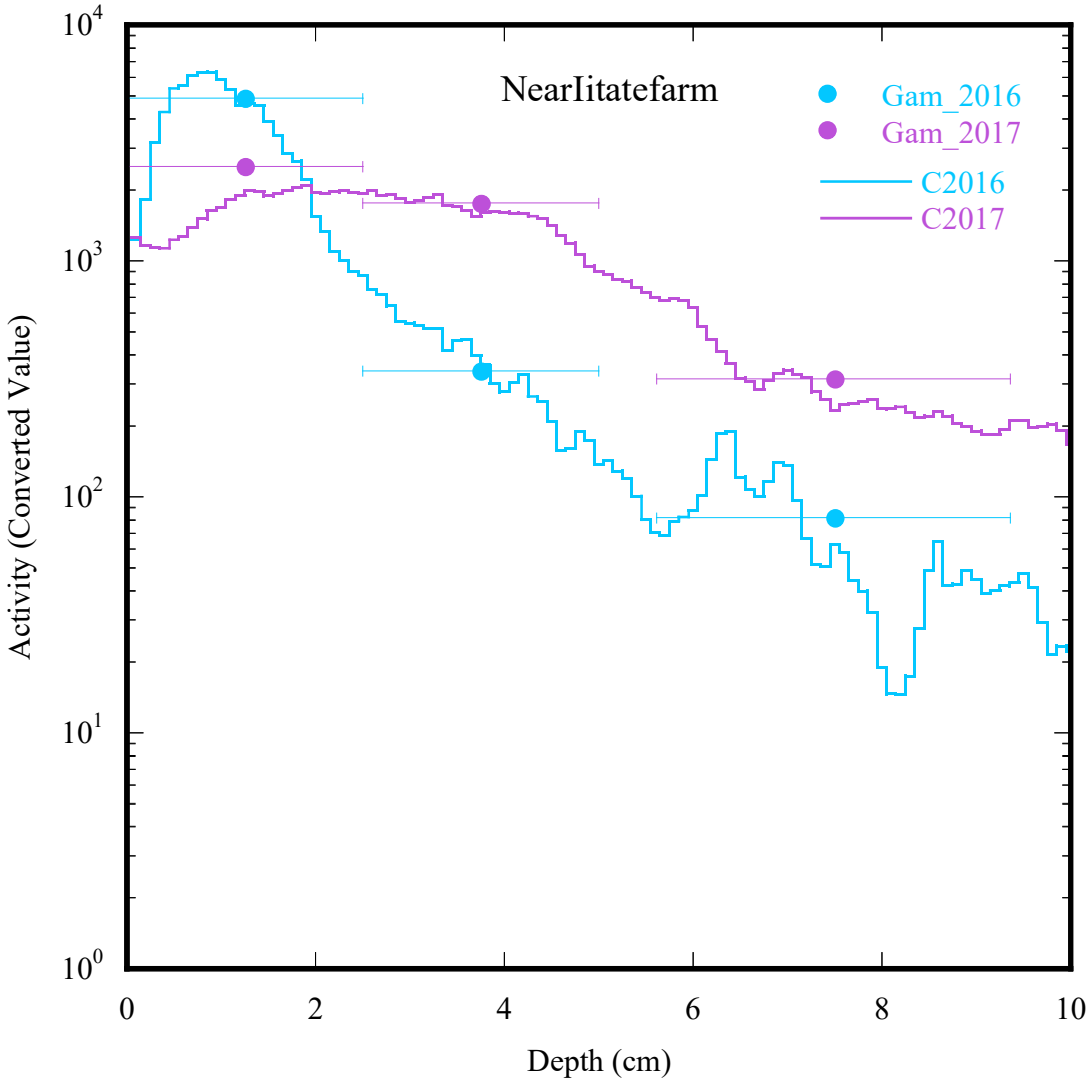

Fig. IV-2 (i): Depth profile of soil cores collected at Near Iitate farm. Light blue and pink solid dots describe for gamma measurement results plotted with the uncertainty bar of cores collected from 2016, and 2017, respectively. Light blue and pink step lines describe for depth profiles of cores collected from 2016, and 2017, respectively, by unfolding method

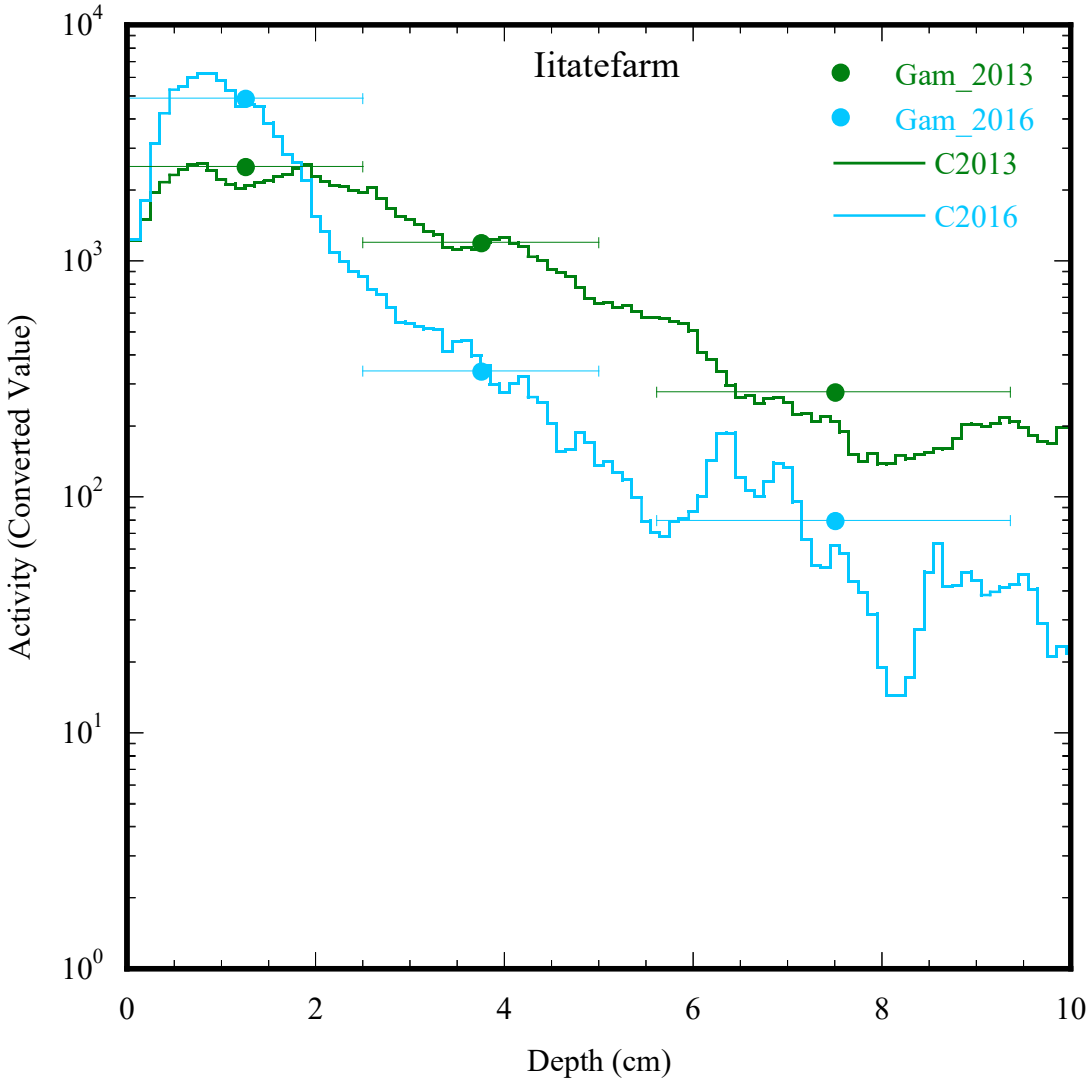

Fig. IV-2 (j): Depth profile of soil cores collected at Iitate farm. Green and pink solid dots describe for gamma measurement results plotted with the uncertainty bar of cores collected from 2013, and 2016, respectively. Green and pink step lines describe for depth profiles of cores collected from 2013, and 2016, respectively, by unfolding method

3. Results

Fitting results are shown in Fig. IV-3 (1)-(7), initial migration velocities have a wide range of values. The difference in the initial migration velocity has a dependence on the type of soil. Notably, the initial migration velocity is quite slow at Warabidaida with Tusima II series brown forest soil (0.09 cm/y) and is fast at Nagadoro Jumonji with Minaniuta Gray Soil (2.1 cm/y).

The obtained values of the diffusion coefficient by fitting are in a range from 0.37 cm^2/y at Nagadoro rice field to 3.6 cm^2/y at Nagadoro Jumonji. The results show that there is not a clear relationship between the diffusion coefficient change and the initial migration velocity at the same location. Particularly, both initial migration velocity and diffusion coefficient are quite high at Nagadoro Jumonji with Minaniuta Gray Soil; however, minimum values of the initial migration velocity and the diffusion coefficient are in different locations as Warabidaida. The initial migration velocity and diffusion coefficient of samples at different forest have a broad range value of 0.09-0.33 cm/y and 0.37-0.88 cm^2/y, respectively.

Absorption factor, *a*, shows the reduction of the migration velocity by time, which has fitting results in a range from $6x10^{-3}$ to 1.73 y^{-1} (min and max values to sample collected at Warabidaida and Nagadoro Magata, respectively). This absorption factor has no dependence on the sampling location and type of soil.

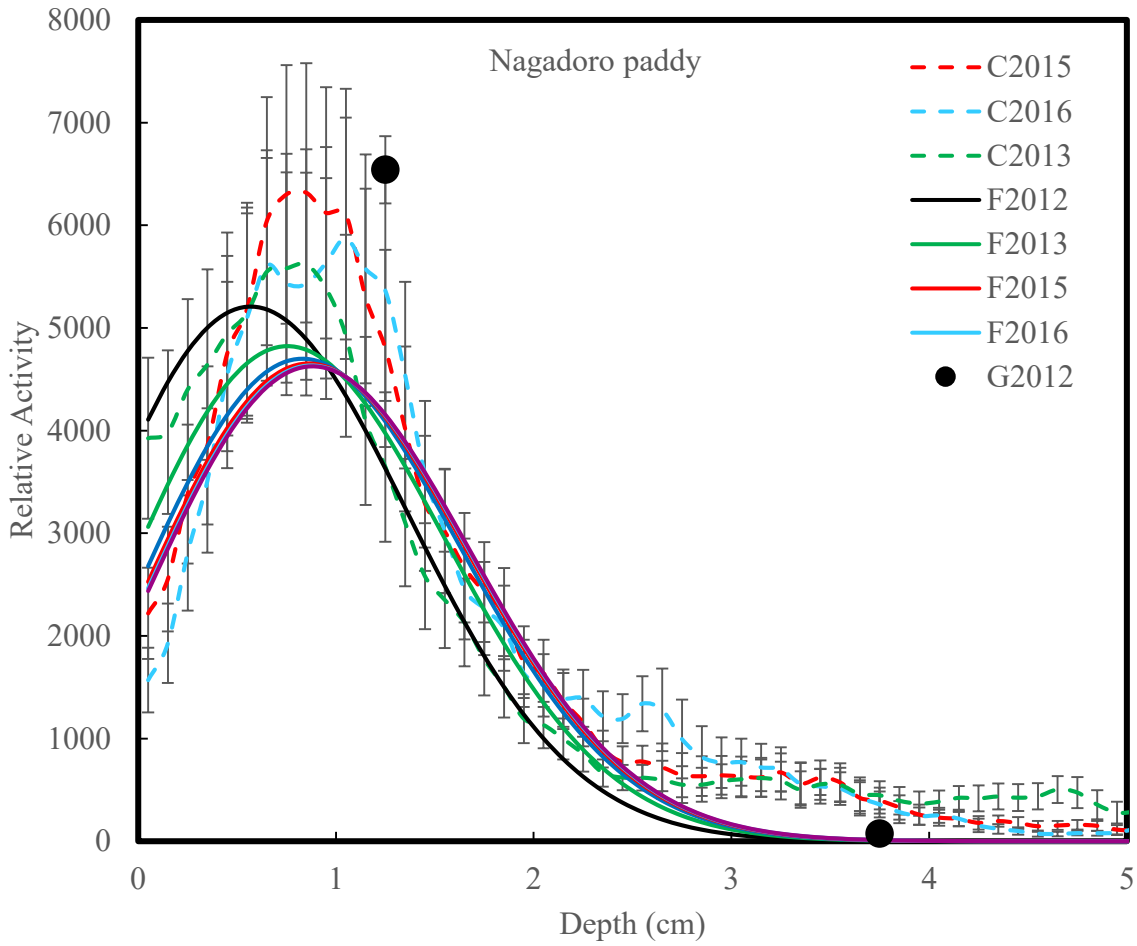

Fig. IV-3 (1): Fitting results of Nagadoro rice field sample by using Eq. (4). Black dot described for data of 2012 by gamma measurement; Green, red, and light blue dashed curves described for data of 2013, 2015, and 2016, respectively; Black, green, red, and light blue smooth curves described for data of 2012, 2013, 2015, and 2016, respectively by fitting.

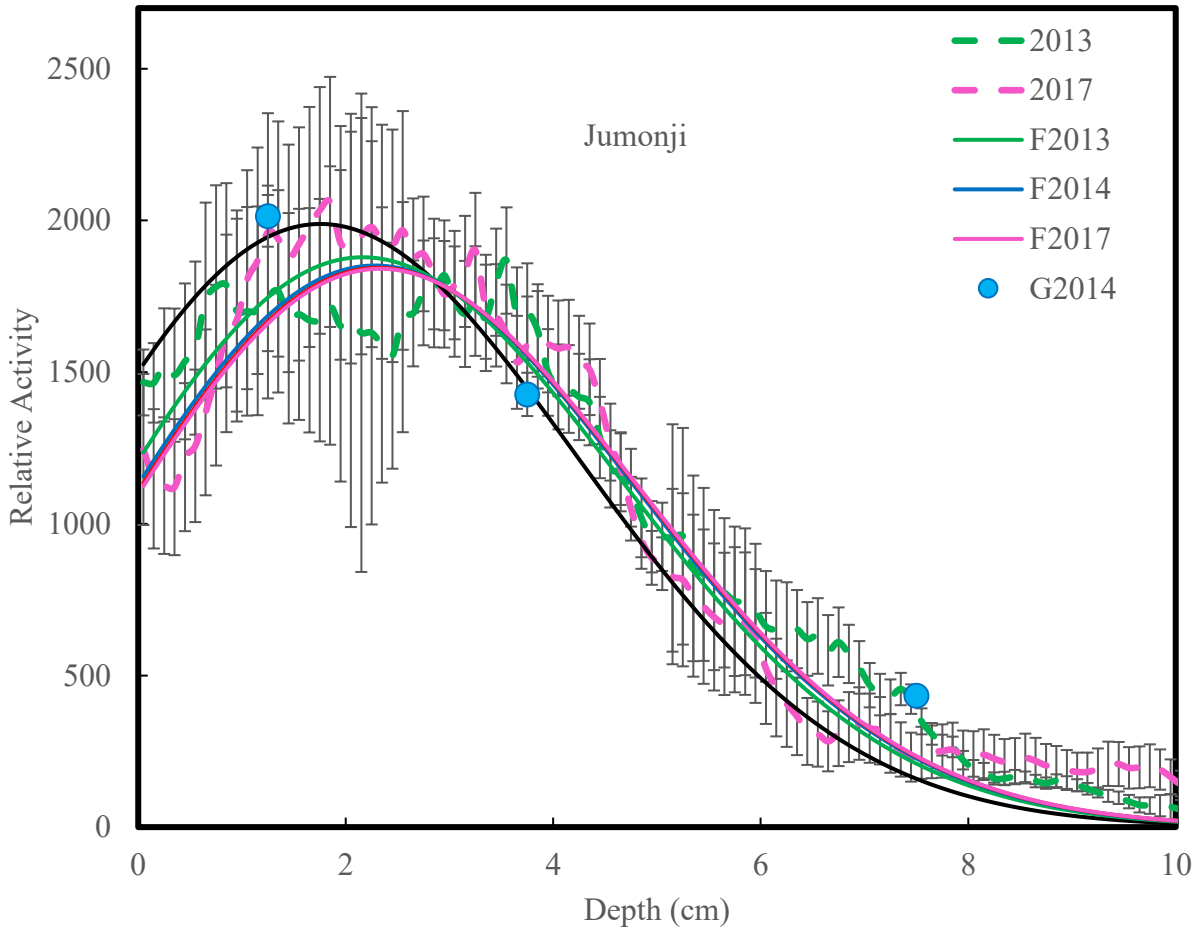

Fig. IV-3 (2) – Fitting results of Nagadoro Jumonji sample by using Eq. (4). Blue dot described for data of 2014 by gamma measurement; Green and pink dashed curves described for data of 2013, and 2017, respectively; Green, blue, and pink smooth curves described for data of 2013, 2014, and 2017, respectively by fitting.

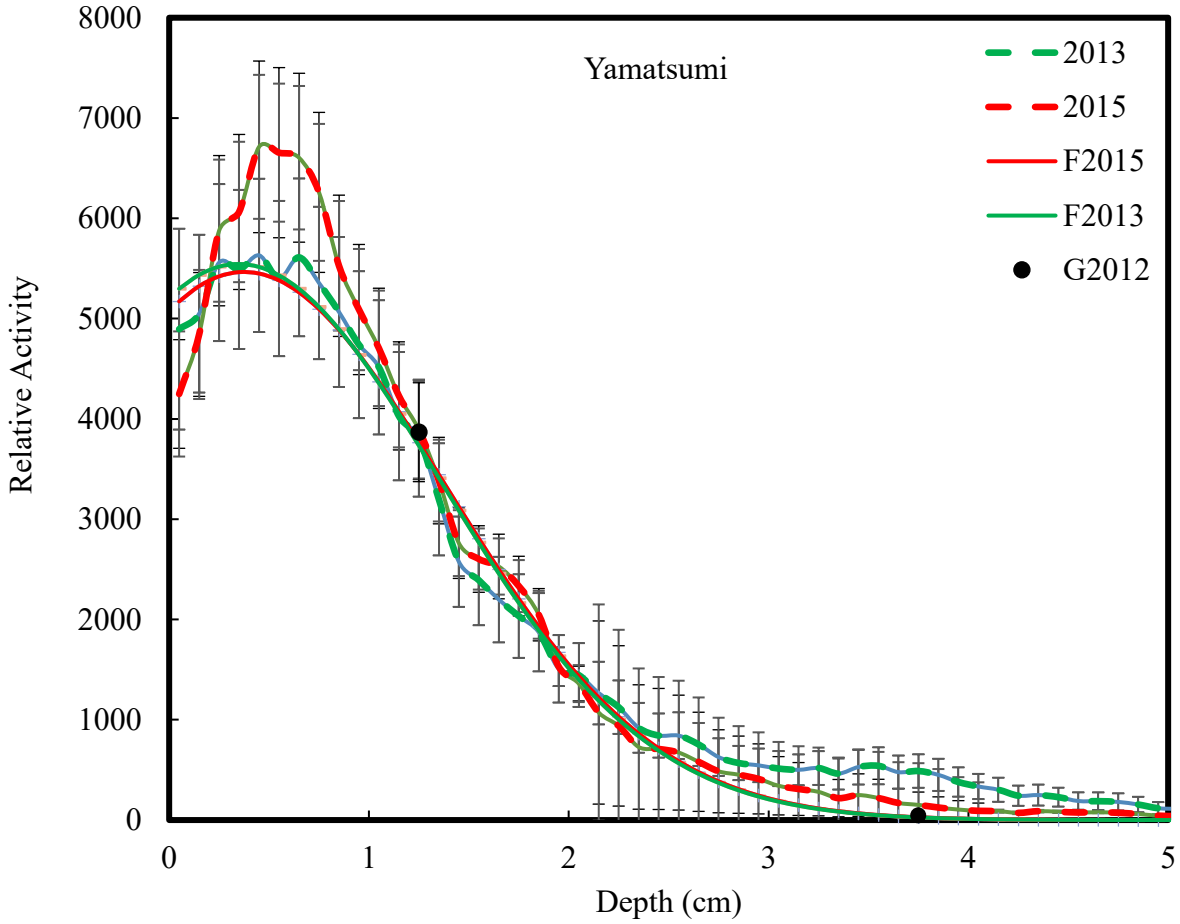

Fig. IV-3 (3) – Fitting results of Yamatsumi Shrine sample by using Eq. (4). Black dot described for data of 2012 by gamma measurement; Green and red dashed curves described for data of 2013, and 2015, respectively; Black, green, and red smooth curves described for data of 2012, 2013, and 2015, respectively by fitting.

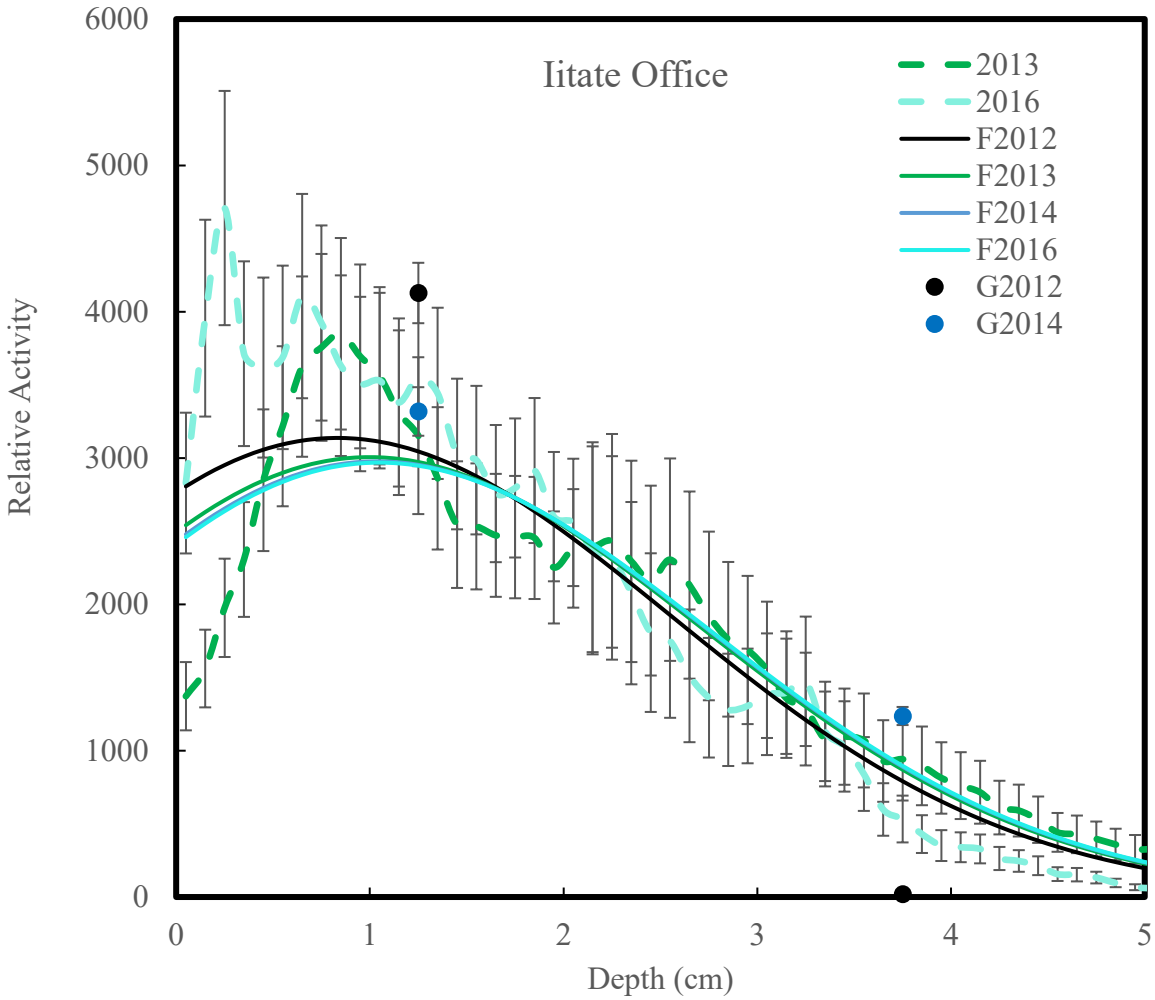

Fig. IV-3 (4) – Fitting results of Iitate Office sample by using Eq. (4). Black and blue dots describe for data of 2012, and 2014 by gamma measurement; Green, and light blue dashed curves describe for data of 2013, and 2016, respectively; Black, green, blue, and light blue smooth curves describe for data of 2012, 2013, 2014, and 2016, respectively by fitting.

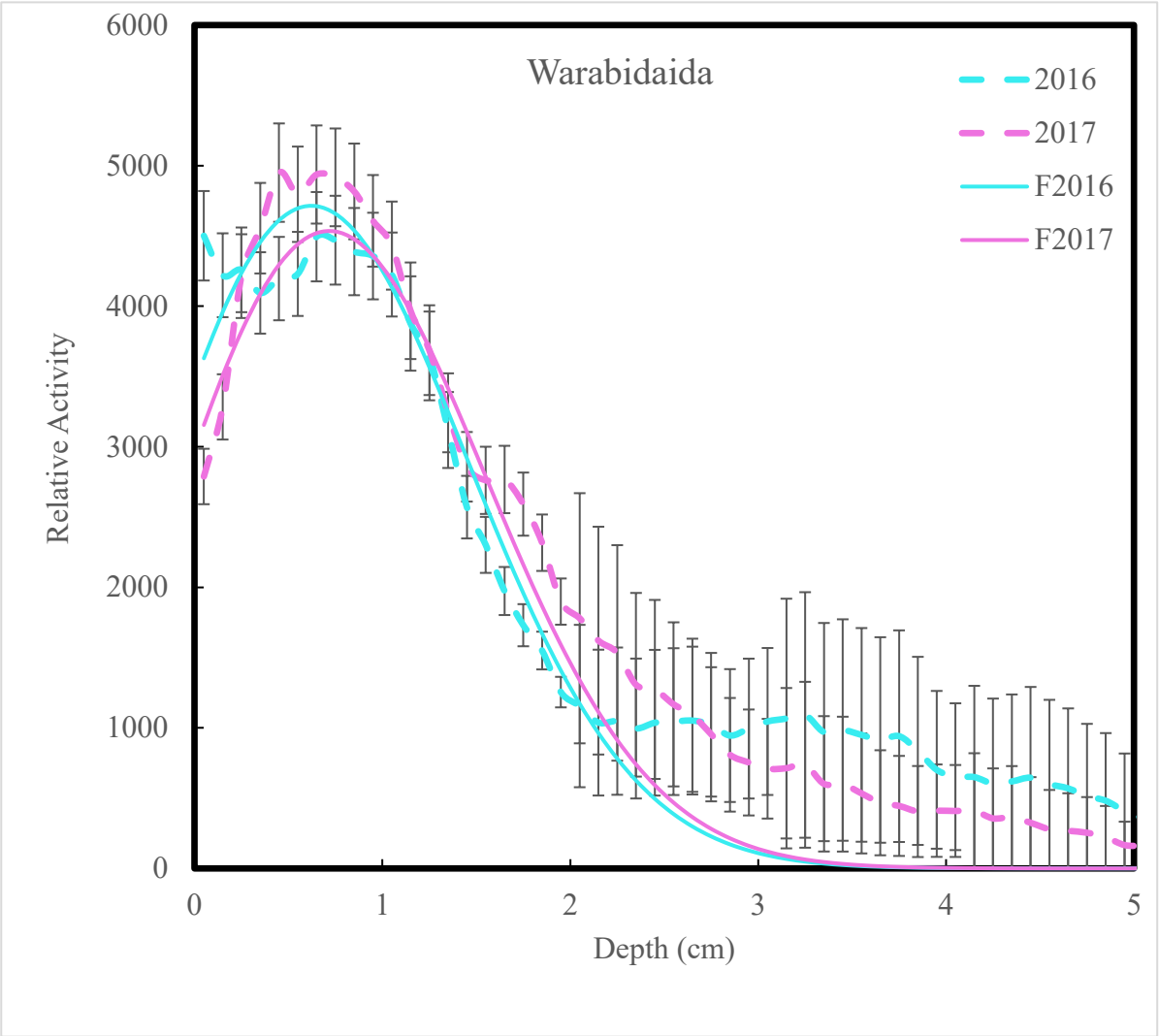

Fig. IV-3 (5) – Fitting results of Warabidaida sample by using Eq. (4). Light blue and pink dashed curves describe for data of 2016, and 2017, respectively; Light blue and pink smooth curves describe for data of 2016, and 2017, respectively by fitting.

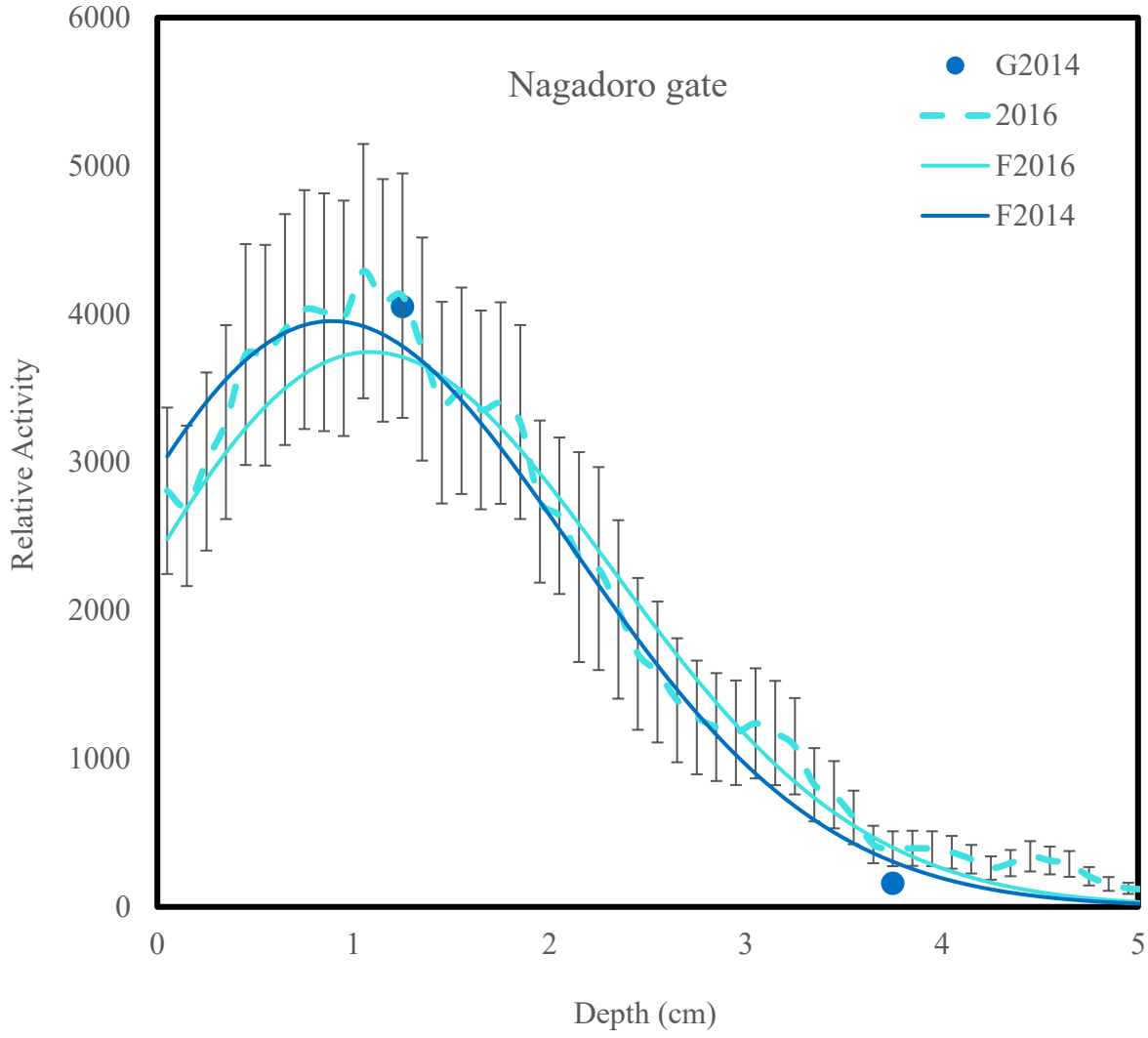

Fig. IV-3 (6) – Fitting results of Nagadoro gate sample by using Eq. (4). Blue dot describes for data of 2014 by gamma measurement; Light blue dashed curve describes for data of 2016; Blue and Light blue smooth curves describe for data of 2014, and 2016, respectively by fitting.

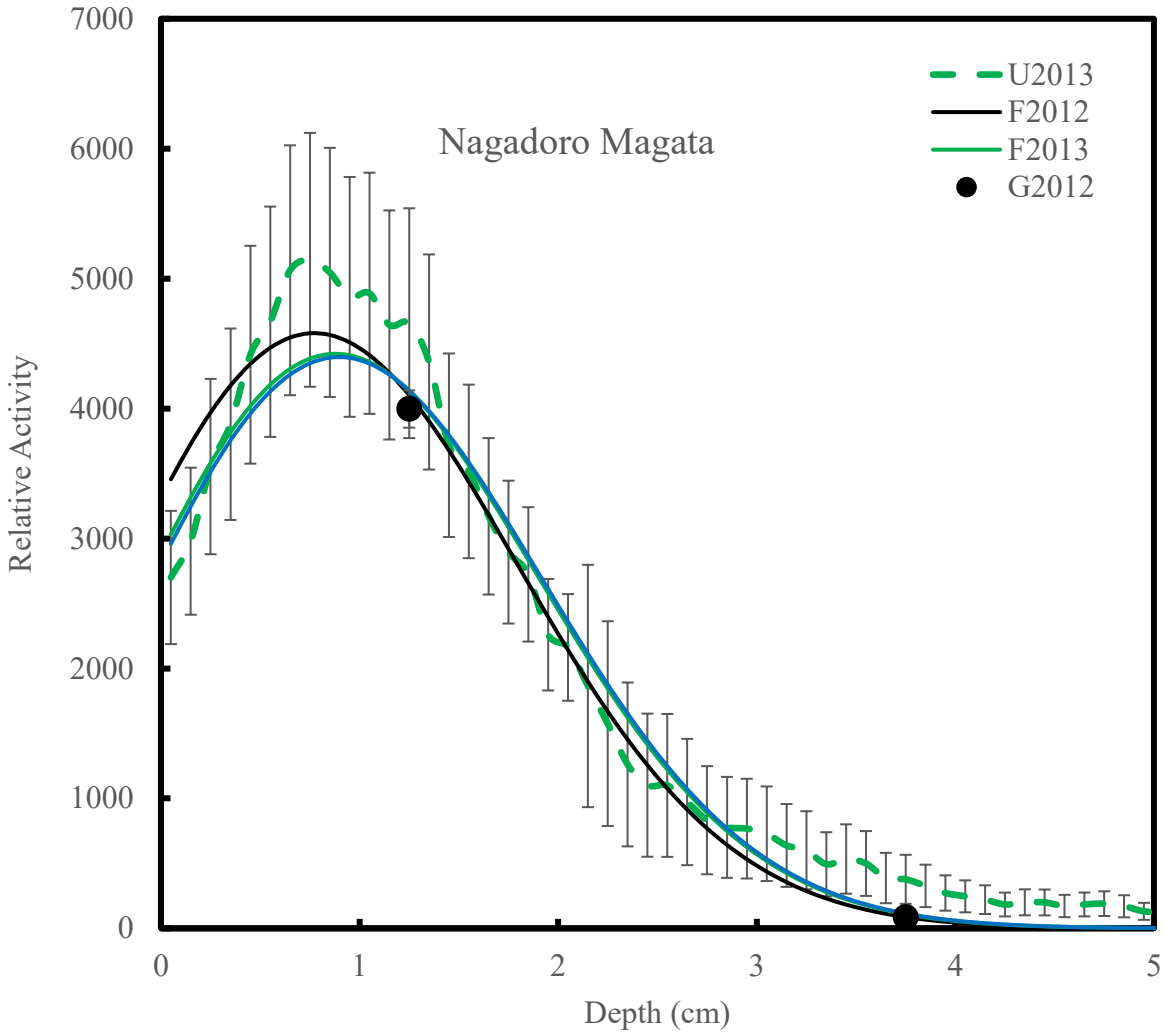

Fig. IV-3 (7) – Fitting results of Nagadoro Magata sample by using Eq. (4). Black dot describes for data of 2012 by gamma measurement; Green dashed curve describes for data of 2013; Black and green smooth curves describe for data of 2012, and 2013, respectively by fitting.

Table IV-1: Fitting results of the parameter, and referred soil types from MLIT and Reduced Chi-square

Location	v_0 (cm/y)		a (1/y)		d (cm^2/y)		Reduced Chi-square	Soil type (referred from MLIT) [6]
	Value	Error	Value	Error	Value	Error		
Nagadoro rice field	0.59	0.01	0.85	0.01	0.37	0.01	1.29	Katakusa-Medium and Coarse-textured gray lowland soil
Nagadoro Jumonji	2.1	0.05	1.2	0.02	3.6	0.04	1.69	Minaniuta-Gray soils
Yamatsumi Shrine	0.27	0.03	1.17	0.17	0.57	0.05	1	Niidono-Brown fForest soil
Iitate Office	0.99	0.09	1.4	0.1	1.7	0.1	2.01	Iidate-Ando soil
Warabidaida	0.09	$2x10^{-3}$	$6x10^{-3}$	0.01	0.41	0.02	1.62	Tusima II series-Brown forest soil
Nagadoro gate	0.33	0.01	0.33	0.02	0.88	0.01	1.17	Hanazuka series II-Brown forest soil
Nagadoro Magata	1.15	0.04	1.73	0.09	0.61	0.01	0.56	Adachi II-Brwown forest soil

4. Discussion

The soil at roadside or hill base is brown-forest soil which has a thin humus layer on surface soil; the paddy field soil is gray lowland soil which is constituted from the medium and coarse soil particle; for farmland soil is gray soil which contains a large amount of humus and is distributed to deep soil layers [6]. As mentioned in **Section 3**, the migration velocity is quite different in sampling locations. It is slow with the samples collected at roadside or hill base (Yamatsumi shrine, Warabidaida, and Nagadoro gate); faster with the samples at the paddy field (Nagadoro rice field) or farmland (Nagadoro Magata); and very fast with samples at farmland (Nagadoro Jumonji). The difference of the initial migration velocity at roadside or hill base, paddy field, and farmland might be affected by the soil type.

The migration velocity of radiocesium is dramatically reduced from centimeter-scale to millimeter-scale following time in first year after the accident. By this investigation results in period from 2012-2017, practically, radiocesium still moves in the soil; however, the migration distance is not so much. The movement of radiocesium for later years is predicted to be same as that in period of 2012-2017. Based on the fitting values of the initial migration velocity and absorption factor, the vertical migration distance of radiocesium in the soil is less than 2 cm from surface soil after 5. The calculated vertical migration distance results are shown in Fig. IV-5. It means radiocesium is almost concentrated mainly in a 5 cm surface soil layer.

The migration velocity of radiocesium is known as quite fast for several months after deposition and then slows down. The migration velocity of radiocesium was estimated 4–7 mm per month during the first 3–4 months after the accident, and 0.4–1.4 mm/y 1 year after the accident [4]. Concretely, the migration velocities were calculated with 1.6 mm/y in meadowland, 3.7 mm/y in farmland, 1.2 mm/y in tobacco fields, and 10.1 mm/y in paddy fields [5]. In this research, the migration velocity of the paddy field and farmland changing follow time are plotted as in Fig. IV-4. The calculated results at 4 months and 10 months after the accident for paddy field and farmland soils by the assumption in this research are consistent with the results reported by previous researchers.

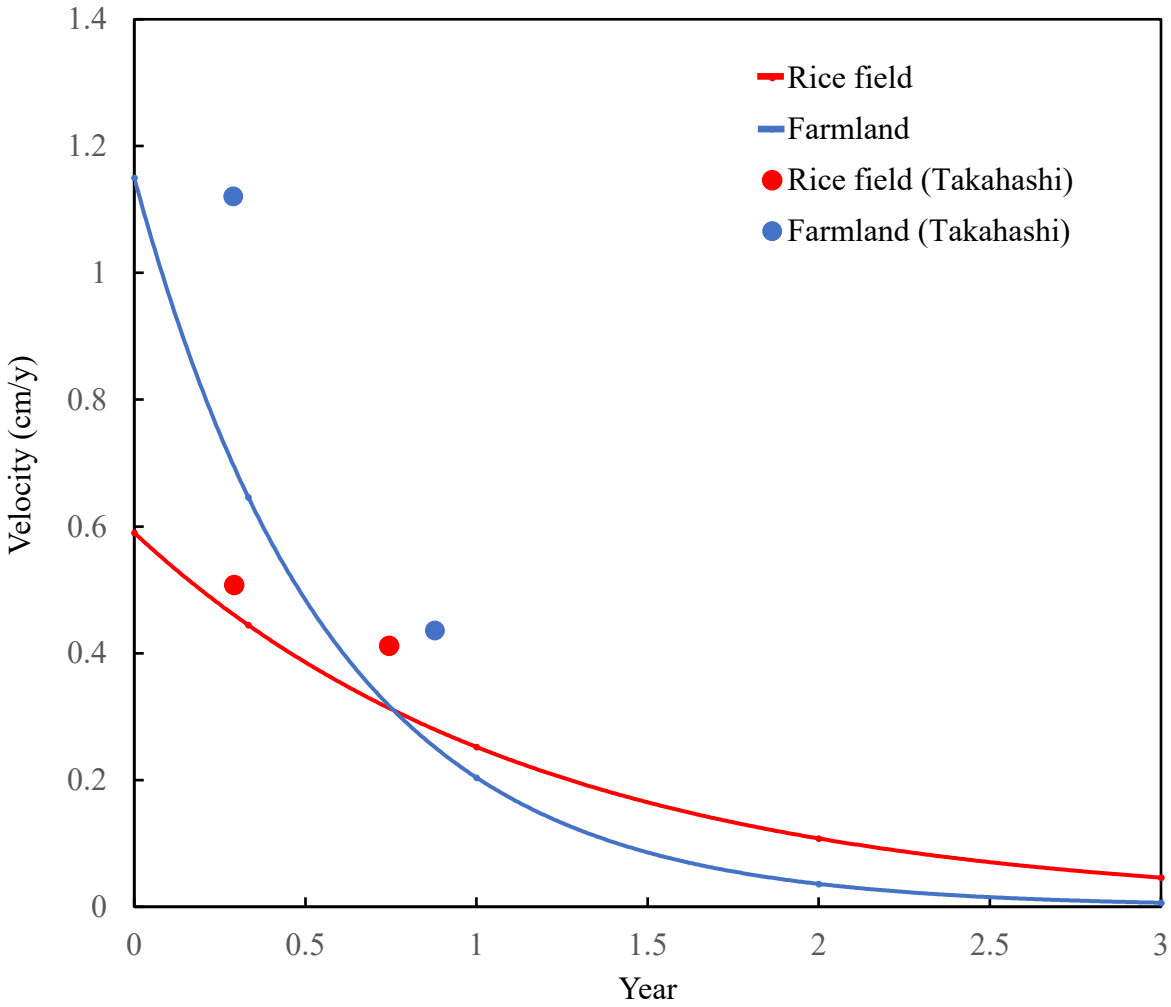

Fig. IV-4: Comparison of migration velocity with reported data by previous researchers.

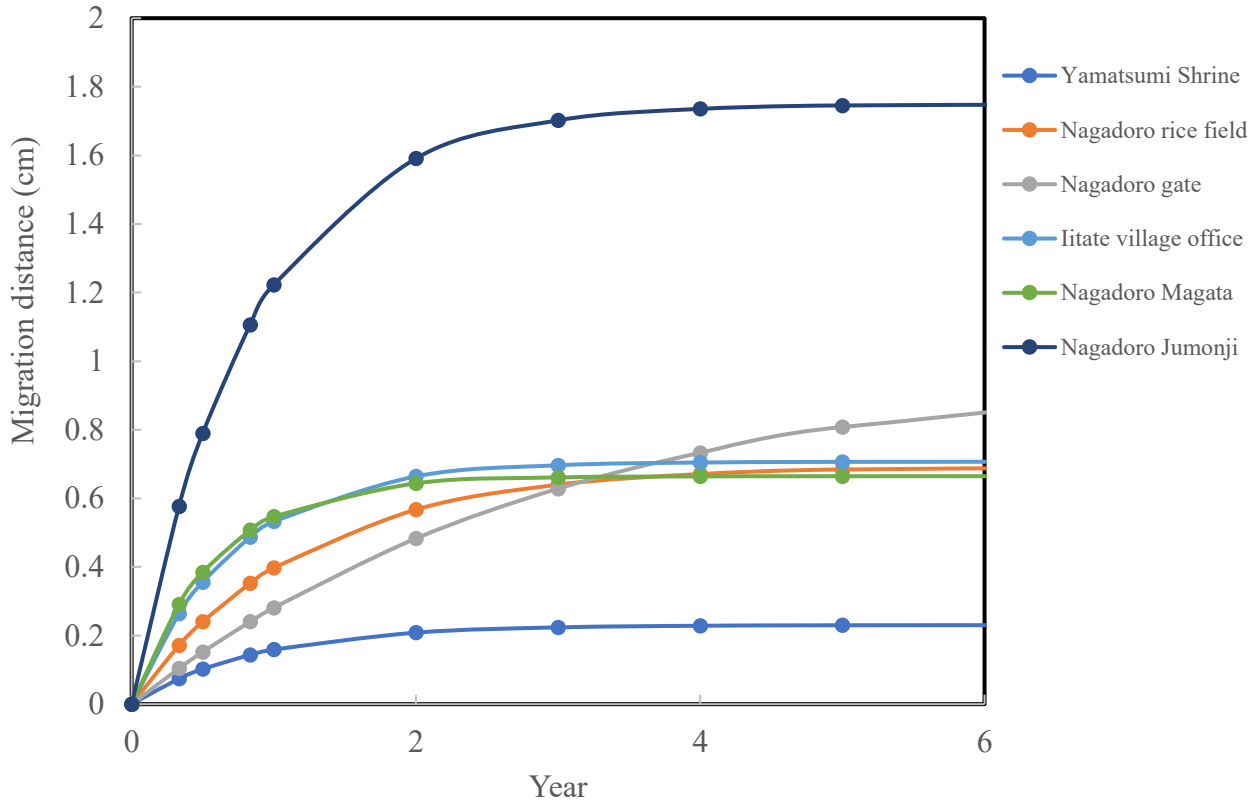

Fig. IV-5: Migration distance following time

5. Conclusion

In this research, a fitting equation was derived from a set of differential equations that were used to describe for 3 processes of the diffusive-convective transport, conservation, and interaction of radionuclides. The fitting equation, which was solved by Bossew and Kirchner, has been modified based on an assuming dependence of the migration velocity of radiocesium on time with the absorption factor. The dependence of the migration velocity as an exponential equation was consistently used for experimental data.

The depth profiles of soil cores which were collected from 2012 to 2017 at some locations of Iitate village, were obtained by a conventional method and new method as in Chapter III. These depth profiles have been applied for fitting with the modified equation. The fitting results of initial migration velocity for roadside or hill base (Yamatsumi shrine, Warabidaida, and Nagadoro gate) had slow migration (0.1-0.3 cm/y); the samples at the rice field (Nagadoro rice field, Nagadoro Magata) had migration velocity from 0.59 – 1.15 (cm/y); and farmland (Nagadoro Jumonji) has quite a high value of migration velocity (2.1 cm/y). Migration velocities calculated based on the initial migration velocities at 4- and 10-months right after the accident of paddy field and farmland were consistent with those of the previous researchers. The diffusion coefficient and absorption factor had values in a range from 0.24 to 3.6 cm^2/y and $6x10^{-3}$ to 1.8 y^{-1}, respectively.

The migration velocity of radiocesium was estimated to be negatable after 5 years of the accident. Vertical migration distance of radiocesium in the soil also predicted to be less than 2 cm from surface soil after 5. It means if a 5 cm surface soil layer is collected, radiocesium is almost removed from the soil.

References

1. Szerbin, P., Koblinger-Bokori, E., Koblinger, L., Vegvari, I., Ugron, A., 1999. Ceasium-137 migration in Hungarian soils. Sci. Total Environ. 227: 215–227.

2. Likar, A., Omahem, G., Lipoglavsek, M., et al., 2001. A theoretical description of diffusion and migration of Cs in soil. J. Environ. Radioact 57: 191-201

3. Bossew, P., Kirchner, G., 2004. Modeling the vertical distribution of radionuclides in soil. Part 1: convection-dispersion equation revisited. J. Environ. Radioact 73: 127-150

4. Shiozawa, S., 2013. Agricultural implications of the Fukushima nuclear accident. In: Nakashima, T.M., Tanoi, K. (Eds.), Agricultural implications of the Fukushima Nuclear accident. Springer, Japan, Tokyo, pp. 49-60

5. Takahashi, J., Tamura. K., Suda, T., *et al*., 2015. Vertical distribution and temporal changes of ^{137}Cs in soil profiles under various land uses after the Fukushima Dai-ichi Nuclear Power Plant accident. J. Environ. Radiact. 139, 351-361.

6. http://www.maff.go.jp/j/seisan/kankyo/hozen_type/h_sehi_kizyun/pdf/ntuti4.pdf (accessed on 2019/05/01)

Chapter V. Soil-to-plant transfer coefficient formulation proposal

1. Introduction

Following the Fukushima nuclear power plant accident, a massive amount of radioactive materials released into the air which had made soil contamination after depositions in the full region surrounding the power plant [1]. After several months of the accident, almost of short half-life radionuclides such as ^{131}I, ^{129}Te, ^{132}Te, ^{136}Cs and so on, have been decayed out, and residual radionuclides are long half-life radionuclides of ^{134}Cs and ^{137}Cs. The migration of radiocesium in the Fukushima soil was estimated to be several millimeters per year after 4 months from the accident occurred for meadow, farmland, and paddy field soil [2, 3]. In addition, research on the migration of radiocesium in a deciduous forest soil shows that only 2% of ^{137}Cs in total deposited amount was penetrated to below a 10 cm depth [4]. These results indicated that the Fukushima surface soil has a high radioactivity concentration of radiocesium. Young trees are quite sensitive to radiation [5,6], which are grown on radioactively contaminated Fukushima soil could be received many effects to become abnormalities in later years.

Radiation impacts on plants (vegetables, rice plants, wood plants so on) are caused by internal and external exposure. The internal exposure of plants comes from the absorption of radionuclides by the plant. Kovalchuk *et al*. (2000) have reported about homologous recombination, which is understood as an index reflecting the repair of induced DNA damage. The reported result indicated the internal exposure to ionizing radiation leads to a higher frequency of the homologous recombination than the external exposure, and the homologous recombination has a strong dependence on radioactivity concentration in plants [7]. Recently, research about morphological abnormalities in Japanese red pine grown in the high air dose rate regions exhibited the dependence of the probability of morphological abnormalities of young pines on the air dose rate. The research results show that internal exposure contributes to the total exposure dose of 20 – 55% [8]. Therefore, it is necessary for the internal exposure to be discussed in the morphological abnormalities of young Japanese red pine induced by exposures.

For estimating the internal exposure of plants, radioactivity concentration in plants is necessary information. Conveniently, radioactivity concentration in the plant could be estimated by a soil-to-plant transfer coefficient (*TF*) and soil contamination. *TF* is normally defined as a ratio of radioactivity concentration in a plant (Bq/(kg dried weight)) to the radioactivity concentration in soil (Bq/(kg dried weight)). The depths from the surface of soil used for *TF* calculation of crop and fruit trees are 20 cm [9], and 15 cm in the case of Fukushima soil [10]. In these calculations, radioactivity concentration in soil is an averaged value corresponding to collected depth. The inhomogeneous distribution of radionuclide in the ground soil is not considered for *TF* calculation. Hence, this study

aims to propose a soil-to-plant transfer coefficient formulation expressed using a soil-to-root transfer factor (β) and root-to-plant translocation factor. β is assumed as a ratio of radioactivity concentration in root to radioactivity concentration in soil at the same soil layer. The proposed formulation is applied for calculating the soil-to-plant transfer coefficient of young pines collected at the Iitate village.

2. Soil-to-tree transfer coefficient formulation

Radioactivity concentration, according to the depth profile of radionuclides, had been analyzed and reported by Albrecht et al. [11] as:

$$C_P = \sum_{i=1}^{n} C_i^s R_i TF \tag{1}$$

where, C_p is radionuclide concentration in plant (Bq/kg dried weight); C_i^s is radionuclide concentration in the *i*-th soil layer (Bq/kg dried weight)*; TF* is the soil-to-plant transfer coefficient; R_i *is* relative root density (dimensionless) in the *i*-th soil layer which is defined with root density, r_i (g.cm^{-3}) and area, A_i (cm^2) of layer *i* as

$$R_i = \frac{r_i A_i}{\sum_{i=1}^{n} r_i A_i} = \frac{m_i / d_i}{\sum_{i=1}^{n} m_i / d_i} \quad (m_i \text{ and } d_i \text{ are mass of root in a length of soil layer } i); \tag{2}$$

Average activity concentration in root ($\overline{C_r}$) which is assumed to insert in the Eq. (1). The soil-to-plant transfer coefficient formulation can be expressed as

$$TF = \frac{C_P}{\overline{C_r}} \frac{1}{\sum_{i=1}^{n} \frac{C_i^s}{\overline{C_r}} R_i} \tag{3}$$

To introduce a soil-to-root transfer factor of *i*-th layer, $C_i^s / \overline{C_r}$ replace to C_i^s / C_i^r. Then the soil-to-root transfer factor, $\beta_i = C_i^r / C_i^s$ is defined by a ratio of radioactivity concentration of root in the *i*-th layer to that of the corresponding soil layer. *TF* is rewritten as follows:

$$TF = \frac{C_P}{\overline{C_r}} \frac{\sum_{i=1}^{n} \frac{m_i}{d_i}}{\sum_{i=1}^{n} \frac{m_i}{d_i \beta_i}} \tag{4}$$

TF in Eq. (4) in the case of homogenous depth distribution, it should correspond to the normal transfer coefficient. For the condition of $C^r = C_1^r = C_2^r = \cdots = C_n^r$, Eq. (4) become

$$TF = \frac{C_p}{\overline{C_r}} \frac{\sum_{i=1}^{n} \frac{m_i}{d_i}}{C^s \sum_{i=1}^{n} \frac{m_i}{d_i C_i^r}}$$

Therefore, when $\overline{C_r}$ is chosen as a harmonic mean of radioactivity concentration in root as $TF = C_P / C^s$

$$\overline{C_r} = \frac{\sum_{i=1}^{n} \frac{m_i}{d_i}}{\sum_{i=1}^{n} \frac{m_i}{d_i C_i^r}} \quad (5).$$

The proposed soil-to-plant transfer coefficient becomes to be the normal transfer coefficient, $TF = C_P / C^s$ which is defined by the ratio of in-plant concentration to the averaged concentration in soil. In this condition, this means that the proposed formulation includes the normal transfer coefficient in case of a homogeneous depth profile and add the soil-to-root transfer factor. The replacement of C_i^s / C_i^r instead of $C_i^s / \overline{C_r}$ is just an assumption. Therefore, this replacement can be checked by the measurement.

3. Results

3.1. Depth profile of radiocesium in soil

Radioactivity concentration of radiocesium and ^{40}K in soil core collected in 2015-2017 are plotted against the depth of the soil layers shown in Fig. V-1. The radiocesium in the soil cores is highly concentrated in the surface layer and lowly distributed in the deep layers. The depth profiles of soil cores collected in 2016 at F1, F4, and F5 have a difference from those collected in 2017 at the same place. The radioactivity concentration of radiocesium is more significant than 90% in 5 cm region from the surface of these locations except soil core collected at F9.

The depth profiles of samples collected in 2015 at F3 and F10 are quite different from those collected in 2017. This because the samples collected at different soil types such as the edge of a rice field (F3) and roadside (F10) in 2015, those collected in 2017 were cultivated for rice planting and forest, respectively. F9 soil core sample was collected at a forested hill with rich humus and organic material, and the measurement result shows that radiocesium is distributed to a 10 cm deep soil layer. The ^{40}K is natural radionuclides in the soil; therefore, distribution is quite homogeneous in the collected soil samples.

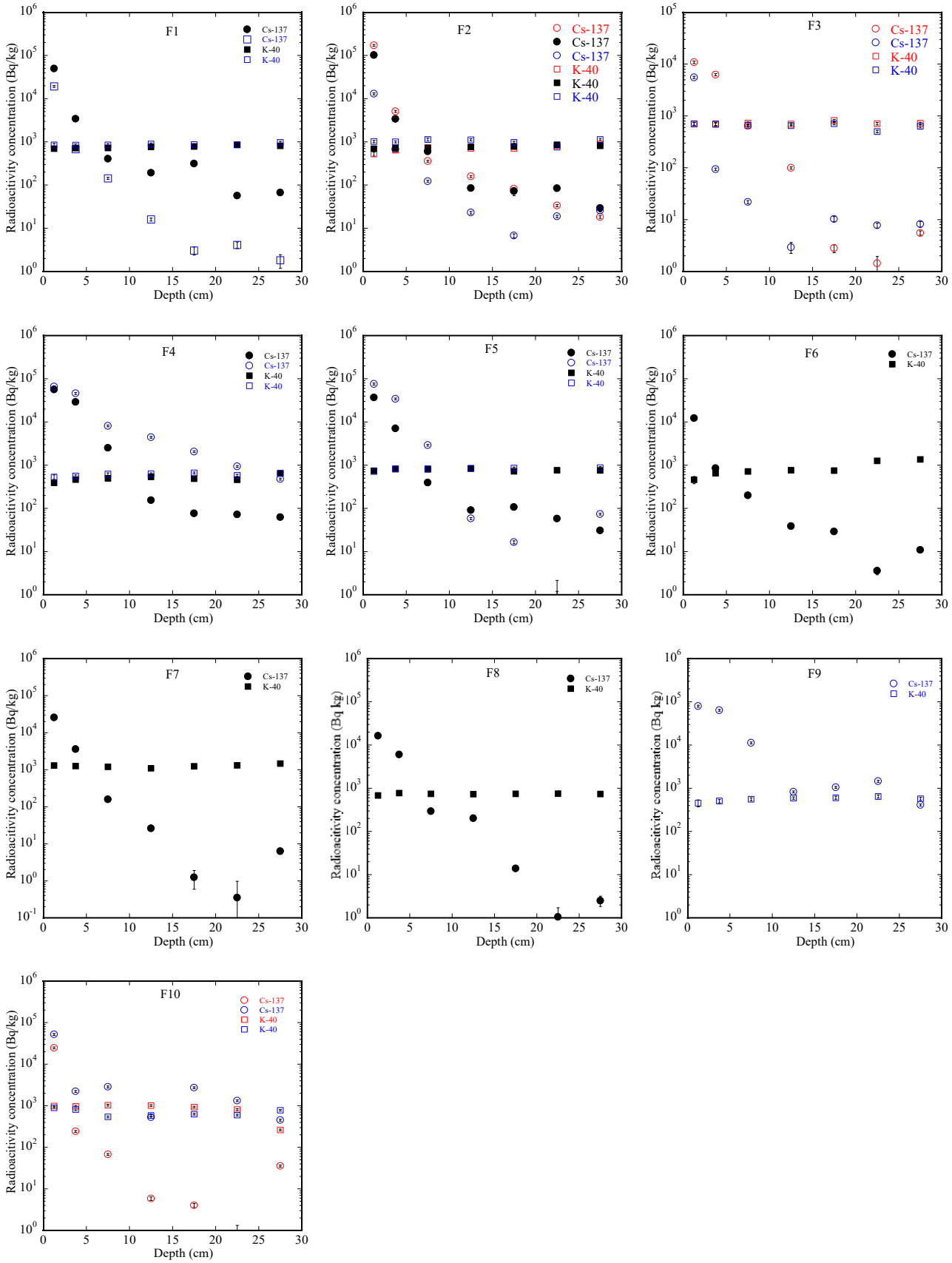

Fig. V-1: Depth profiles of radiocesium and ^{40}K in soil. The red, black and blue circles show for radiocesium of 2015, 2016, and 2017, respectively; The red, black and blue squares illustrate for ^{40}K of 2015, 2016, and 2017, respectively.

3.2. Radioactivity concentration in the root

The radioactivity concentration of radiocesium and ^{40}K in root corresponding to soil layers are shown as in Fig. V-2. The results indicate that the distribution of ^{40}K in root is the same tendency as in soil. The radiocesium radioactivity concentration tends to be higher than that of ^{40}K in root of samples collected at the rice field (F2, F3, F4 and F8) and in samples collected at the forest (F1, F5(2016), F6, F7, F9 and F10(2017)) except for F3 (2015). The young trees at the roadside as F5 (2017), F6 and F10 (2015) have a similarity of radioactivity concentration of radiocesium and ^{40}K in the root.

Radioactivity concentration of radiocesium in collected trees and inventory are listed in Table 1. The radioactivity concentration in roots and inventory of ^{137}Cs is in a range from 20 to 5291 Bq/kg and from 30 to 2044 kBq/m2, respectively. The radioactivity concentration in trees is proportional to those in roots.

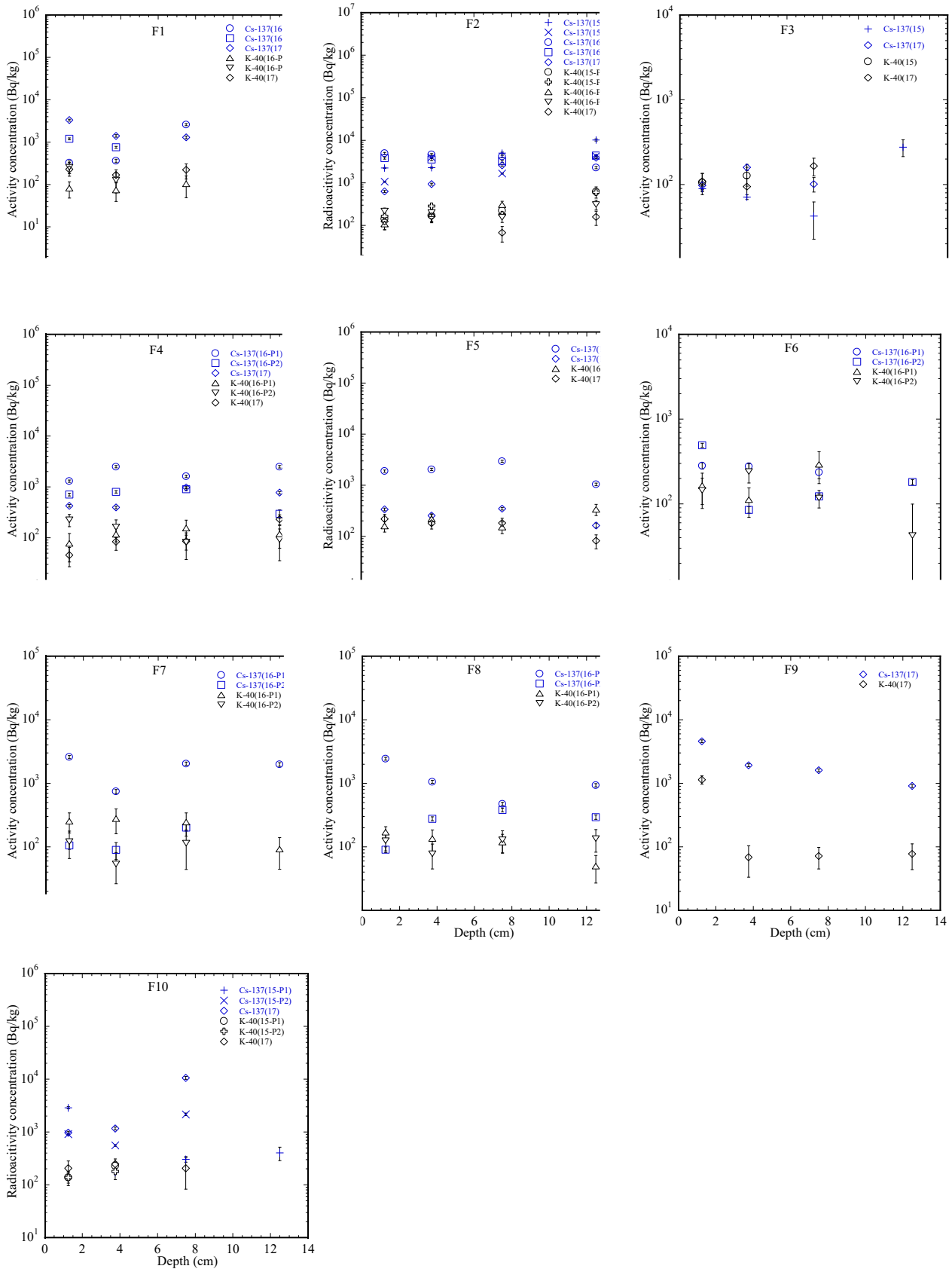

Fig. V-2: Radioactivity concentration of ^{137}Cs and ^{40}K in the root of tree collected from 2015-2017 (P1: represented for first plant, P2: represented for second plant in each year)

3.3. Soil-to-root transfer factor and soil-to-plant transfer coefficient

An example of a soil-to-root transfer factor, β of samples collected in March 2016 and 2017 are plotted in Fig. V-3. β is the ratio of radioactivity concentration in root grown in a soil layer to radioactivity concentration of that soil layer. Radioactivity concentration of radiocesium in the soil layer of 5 cm from the surface is a few hundred to thousand times higher than those in deep soil layers (section 3.1). This distribution of radiocesium leads to β values of the root are increasing with the depth. The root-to-plant translocation factor for ^{137}Cs is listed in table V-1. Translocation factors are less than 1 in almost samples collected at Iitate village except for 3 samples in F2, F6, and F8 with translocation factors of 1.9, 3.68 and 5.61, respectively. The samples in these locations were not washed off properly, they were contaminated by radiocesium in soil attached to these 3 young trees. These samples are neglected for *TF* calculation.

The calculated transfer coefficient of young trees with radiocesium by the proposed formulation is in a range from $3x10^{-3}$ to 0.073 with a mean value of 0.021. The *TF* is quite a similarity for 1-year plants, and these values are in a range from $3x10^{-3}$ to 0.026 with a mean value of 0.011±0.008. The *TF* of 2-year plant samples has a substantial scatter value of a range from 0.011 to 0.073 with a mean value of 0.039±0.026. The *TF* calculated based on IAEA recommendation for crop and fruit trees [10] is in a range from $9x10^{-3}$ to 0.305. *TF* results by both calculation methods are listed in Table V-2.

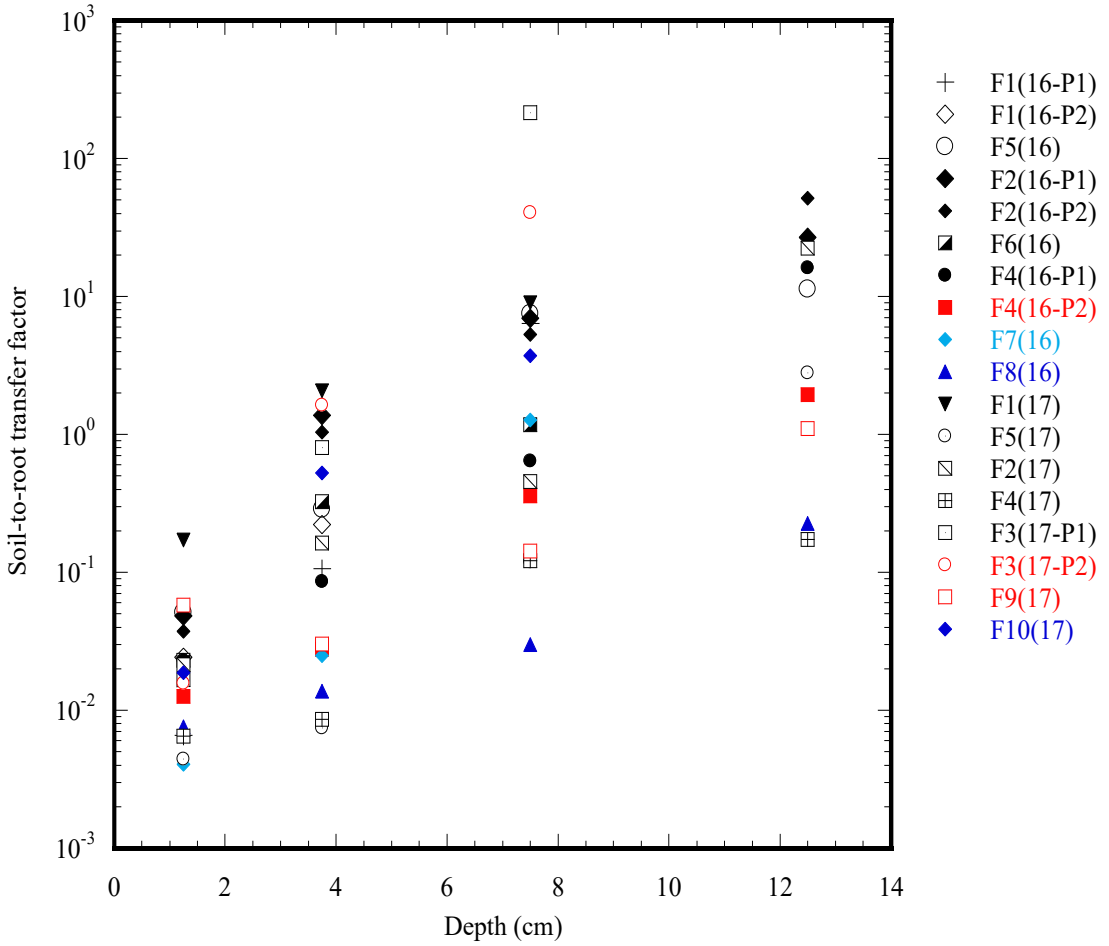

Fig. V-3: Example of soil-to-root transfer factor (β) of plants collected in March 2016 and 2017

Table V-1: Root-to-plant translocation factor for ^{137}Cs

Location	Root-to-plant translocation factor for ^{137}Cs		
	2015	2016	2017
F1	-	$0.82^{(1)\,i}$ $0.26^{(2)\,i}$	$0.07^{\,i}$
F2	$1.90^{(1)\,ii}$ $0.83^{(2)\,ii}$	$0.81^{(1)\,ii}$ $0.42^{(2)\,ii}$	$0.43^{\,i}$
F3	$0.52^{\,i}$	-	$0.21^{\,i}$
F4	-	$0.20^{(1)\,i}$ $0.57^{(2)\,i}$	$0.34^{\,i}$
F5	-	$0.39^{\,ii}$	$0.59^{\,i}$
F6	-	$3.68^{(1)\,ii}$	-
F7	-	$0.52^{\,i}$	-
F8	-	$5.61^{\,ii}$	-
F9	-	-	$0.28^{M\,ii}$
F10	$0.33^{(1)\,ii}$ $0.96^{(2)\,ii}$	-	$0.84^{M\,i}$

$^{(1)}$ and $^{(2)}$ mean for the first and second tree, respectively; ^{M} is shown for fir tree; ^{i}: 0-1 year plant; ^{ii}:1- 2 years plant

Table V-2: Radioactivity concentration of radiocesium in plants collected in 2016 and 2017; transfer coefficient calculated from our formulation and IAEA [6]

Location	radiocesium concentration in plant Bq/kg[#]			Inventory (kBq/m^2)[*]			Transfer coefficient (*TF*) for ^{137}Cs					
							Present			IAEA		
	2015	2016	2017	2015	2016	2017	2015	2016	2017	2015	2016	2017
F1	-	305±19$^{(1)}$ 248±13$^{(2)}$	133±8	-	1198	372	-	0.011$^{(1)\,i}$ 0.012$^{(2)\,i}$	0.020 ^{i}	-	0.038$^{(1)\,i}$ 0.031$^{(2)\,i}$	0.051 ^{i}
F2	5291±266$^{(1)}$ 1450±74$^{(2)}$	3556±178$^{(1)}$ 1542±78$^{(2)}$	441±22	2035	1441	808	0.015$^{(2)\,ii}$	0.011$^{(1)\,ii}$ 0.045$^{(2)\,ii}$	0.021 ^{i}	0.09$^{(2)\,ii}$	0.305$^{(1)\,ii}$ 0.132$^{(2)\,ii}$	0.067 ^{i}
F3	38±3	-	20±5	497	-	30	6x10$^{-3\,i}$	-	7x10$^{-3\,i}$	0.013 ^{i}	-	0.023 ^{i}
F4	-	334±17$^{(1)}$ 414±22$^{(2)}$	168±6	-	1415	1734	-	8x10$^{-3(1)\,i}$ 0.011$^{(2)\,i}$	4x10$^{-3\,i}$	-	0.027$^{(1)\,i}$ 0.033$^{(2)\,i}$	9x10$^{-3\,i}$
F5	-	757±38	-	-	1062	2044	-	0.039 ^{ii}	4x10$^{-3\,i}$	-	0.106 ^{ii}	0.011 ^{i}
F6	-	167±10$^{(1)}$	-	-	169	-	-	-	-	-	-	-
F7	-	58±7$^{(1)}$	-	-	509	-	-	3x10$^{-3\,i}$	-	-	0.020 ^{i}	-
F8	-	992±51	-	-	1195	-	-	-	-	-	-	-
F9	-	-	509±26^{M}	-	-	1689	-	-	0.017$^{(M)\,ii}$	-	-	0.026$^{(M)\,ii}$
F10	120±7$^{(1)}$ 764±39$^{(2)}$	-	960±50^{M}	622	-	958	0.073$^{(1)\,ii}$ 0.072$^{(2)\,ii}$	-	0.026$^{(M)\,i}$	0.033$^{(1)\,ii}$ 0.208$^{(2)\,ii}$	-	0.178$^{(M)\,i}$

[*]: Error of inventory value including statistical and systematical errors was estimated to be less than 5%; [#]: unit calculated by Bq/(kg dried weight)

$^{(1)}$ and $^{(2)}$ mean for the first and second tree, respectively; ^{M} is shown for fir tree; ^{i}: 0-1 year plant; ^{ii}: 1-2 years plant

4. Discussion

The proposed formulation was used to calculate for a homogeneous distribution of ^{40}K in soil, and the results were listed in Table V-3. *TFs* of ^{40}K by proposed formulation were compared to those calculated based on IAEA recommendations for crop and fruit trees [9]. The results show that *TF* values of ^{40}K by our formulation are agreed well with the normal definition within error. This shows that our formulation includes the normal definition for the homogeneous depth profile condition.

To evaluate the dependence of *TF* on the depth of soil core used for calculation with our formulation and normal definition, *TF* results of some locations as forest (F1-2016), rice field (F2-2016), disturbed rice field (F3-2017) and wide distribution of radiocesium in soil (F9-2017) were plotted as in Fig. V-4 for comparison. The dashed and solid lines indicate for *TF* calculated based on the normal definition and proposed formulation, respectively. The results show that *TF* calculated by normal definition has a strong dependence on the depth of soil core for calculation. *TF* is dramatically increased with the depth of soil core. This increase of *TF* is caused by decreasing average radioactivity concentration in the soil core.

According to recommendations of IAEA [6] and the Japanese Ministry of Agriculture, Forestry and Fisheries (JMAFF) [9], soil core of 20 cm and 15 cm depth, respectively, is suitable for *TF* calculation with crop and fruit trees. Calculations for our samples by normal definition show *TF* of 20 cm soil core is higher than that of 15 cm soil core. The difference of *TF* from IAEA and JMAFF recommendations leads to difficulty in the application of the transfer coefficient for the estimation of radioactivity concentration in the plant. *TF* calculated by the proposed formulation has the same tendency as that calculated based on the normal definition for 5 cm depth of soil core. However, *TF* for soil core with depth more than 5 cm by the proposed formulation does not change so much comparing to that of 5 cm depth soil core. This because in the proposed formulation, *TF* was taken into account the depth profile of soil core presented in the soil-to-root transfer factor. Besides, with harmonic mean calculated for radioactivity concentration in root and soil-to-root transfer factor, *TF* was expressed by the contribution of root density in each soil layer.

The means of *TF* have a dependence on the years of the collected young pines, in which the means of *TF* for 0-1 year pines and 1-2 years pines are 0.01 and 0.05, respectively. The increase of the *TF* with the year of pines might come from the nutrient supply, and root uptake increased with the age of the tree to make them grow up (Edwards and Asher (1974) [12]. Besides, Stauton et al. (2003) have assessed the redistribution of radiocesium in root and shoot of young plants for the calculation of *TF* with 10-types of young trees. The reported results of the *TF*s are in a range from 0.005 to 0.037 [13]. In my research, the *TF* values were scattered from 3×10^{-3} to 0.073; however, the mean of the *TF* is 0.021 and this value is consistent with the reported results.

Table V-3: Transfer coefficient of ^{40}K

Location	Transfer coefficient (*TF*) for ^{40}K					
	Present			IAEA		
	2015	2016	2017	2015	2016	2017
F1	-	0.264(1) 0.172(2)	-	-	0.256(1) 0.167(2)	-
F2	0.163(1) 0.049(2)	0.278(1) 0.212(2)	0.078	0.161(1) 0.049(2)	0.277(1) 0.217(2)	0.078
F3	0.1	-	-	0.099	-	-
F4	-	0.303(1) 0.250(2)	0.398	-	0.238(1) 0.219(2)	0.349
F5	-	0.218	-	-	0.210	-
F6	-	0.065(1)	-	-	0.055(1)	-
F7	-	0.016	-	-	0.071	-
F8	-	0.279	-	-	0.258	-
F9	-	-	-	-	-	-
F10	0.013(1) 0.048(2)	-	-	0.013(1) 0.047(2)	-	-

(1) and (2) mean for the first and second trees, respectively.

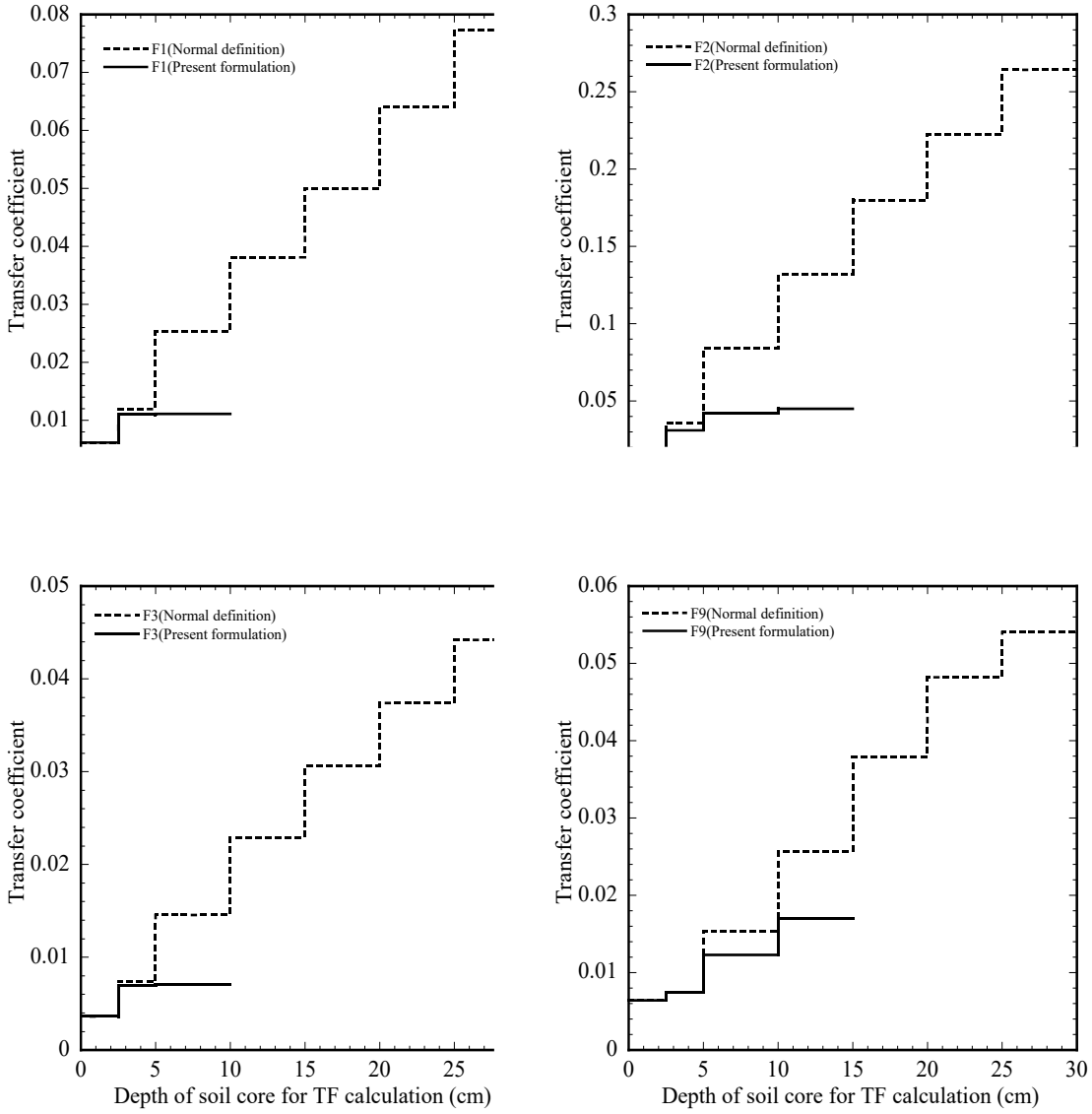

Fig. V-4: Transfer coefficient calculated with different depth of soil core of samples collected at the forest (F1), rice field (F2), disturbed rice field (F3) and deeply distributed radiocesium in soil (F9). Solid lines indicate for the calculation by proposed formulation; dashed lines illustrated for the calculation by normal definition.

Contribution of the root in soil layers to soil-to-plant transfer coefficient of samples collected at Iitate village from 2015 to 2017 were calculated, and some results of samples collected in 2016 and 2017 are shown in Fig. V-5. The results of samples in regions of 0-2.5 cm, 2.5-5 cm, 5-10 cm are broadly scattered, however, the contribution of the root in these regions to *TF* is more than 95%. Interestingly, the contribution of the root in soil layers to *TF* in this investigation is similar to the contribution of the organic layers and organo-mineral layers to the radiocesium soil-to-plant transfer reported by Thiry *et al*. (2000) [14]. With the obtained results of the contribution of the root in soil layer to *TF*, soil core is collected with a depth of 10 cm for narrowly distributed radiocesium, and 15 cm for widely distributed radiocesium in the soil is enough for *TF* calculation with 95% confidence by using the proposed formulation.

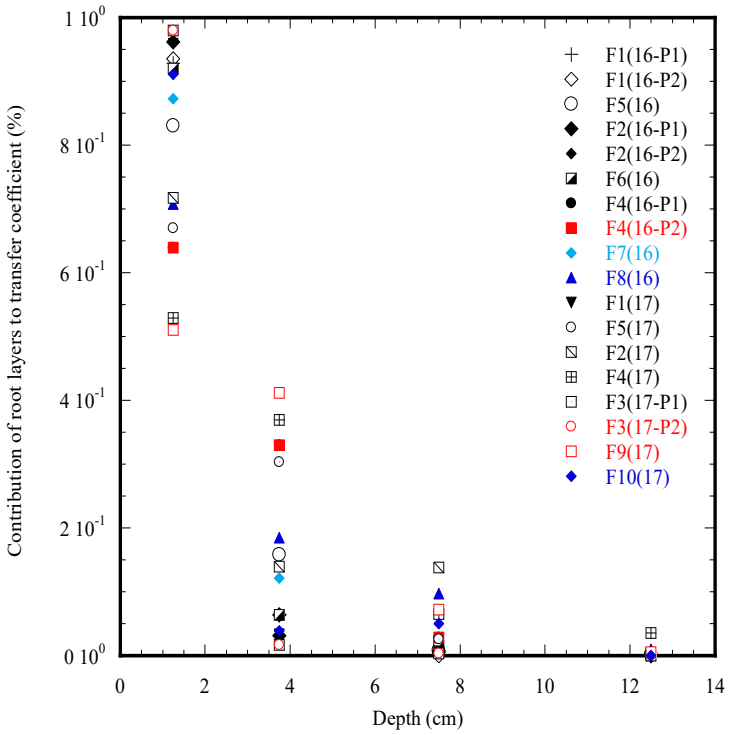

Fig. V-5: Contribution of root layers to soil-to-plant transfer coefficient

5. Conclusion

A transfer coefficient formation of radiocesium from soil to plant, aiming to apply for the depth profile soil by using a transfer factor soil-to-root, was proposed. To take into account the depth profile of soil, the soil-to-root factor was introduced corresponding to the several soil layers. The transfer coefficient is defined by the product of the soil-to-root transfer factor and root-to-plant translocation factor and consistently defined with normal transfer factor, which is the concentration ratio of in-plant to in-soil. The proposed formulation was used to calculate for a homogeneous distribution of ^{40}K in soil, and obtained results show that our formulation includes the normal transfer factor for the homogeneous depth profile condition. The transfer coefficient proposed in this research was considered to the contribution of the root in each soil layer and soil layers by selecting a harmonic mean.

In this investigation, the soil-to-plant transfer coefficient values were scattered from $3x10^{-3}$ to 0.073; however, the mean of the *TF* is 0.021 and this value is consistent with the previous results of other researchers. The soil-to-plant transfer coefficient was in a range from $3x10^{-3}$ to 0.026 with the mean value of 0.011±0.008 for 1-year plants and in a range 0.011 to 0.073 with a mean value of 0.039±0.026 for 2-year plants. For approximation in the application of the proposed formulation, 10 cm and 15 cm soil core are used instead of 30 cm soil core with narrowly and widely distributed radiocesium in soil within 95% confidence of the *TF*.

References

1. Saito K, Tanihata I, Fujiwara M et al., 2015. Detailed deposition density maps constructed by large-scale soil sampling for gamma-ray emitting radioactive nuclides from the Fukushima Dai-ichi Nuclear Power Plant accident. J. Environ. Radiact. 139:308-319.

2. Takahashi J, Tamura K, Suda T, et al., 2015. Vertical distribution and temporal changes of ^{137}Cs in soil profiles under various land uses after the Fukushima Dai-ichi Nuclear Power Plant accident. J. Environ. Radiact. 139:351-361.

3. Shiozawa S. Agricultural implications of the Fukushima nuclear accident. In: Nakashima, T.M., Tanoi, K. (Eds.), 2013. Agricultural implications of the Fukushima Nuclear accident. Springer, Japan, Tokyo. pp. 49-60.

4. Nakanishi T, Matsunaga T, Koarashi J et al., 2014. ^{137}Cs vertical migration in a deciduous forest soil following the Fukushima Dai-ichi Nuclear Power Plant accident. J. Environ. Radiact. 128:9-

5. Sigh S, Eapen S, Thorat V, et al., 2008. Phytoremediation of 137Cs and ^{90}Sr from solutions and low-level nuclear waste by Vetiveria zizanoides. Ecotoxicol. Environ. Safe. 69:2071-2073.

6. International Union of Radioecologists. Handbook of parameter values for the prediction of radionuclide transfer in temperate environments. Technical reports series no. 364. 1994. Vienna: International Atomic Energy Agency (IAEA).

7. Kovalchuk O, Arkhipov A, Barylya I et al., 2000. Plants experiencing chronic internal exposure to ionizing radiation exhibit higher frequency of homologous recombination than acutely irradiated plants. Mutation research. 449:47-56

8. Yoschenko Y, Nanba K, Yoshida S, Watanabe Y et al., 2016. Morphological abnormalities in Japanese red pine (Pinus densiflora) at the territories contaminated as a result of the accident at Fukushima Dai-Ichi Nuclear Power Plant. J. Environ. Radiact. 165:60-67

9. Ministry of Agriculture, Forestry and Fisheries of Japan (MAFF). Transfer of cesium from agricultural soil to fruit tree and vegetable. www.maff.go.jp/j/press/syouan/nouan/pdf/110527-01.pdf accessed in 2018/03/15

10. Endo S, Kajimoto T, Shizuma K., 2013. Paddy-field contamination with ^{134}Cs and ^{137}Cs due to Fukushima Dai-ichi Nuclear Power Plant accident and soil-to-rice transfer coefficients. J. Environ. Radiact. 116: 59-64.

11. Albrecht A, Schultze U, Liedgens M et al., 2002. Incorporating soil structure and root distribution into plant uptake models for radionuclides: toward a more physically based transfer model. J. Environ. Radiact. 59(3):329-350

12. Edwards D. G and Asher C J, 1974. The significance of solution flow rate in flowing culture experiments. Plant and Soil. 41(1):161-175

13. Staunton S, Hinsinger P, Guivarch A et al., 2003. Root uptake and translocation of radiocaesium from agricultural soils by various plant species. Plant and Soil. 254:443-455

12. Thiry Y, Kruyts N, Delvaux B., 2000. Respective horizon contributions to cesium-137 soil-to-plant transfer: A pot experiment approach. J. Environ.Qual. 29:1194-1199

Chapter VI. Summary

Investigation of the environmental dynamics of radiocesium released from the Fukushima Daiichi Nuclear Power Plant has been conducted in this doctoral thesis. In order to make clear the environmental dynamics and transfer of radiocesium from the soil to plant, some works have been implemented step by step as below,

A new technique for determining the shape of the depth profile of radiocesium in soil by using an imaging plate combined with the unfolding algorithm and PHITS code simulation was developed. By the proposed technique, the depth profile of radiocesium can be plotted with millimeter depth-bin width, which is quite difficult to be obtained by ordinary techniques such as sliding soil core to thin soil layers. The distribution level following depth soil layers was presented clearer.

Migration velocity was assumed to be an exponential function time and used for modifying the equation derived from Bossew and Kirchner-model for the transportation of radionuclides in soil. Obtained results from the modified equation show a consistent with the results of previous researchers. By these results, the vertical migration distance of radiocesium was predicted to be stopped around 5 cm of surface soil layer after 5 years.

The final step of the investigation, a soil-to-plant transfer coefficient formulation expressed using a soil-to-root transfer factor and root-to-plant translocation factor. The proposed formulation is applied for calculating the soil-to-plant transfer coefficient of young pines collected at the Iitate village. The calculated *TF* were consistent with previous results of other researchers for young tree types. The proposed soil-to-plant transfer coefficient formulation can be applied in the homogeneous distribution and inhomogeneous distribution of radionuclides in soil. Based on the soil-to-plant transfer coefficient, the amount of radiocesium absorbed by plants growing on the contaminated soil is estimated easily and conveniently.

In conclusion, the radiocesium after released from Fukushima Daiichi Nuclear Power Plant deposited on soil. The environmental dynamics of radiocesium in soil with one movement direction from soil to young trees have been evaluated in this thesis. For further research, the existence of a small amount of radiocesium in deep layers of soil and the change of underground water contamination by this radiocesium following time, are considered as the new theme of research in the future.

Acknowledgment

Firstly, I would like to express my deep and sincere gratitude to my Supervisor uniquely, Professor ENDO Satoru of the Quantum Energy Applications for his enthusiasm and guiding me to do this research as well as the other supports outside research field. It is really the best chance when contacted and received the knowledge and logical way to solve problems from him. His hospitality, encouraging, and personal guidance has provided a sound basis for me in the present thesis.

Next, along with my Supervisor, I would like to thank all my sub-advisors: Professor SHIZUMA Kyoshi- former professor of the Quantum Energy Applications, Associate Professor TANAKA Kenichi, Assistant Professor KAJIMOTO Tsuyoshi for their comment and strong support in my scientific journal and other parts. I would like to send my thanks to Professor NAMBA Shinichi, Professor TSUCHIDA Takashi, Professor MATSUURA Shinya, Professor SAKATA Kiriko for their encouragement insightful comments and provided me much good basic knowledge in the energy applications fields. I am deeply grateful to Professor PHUNG Van Duan and Professor NISHIYAMA Atsushi who gave me a big chance to be here and supported me a lot in my research field and living manner. I also express my sincere gratitude to Professors and Staff of the Phoenix Leader Education Program for their guidance and strong support for me to complete my works.

Then, I thank my fellow labmates in the Quantum Energy Applications Laboratory for their friendly help during the time I live in Japan. Also, I thank all Vietnamese Students at Hiroshima University who make me feel at home country during the time I live here. Moreover, I also would like to express my warm and sincere thanks to my host-family, Mr/Mrs. MORIMOTO and my Japanese Teacher Yamamoto sensei, who have given me good chances to find and understand more about the Japanese culture and the hospitality of Japanese people.

Finally, I owe my loving thanks to my wife DINH Thi Hai, my children NGUYEN Tat Vinh, NGUYEN Quoc Toan, NGUYEN Tue An. Sometimes, I had ever thought about giving up due to much pressure. However, their encouragement is a big motivation for me to continue. My special gratitude is due to my parents, my sisters, and my brothers for their loving support.

Thank you all,

NGUYEN Tat Thanh

Appendixes

Appendix 1: Gamma measurement results of Soil cores

Warabidaida							
Depth (cm)	Cs-137		Cs-134		K-40		Mass (g)
	Radioact. (kBq/g)	Error (kBq/g)	Radioact. (kBq/g)	Error (kBq/g)	Radioact. (kBq/g)	Error (kBq/g)	
2016							
1.25	49.55	2.48	49.65	2.49	0.70	0.05	38.89
3.75	3.41	0.17	3.46	0.18	0.72	0.05	42.53
7.5	0.41	0.02	0.40	0.02	0.73	0.04	94.33
12.5	0.19	0.01	0.19	0.01	0.76	0.04	90.52
17.5	0.31	0.02	0.32	0.02	0.78	0.04	88.2
22.5	0.06	0.00	0.06	0.00	0.86	0.05	99.7
27.5	0.07	0.00	0.07	0.00	0.81	0.04	96.12
2017							
1.25	19.27	0.96	17.42	0.87	0.85	0.07	32.42
3.75	0.68	0.03	0.53	0.03	0.84	0.06	49.15
7.5	0.14	0.01	0.11	0.01	0.85	0.06	93.57
12.5	0.02	0.00	0.01	0.01	0.89	0.05	84.6
17.5	0.00	0.00	-	-	0.87	0.05	106.05
22.5	0.00	0.00	-	-	0.85	0.05	85.89
27.5	0.00	0.00	-	-	0.98	0.05	84.93

Nagadoro rice field							
Depth (cm)	Cs-137		Cs-134		K-40		Mass (g)
	Radioact. (kBq/g)	Error (kBq/g)	Radioact. (kBq/g)	Error (kBq/g)	Radioact. (kBq/g)	Error (kBq/g)	
2012							
1.25	219.78	0.33	233.61	0.39	0.41	0.11	17.70
3.75	2.50	0.01	2.60	0.01	0.61	0.02	35.82
7.50	1.85	0.01	1.97	0.01	0.61	0.02	68.70
12.50	0.38	0.00	0.38	0.00	0.55	0.01	73.49
17.50	0.21	0.00	0.21	0.00	0.65	0.01	77.70
22.50	0.03	0.00	0.04	0.00	0.72	0.01	76.75
27.50	0.03	0.00	0.03	0.00	0.79	0.02	71.03
2013							

2013							
1.25	218.16	0.09	204.81	0.12	0.50	0.03	14.88
3.75	17.40	0.02	17.12	0.03	0.64	0.02	30.88
7.5	3.69	0.01	3.45	0.01	0.60	0.01	84.23
12.5	0.80	0.00	0.76	0.01	0.62	0.01	79.15
17.5	0.18	0.00	0.16	0.00	0.63	0.01	81.33
22.5	0.10	0.00	0.09	0.00	0.63	0.01	81.06
27.5	0.12	0.00	0.11	0.00	0.92	0.02	85.74
2014							
1.25	71.05	3.55	75.96	3.80	0.25	0.03	28.51
3.75	4.34	0.22	4.47	0.23	0.40	0.03	31.6
7.5	1.34	0.07	1.39	0.07	0.53	0.03	67.83
12.5	0.06	0.00	0.06	0.00	0.63	0.03	68.69
17.5	0.12	0.01	0.12	0.01	0.69	0.04	77.74
22.5	0.08	0.00	0.08	0.00	0.94	0.05	76.35
27.5	0.06	0.00	0.05	0.00	0.71	0.04	67.42
2015							
1.25	171.16	8559.09	171.18	8.56	0.52	0.06	20.15
3.75	5.09	255.36	5.04	0.26	0.65	0.04	34.57
7.5	0.36	18.30	0.32	0.02	0.73	0.04	88.08
12.5	0.16	8.13	0.15	0.01	0.71	0.04	85.71
17.5	0.08	4.34	0.08	0.00	0.71	0.04	88.77
22.5	0.03	1.95	0.03	0.00	0.82	0.04	85.51
27.5	0.02	1.17	0.02	0.00	0.88	0.05	85.65
2016							
1.25	102.20	5.11	102.88	5.17	0.53	0.08	23.67
3.75	3.38	0.17	3.40	0.17	0.69	0.04	34.86
7.5	0.60	0.03	0.60	0.03	0.61	0.03	82.41
12.5	0.09	0.00	0.08	0.00	0.56	0.03	81.16
17.5	0.07	0.00	0.07	0.00	0.60	0.03	81.64
22.5	0.08	0.00	0.07	0.00	0.53	0.03	72.41
27.5	0.03	0.00	0.02	0.00	0.37	0.02	70.74

2017							
1.25	75.61	3.78	74.99	3.76	0.71	0.05	28.61
3.75	34.26	1.71	30.28	1.52	0.83	0.08	36.47
7.5	2.91	0.15	2.89	0.15	0.83	0.05	93.57
12.5	0.06	0.00	0.06	0.01	0.85	0.05	87.66
17.5	0.02	0.00	-	-	0.86	0.05	106.05
22.5	0.03	0.00	0.02	0.01	1.37	0.07	97.25
27.5	0.07	0.00	0.07	0.01	0.87	0.05	88.55

Iitate Farm							
Depth (cm)	Cs-137		Cs-134		K-40		Mass (g)
	Radioact. (kBq/g)	Error (kBq/g)	Radioact. (kBq/g)	Error (kBq/g)	Radioact. (kBq/g)	Error (kBq/g)	
2012							
1.25	49.72	0.19	52.51	0.22	0.24	0.09	32.16
3.75	1.52	0.01	1.71	0.01	0.37	0.02	37.72
7.5	0.19	0.00	0.20	0.00	0.51	0.02	58.58
12.5	0.02	0.00	0.02	0.00	0.45	0.01	82.77
17.5	0.02	0.00	0.02	0.00	0.53	0.01	87.66
22.5	0.01	0.00	0.00	0.00	0.55	0.01	94.68
27.5	0.01	0.00	0.01	0.00	0.53	0.01	68.35
2013							
1.25	9.30	0.02	8.80	0.03	0.60	0.02	23.61
3.75	4.38	0.02	4.29	0.02	0.53	0.02	25.98
7.5	1.02	0.00	0.98	0.01	0.49	0.01	57.94
12.5	0.59	0.00	0.55	0.00	0.51	0.01	68.80
17.5	0.05	0.00	0.03	0.00	0.54	0.01	68.86
22.5	0.03	0.00	0.01	0.00	0.50	0.01	67.13
27.5	0.02	0.00	0.01	0.00	0.41	0.01	88.46
2014							
1.25	42.68	2.14	43.24	2.17	0.48	0.05	17.57
3.75	12.76	0.64	12.21	0.61	0.63	0.04	37.17
7.5	0.08	0.00	0.07	0.01	0.58	0.04	73.29
12.5	0.05	0.00	0.05	0.00	0.58	0.03	67.67
17.5	0.03	0.00	0.03	0.00	0.79	0.04	94.11
22.5	0.00	0.00	0.00	0.00	0.61	0.03	74.55
27.5	0.01	0.00	0.01	0.00	0.71	0.04	93.69

2015							
1.25	10.86	570.08	10.96	0.59	0.70	0.05	45.15
3.75	6.25	313.53	6.14	0.31	0.69	0.05	53.81
7.5	0.64	32.43	0.64	0.03	0.72	0.04	92.35
12.5	0.10	5.17	0.10	0.01	0.70	0.04	117.94
17.5	0.00	0.50	0.00	0.00	0.82	0.04	119.75
22.5	0.00	0.51	0.00	0.01	0.71	0.04	124.45
27.5	0.01	0.54	0.00	0.00	0.72	0.04	125.49
2016							
1.25	16.24	0.81	16.07	0.81	0.69	0.05	49.52
3.75	6.04	0.30	5.97	0.30	0.77	0.05	47.5
7.5	0.29	0.02	0.29	0.02	0.75	0.04	91.86
12.5	0.20	0.01	0.20	0.01	0.73	0.04	90.14
17.5	0.01	0.00	0.01	0.00	0.74	0.04	104.29
22.5	0.00	0.00	0.00	0.00	0.75	0.04	108.04
27.5	0.00	0.00	0.00	0.00	0.74	0.04	111.11
2017							
1.25	5.55	0.28	5.68	0.29	0.71	0.05	44.93
3.75	0.09	0.00	0.09	0.01	0.70	0.05	47.76
7.5	0.02	0.00	0.02	0.00	0.66	0.04	92.75
12.5	0.00	0.00	0.00	0.00	0.65	0.04	107.14
17.5	0.01	0.00	-	-	0.71	0.04	99.7
22.5	0.01	0.00	-	-	0.50	0.03	88.37
27.5	0.01	0.00	0.01	0.00	0.63	0.04	89.09

Near Iitate Farm 1							
Depth (cm)	Cs-137		Cs-134		K-40		Mass (g)
	Radioact. (kBq/g)	Error (kBq/g)	Radioact. (kBq/g)	Error (kBq/g)	Radioact. (kBq/g)	Error (kBq/g)	
2016							
1.25	16.07	0.81	16.24	0.81	0.69	0.05	49.52
3.75	5.97	0.30	6.04	0.30	0.77	0.05	47.50
7.5	0.29	0.02	0.29	0.02	0.75	0.04	91.86
12.5	0.20	0.01	0.20	0.01	0.73	0.04	90.14
17.5	0.01	0.00	0.01	0.00	0.74	0.04	104.29
22.5	0.00	0.00	0.00	0.00	0.75	0.04	108.04
27.5	0.00	0.00	0.00	0.00	0.74	0.04	111.11

2017							
1.25	65.79	3.29	64.72	3.26	0.39	0.05	16.03
3.75	45.91	2.30	45.18	2.27	0.46	0.05	24.07
7.5	8.11	0.41	8.12	0.41	0.50	0.03	58.85
12.5	4.44	0.22	4.43	0.22	0.54	0.03	60.21
17.5	2.06	0.10	2.03	0.10	0.49	0.03	58.72
22.5	0.94	0.05	0.84	0.04	0.46	0.04	87.98
27.5	0.48	0.02	0.48	0.02	0.65	0.04	61.93

Nagadoro gate							
Depth (cm)	Cs-137		Cs-134		K-40		Mass (g)
	Radioact. (kBq/g)	Error (kBq/g)	Radioact. (kBq/g)	Error (kBq/g)	Radioact. (kBq/g)	Error (kBq/g)	
2014							
1.25	22.92	1.15	21.96	1.10	0.78	0.05	46.79
3.75	0.89	0.05	0.88	0.05	0.76	0.05	45.52
7.5	0.04	0.00	0.03	0.00	0.81	0.05	101.21
12.5	0.02	0.00	0.01	0.00	0.79	0.04	88.86
17.5	0.01	0.00	0.01	0.00	0.82	0.04	89.66
22.5	0.02	0.00	0.02	0.00	0.84	0.05	88.73
27.5	0.02	0.00	0.02	0.00	0.80	0.04	69.56
2016							
1.25	37.11	1.86	36.83	1.85	0.74	0.05	42.1
3.75	7.10	0.36	7.12	0.36	0.81	0.05	41.98
7.5	0.39	0.02	0.39	0.02	0.81	0.04	91.75
12.5	0.09	0.00	0.09	0.01	0.83	0.04	91.44
17.5	0.11	0.01	0.11	0.01	0.72	0.04	83.43
22.5	0.06	0.00	0.06	0.00	0.77	0.04	95.54
27.5	0.03	0.00	0.03	0.00	0.76	0.04	87.86
2017							
1.25	75.61	3.78	74.99	3.76	0.71	0.05	28.61
3.75	34.26	1.71	30.28	1.52	0.83	0.08	36.47
7.5	2.91	0.15	2.89	0.15	0.83	0.05	93.57
12.5	0.06	0.00	0.06	0.01	0.85	0.05	87.66
17.5	0.02	0.00	-	-	0.86	0.05	106.05
22.5	0.03	0.00	0.02	0.01	1.37	0.07	97.25
27.5	0.07	0.00	0.07	0.01	0.87	0.05	88.55

Manodam							
Depth (cm)	Cs-137		Cs-134		K-40		Mass (g)
	Radioact. (kBq/g)	Error (kBq/g)	Radioact. (kBq/g)	Error (kBq/g)	Radioact. (kBq/g)	Error (kBq/g)	
2016							
1.25	12.23	0.62	12.00	0.64	0.46	0.09	21.42
3.75	0.85	0.04	0.84	0.05	0.65	0.05	30.48
7.5	0.20	0.01	0.20	0.01	0.72	0.04	67.57
12.5	0.04	0.00	0.04	0.00	0.77	0.04	55.39
17.5	0.03	0.00	0.03	0.00	0.75	0.04	56.03
22.5	0.00	0.00	0.01	0.00	1.26	0.07	78.64
27.5	0.01	0.00	0.01	0.00	1.36	0.07	70.22

Nimabashi							
Depth (cm)	Cs-137		Cs-134		K-40		Mass (g)
	Radioact. (kBq/g)	Error (kBq/g)	Radioact. (kBq/g)	Error (kBq/g)	Radioact. (kBq/g)	Error (kBq/g)	
2016							
1.25	25.90	1.30	25.57	1.29	1.30	0.09	29.34
3.75	3.62	0.18	3.57	0.18	1.26	0.07	38.44
7.5	0.16	0.01	0.15	0.01	1.21	0.07	113.74
12.5	0.03	0.00	0.02	0.00	1.10	0.06	131.81
17.5	0.00	0.00	-	-	1.24	0.06	123.76
22.5	0.00	0.00	-	-	1.30	0.07	126.16
27.5	0.01	0.00	0.00	0.00	1.47	0.08	124.53

Nagadoro Jumonji							
Depth (cm)	Cs-137		Cs-134		K-40		Mass (g)
	Radioact. (kBq/g)	Error (kBq/g)	Radioact. (kBq/g)	Error (kBq/g)	Radioact. (kBq/g)	Error (kBq/g)	
2012							
1.25	74.61	0.06	70.65	0.08	0.44	0.03	24.90
3.75	53.79	0.06	53.17	0.07	0.50	0.03	29.48
7.5	8.23	0.01	7.81	0.02	0.47	0.01	56.18
12.5	0.32	0.00	0.28	0.00	0.46	0.01	61.18
17.5	0.08	0.00	0.07	0.00	0.39	0.01	59.54
22.5	0.03	0.00	0.02	0.00	0.29	0.01	56.34
27.5	0.05	0.00	0.05	0.00	0.28	0.01	43.15

2013							
1.25	50.62	0.15	52.88	0.17	0.44	0.08	29.11
3.75	22.69	0.05	23.57	0.06	0.51	0.03	30.60
7.5	2.57	0.01	2.70	0.01	0.22	0.01	53.53
12.5	0.14	0.00	0.14	0.00	0.67	0.01	56.81
17.5	0.07	0.00	0.07	0.00	0.51	0.01	64.74
22.5	0.03	0.00	0.02	0.00	0.52	0.01	72.90
27.5	0.02	0.00	0.01	0.00	0.58	0.01	56.12
2014							
1.25	26.54	1.33	26.99	1.35	0.40	0.04	21.75
3.75	18.70	0.94	19.14	0.96	0.45	0.04	29.64
7.5	5.68	0.28	5.85	0.29	0.49	0.03	57.56
12.5	0.21	0.01	0.21	0.01	0.44	0.02	57.59
17.5	0.10	0.01	0.08	0.00	0.39	0.02	63.35
22.5	0.06	0.00	0.04	0.00	0.40	0.02	66.54
27.5	0.06	0.00	0.04	0.00	0.34	0.02	51.85
2015							
1.25	59.88	3.00	59.61	2.99	0.42	0.05	21.83
3.75	44.97	2.25	44.59	2.23	0.50	0.04	26.29
7.5	5.68	0.28	5.52	0.28	0.45	0.03	55.6
12.5	5.75	0.29	5.70	0.29	0.46	0.03	58.65
17.5	0.02	0.00	0.02	0.00	0.47	0.03	62.13
22.5	0.03	0.00	0.03	0.00	0.45	0.03	58.74
27.5	0.02	0.00	0.03	0.00	0.41	0.03	50.46
2017							
1.25	79.20	3.96	77.05	3.89	0.45	0.08	9.7
3.75	63.93	3.20	63.81	3.20	0.51	0.04	22.79
7.5	11.20	0.56	11.13	0.57	0.56	0.04	52.48
12.5	0.82	0.04	0.82	0.04	0.60	0.04	59.44
17.5	1.05	0.05	0.96	0.05	0.60	0.05	74.54
22.5	1.45	0.07	1.31	0.07	0.64	0.05	68.97
27.5	0.41	0.02	0.40	0.02	0.57	0.04	36.51

Yamatsumi							
Depth (cm)	Cs-137		Cs-134		K-40		Mass (g)
	Radioact. (kBq/g)	Error (kBq/g)	Radioact. (kBq/g)	Error (kBq/g)	Radioact. (kBq/g)	Error (kBq/g)	
2012							
1.25	12.48	0.06	12.95	0.07	0.31	0.05	64.06
3.75	0.14	0.00	0.14	0.00	0.72	0.02	66.95
7.5	0.05	0.00	0.05	0.00	0.70	0.02	121.49
12.5	0.02	0.00	0.02	0.00	0.78	0.01	137.40
17.5	0.00	0.00	0.00	0.00	0.89	0.02	139.46
22.5	0.00	0.00	0.00	0.00	0.89	0.02	134.76
27.5	0.01	0.00	0.01	0.00	0.95	0.02	119.51
2013							
1.25	38.36	0.03	36.10	0.03	0.99	0.02	46.05
3.75	1.32	0.01	1.27	0.01	1.09	0.02	48.17
7.5	0.11	0.00	0.10	0.00	0.96	0.02	100.76
12.5	0.02	0.00	0.02	0.00	0.98	0.02	111.58
17.5	0.01	0.00	0.01	0.00	1.03	0.02	117.77
22.5	0.01	0.00	0.01	0.00	1.02	0.02	115.92
27.5	0.05	0.00	0.04	0.00	1.10	0.02	118.90
2014							
1.25	87.80	4.39	75.69	3.79	0.86	0.06	27.52
3.75	3.87	0.19	3.32	0.17	0.99	0.06	69.32
7.5	0.33	0.02	0.32	0.02	0.88	0.05	138.79
12.5	0.01	0.00	0.01	0.00	0.79	0.04	138.32
17.5	0.01	0.00	0.01	0.00	0.82	0.04	152.52
22.5	0.02	0.00	0.02	0.00	0.78	0.04	143.79
27.5	0.02	0.00	0.02	0.00	0.75	0.04	135.72
2015							
1.25	24.63	1232.08	24.28	1.22	0.98	0.06	44.88
3.75	0.24	12.34	0.24	0.01	0.98	0.05	43.3
7.5	0.07	3.71	0.07	0.00	1.04	0.06	105.29
12.5	0.01	0.55	0.01	0.00	1.01	0.05	111.63
17.5	0.00	0.47	0.00	0.00	0.93	0.05	112.87
22.5	0.00	0.34	0.00	0.00	0.81	0.04	87.44
27.5	0.04	2.01	0.03	0.00	0.26	0.02	60.73
2016							

2016							
1.25	25.37	1.27	24.90	1.26	0.30	0.04	13.92
3.75	3.95	0.20	3.89	0.20	0.34	0.03	24.35
7.5	0.23	0.01	0.21	0.01	0.35	0.03	59
12.5	0.07	0.00	0.06	0.01	0.34	0.02	69.26
17.5	0.02	0.00	0.02	0.00	0.38	0.02	72.12
22.5	0.02	0.00	0.02	0.00	0.41	0.02	75.01
27.5	0.07	0.00	0.06	0.01	0.45	0.03	58.73
2017							
1.25	51.96	2.60	51.16	2.57	0.11	0.03	7.98
3.75	2.22	0.11	2.09	0.11	0.81	0.07	16.61
7.5	2.84	0.14	2.86	0.15	0.54	0.04	37.2
12.5	0.53	0.03	0.51	0.03	0.59	0.04	46.1
17.5	2.72	0.14	2.71	0.14	0.63	0.04	51.81
22.5	1.33	0.07	1.21	0.06	0.60	0.05	47.99
27.5	0.45	0.02	0.44	0.02	0.78	0.05	54.23

Iitate Office							
Depth (cm)	Cs-137		Cs-134		K-40		Mass (g)
	Radioact. (kBq/g)	Error (kBq/g)	Radioact. (kBq/g)	Error (kBq/g)	Radioact. (kBq/g)	Error (kBq/g)	
2012							
1.25	27.04	0.09	29.18	0.10	0.36	0.06	45.73
3.75	0.14	0.00	0.13	0.00	0.58	0.02	47.01
7.5	0.01	0.00	0.01	0.00	0.55	0.02	97.22
12.5	0.02	0.00	0.01	0.00	0.64	0.01	80.16
17.5	0.00	0.00	0.00	0.00	0.71	0.01	96.37
22.5	-	-	-	-	-	-	-
27.5	-	-	-	-	-	-	-
2013							
1.25	24.71	0.02	23.57	0.03	0.43	0.01	60.00
3.75	3.44	0.01	3.42	0.01	0.71	0.01	38.58
7.5	0.34	0.00	0.32	0.00	0.74	0.01	98.94
12.5	0.02	0.00	0.02	0.00	0.69	0.01	94.82
17.5	0.03	0.00	0.03	0.00	0.71	0.01	93.49
22.5	0.01	0.00	0.01	0.00	0.68	0.01	92.34
27.5	-	-	-	-	-	-	-

2014							
1.25	54.11	2.71	54.93	2.75	0.62	0.05	30.45
3.75	20.26	1.01	20.46	1.03	0.59	0.04	39.05
7.5	0.48	0.02	0.47	0.02	0.62	0.04	82.22
12.5	0.02	0.00	0.01	0.00	0.56	0.03	100.01
17.5	0.01	0.00	0.00	0.00	0.56	0.03	97.57
22.5	0.00	0.00	0.00	0.00	0.44	0.03	68.11
27.5	0.01	0.00	0.01	0.00	0.40	0.02	59.91
2015							
1.25	36.91	1.85	36.52	1.83	0.52	0.04	25.1
3.75	1.45	0.07	1.50	0.08	0.52	0.04	50.73
7.5	0.03	0.00	0.03	0.00	0.56	0.03	91.88
12.5	0.01	0.00	0.01	0.00	0.58	0.03	100.09
17.5	0.02	0.00	0.02	0.00	0.54	0.03	87.21
22.5	0.00	0.00	0.00	0.00	0.43	0.03	88.52
27.5	0.00	0.00	0.00	0.00	0.54	0.03	71.05
2016							
1.25	39.04	1.95	39.31	1.97	0.48	0.04	25.51
3.75	6.74	0.34	6.70	0.34	0.49	0.04	29.02
7.5	0.83	0.04	0.82	0.04	0.48	0.03	72.17
12.5	0.05	0.00	0.04	0.00	0.51	0.03	78.18
17.5	0.01	0.00	0.01	0.00	0.49	0.03	84.45
22.5	0.01	0.00	0.01	0.00	0.44	0.03	77.16
27.5	0.00	0.00	0.00	0.00	0.50	0.03	80
2017							
1.25	31.46	1.57	31.45	1.58	0.54	0.04	32.42
3.75	23.59	1.18	21.28	1.07	0.57	0.08	35.94
7.5	5.60	0.28	5.56	0.28	0.62	0.04	82.79
12.5	0.02	0.00	0.03	0.01	0.75	0.05	84.6
17.5	0.01	0.00	0.01	0.01	0.53	0.03	85.83
22.5	0.03	0.00	0.03	0.01	0.70	0.05	85.89
27.5	0.01	0.00	0.00	0.00	0.63	0.03	84.93

Nagadoro Magata							
Depth (cm)	Cs-137		Cs-134		K-40		Mass (g)
	Radioact. (kBq/g)	Error (kBq/g)	Radioact. (kBq/g)	Error (kBq/g)	Radioact. (kBq/g)	Error (kBq/g)	
2012							
1.25	86.93	0.19	89.54	0.22	0.55	0.09	37.82
3.75	1.83	0.01	1.88	0.01	0.91	0.03	43.95
7.5	0.24	0.00	0.24	0.00	0.75	0.03	70.84
12.5	0.04	0.00	0.05	0.00	0.77	0.01	74.39
17.5	0.01	0.00	0.01	0.00	0.81	0.02	95.78
22.5	0.01	0.00	0.00	0.00	0.64	0.01	86.91
27.5	0.05	0.00	0.06	0.00	0.86	0.01	74.52
2013							
1.25	92.86	0.06	87.73	0.07	1.03	0.03	34.37
3.75	2.84	0.01	2.79	0.01	0.93	0.02	55.02
7.5	0.57	0.00	0.53	0.00	0.90	0.02	66.37
12.5	0.14	0.00	0.13	0.00	0.88	0.02	88.74
17.5	0.01	0.00	0.01	0.00	0.95	0.02	98.58
22.5	0.01	0.00	0.01	0.00	0.94	0.02	93.67
27.5	0.08	0.00	0.07	0.00	0.95	0.02	107.15

Appendix 2: Gamma measurement results of Roots and Plants

Warabidaida			
Root	Concentration (Bq/kg)	Weight (g)	Concentration of Plant (Bq/kg)
2016			
Root 1			
1.25	326.50	0.10	309.59
3.75	362.37	0.10	
7.5	2600.31	0.04	
12.5	-	-	
Root 2			
1.25	1201.28	0.42	247.72
3.75	755.78	0.44	
7.5	-	-	
10	-	-	
2017			
Root 1			
1.25	3309.02	0.06	133.00
3.75	1400.89	0.03	
7.5	1295.22	0.04	
10	-	-	

Nagadoro rice field			
Root	Concentration (Bq/kg)	Weight (g)	Concentration of Plant (Bq/kg)
2015			
Root 1			
1.25	2244.12	0.75	5290.59
3.75	2285.45	0.59	
7.5	5038.67	1.04	
12.5	10201.80	0.15	
Root 2			
1.25	1065.27	0.42	1450.19
3.75	3984.37	0.44	
7.5	1668.55	0.58	
10	4280.41	0.14	
2016			
Root 1			
1.25	4943.85	0.42	3556.42
3.75	4662.67	0.44	
7.5	4201.78	0.58	
10	2286.65	0.14	
Root 2			
1.25	3820.20	0.6	1541.66
3.75	3536.09	0.63	
7.5	3223.25	0.79	
10	4389.85	0.28	
2017			
Root			
1.25	631.24	0.21	441.21
3.75	933.14	0.11	
7.5	2584.07	0.08	
10	3916.91	0.31	

Iitate farm			
Root	Concentration (Bq/kg)	Weight (g)	Concentration of Plant (Bq/kg)
2015			
Root			
1.25	89.35	0.98	37.96
3.75	71.12	0.91	
7.5	42.47	0.69	
12.5	275.13	0.30	
2017			
Root 1			
1.25	92.52	0.24	20.06
3.75	75.56	0.19	
7.5	4747.96	0.13	
10	-	-	
Root 2			
1.25	87.22	0.17	2.02
3.75	153.60	0.13	
7.5	889.55	0.11	
10	-	-	

Near Iitate farm 1			
Root	Concentration (Bq/kg)	Weight (g)	Concentration of Plant (Bq/kg)
2016			
Root 1			
1.25	1302.00	0.46	334.81
3.75	2496.77	0.37	
7.5	1617.83	0.17	
12.5	2493.90	0.08	
Root 2			
1.25	707.99	0.35	413.99
3.75	803.13	0.25	
7.5	899.81	0.18	
10	297.64	0.05	
2017			
Root 1			
1.25	426.63	0.6	168.62
3.75	394.80	0.64	
7.5	981.23	0.78	
10	772.30	0.45	

Nagadoro gate			
Root	Concentration (Bq/kg)	Weight (g)	Concentration of Plant (Bq/kg)
2016			
Root			
1.25	1893.76	0.71	757.13
3.75	2049.20	0.46	
7.5	2950.85	0.60	
12.5	1041.09	0.21	
2017			
Root			
1.25	336.52	0.32	168.00
3.75	255.17	0.26	
7.5	347.82	0.23	
12.5	163.51	0.10	

Manodam			
Root	Concentration (Bq/kg)	Weight (g)	Concentration of Plant (Bq/kg)
2016			
Root 1			
1.25	282.14	0.19	166.68
3.75	276.88	0.25	
7.5	235.51	0.08	
12.5	-	-	
Root 2			
1.25	491.80	0.85	543.45
3.75	85.13	0.69	
7.5	122.95	1.38	
10	181.52	0.54	

Nimabashi			
Root	Concentration (Bq/kg)	Weight (g)	Concentration of Plant (Bq/kg)
2016			
Root 1			
1.25	0.24	0.03	58.15
3.75	0.10	0.01	
7.5	0.14	0.03	
12.5	-	-	

Near Iitate farm 2			
Root	Concentration (Bq/kg)	Weight (g)	Concentration of Plant (Bq/kg)
2016			
Root 1			
1.25	295.98	0.28	991.03
3.75	141.46	0.24	
7.5	162.22	0.25	
12.5	126.26	0.21	

Nagadoro Jumonji			
Root	Concentration (Bq/kg)	Weight (g)	Concentration of Plant (Bq/kg)
2017			
Root			
1.25	4597.64	0.29	509.00
3.75	1923.88	0.31	
7.5	1609.22	0.64	
12.5	910.01	0.30	

Yamatsumi Shrine			
Root	Concentration (Bq/kg)	Weight (g)	Concentration of Plant (Bq/kg)
2015			
Root 1			
1.25	2881.65	0.92	120.09
3.75	171.90	0.64	
7.5	305.37	0.70	
12.5	401.84	0.14	
Root 2			
1.25	910.59	0.69	764.18
3.75	555.95	0.51	
7.5	2166.41	0.40	
10	-	-	
2017			
Root 1			
1.25	970.62	0.21	960.42
3.75	1166.45	0.11	
7.5	10591.48	0.08	
10	-	-	